INVESTIGATION ON THERMO-MECHANICAL INSTABILITY OF POROUS LOW DIELECTRIC CONSTANT MATERIALS

by

EMIL HYUNBAE ZIN

Presented to the Faculty of the Graduate School of

The University of Texas at Arlington in Partial Fulfillment

of the Requirements

for the Degree of

DOCTOR OF PHILOSOPHY

THE UNIVERSITY OF TEXAS AT ARLINGTON

August 2012

Copyright © by Emil Hyunbae Zin 2012

All Rights Reserve

ACKNOWLEDGEMENTS

First and foremost, I would like to express the deepest appreciation to my advisor, Prof. Choong-Un Kim for leading me into the semiconductor industry, offering me the opportunities to get involved into various projects, providing continuous support and assistance throughout my doctoral research. Without his guidance and persistent help this dissertation would not have been possible. In addition, special thanks are extended to the other committee members Prof. Wen Chan, Prof. Seong Jin Koh, Prof. Yaowu Hao, and Prof. Fuqiang Liu for their thoughtful questions, encouraging words, and valuable feedback.

Second, I would like to thank with my heart to my group members and friends, Dr. Nancy Michael, Dr. Woong Ho Bang, Dr. Liangshan Chen, Huili Xu, Tingqin Zhao, Rodriguez, Patricia A, Rahmat S Duryat, Swathi Murthi, Mehmet Eray Erkan, Jie He, Mook, Koi and others. My boundless gratitude goes to Dr. Woong Ho Bang whose professional help for doing researches and instructions in many aspects. Also, my deepest gratitude goes to my Korean younger and elder brothers, Dr. Bo Hoon Kim, Dr. Suk Hoon Kang, Dr. Kun Hee Han, Dr. Jae Sung Cho, Soo Kim, Yoon Ki Sa, Dr. Jong Kwan Lee, Dr. Ki Hyun Kim, Dr. Dong Hyun Lee, Dr. Yoon Chul Na, Dr. Jae Woong Yoon, Dr. In Pyo Hong, Dr. Hyo Sung Wi, Dr. Hoon Jung, Byung Soo Moon, Jung

Hyun Lee, Dr. Yeon Ho Park, Jung Pil Ki and others. In addition, I am greatly grateful to Yu Sin Kim and So young Lee as my senior of life.

Third, I would sincerely like to thank my two younger sisters and one brother, and my parents-in-law, and sister-in-law for their countless love and belief.

Last, I with true heart want to thank my parents. Their concern, understanding and encouragement have been the cornerstone to my success. I want to dedicate this thesis to them and express all my respects to them. I especially wish to express the most heartfelt thanks and my love to my wife, Hae Kyoung Kim who makes it all possible and is always standing behind me firmly.

July 12, 2012

ABSTRACT

INVESTIGATION ON THERMO-MECHANICAL INSTABILITY OF POROUS LOW DIELECTRIC CONSTANT MATERIALS

Emil H. Zin, PhD

The University of Texas at Arlington, 2012

Supervising Professor: Choong-Un Kim

This study investigates the structural stability of porous low dielectric constant materials (PLK) under thermal and mechanical load and the influence of contributing factors including porosity as intrinsic factor and plasma damage and moisture absorption as extrinsic factors on thermo-mechanical instability of PLK in advanced Cu/PLK interconnects. For this purpose, a ball indentation creep test technique was developed to examine the thermal and mechanical instability of PLK at relevant load and temperature conditions in the interconnect structure.

Our exploration with the ball indentation creep test found that PLK films plastically deforms with time, indicating that viscoplastic deformation does occur under relevant conditions of PLK processing. On the basis of the results that the increase of the indentation depth with time shows more noticeable difference in PLK films with

higher porosity, plasma exposure, and moisture absorption, it is our belief that PLK stability is greatly affected by porosity, plasma damage and moisture.

Viscous flow was found to be mechanism for the viscoplastic deformation at the temperature and load of real PLK integration processing. This finding was obtained from the facts that the kinetics of the indentation creep fit very well with the viscous flow model and the extracted stress exponent is close to unity. Based on the results of temperature dependence in all PLK films, the activation energy(~1.5eV) of the viscosity back calculated from the experimental value of the kinetics was found to be much small than that of a pure glass (> 4eV). This suggests that the viscous flow of PLK is controlled by chemical reaction happening in PLK matrix. The FT-IR measurement for the examination of chemical bond reconfiguration shows that the intensity of Si-OH bonds increases with the flow while that of Si-O-Si, $-CH_X$ and $Si-CH_3$ bonds decreases, indicating that chemical reactions are involved in the deformation process.

From these findings, it is concluded that the viscoplastic deformation in PLK films proceeds mainly by the viscous flow but is assisted by chemical reaction that reconfigure bonding configuration in the network (Si-OH or Si-H).

In addition, the effect of integration process steps on the PLK stability with a variety of integration processes such as plasma etching/ashing, chemical-mechanical polishing (CMP) and Ultra-Violet (UV) irradiation cure processes has been investigated. With the use of the ball indentation creep test, the damage to PLK film was found to be cumulative due to the each process step and was the most pronounced when PLK films were exposed to plasma etching and ashing processes.

TABLE OF CONTENTS

ACKNOWLEDGEMENTS... ……………..iii

ABSTRACT v

LIST OF ILLUSTRATIONS..xi

LIST OF TABLES...xv

Chapter Page

1. INTRODUCTION 1

1.1 Research Motivation 1

1.2 Low-k dielectric materials in advanced microelectronics 3

1.2.1 RC time delay 3

1.2.2 Copper metallization as interconnect Metal 5

1.2.3 Low Dielectric constant materials 8

1.2.3.1 How to lower a dielectric constant value.................9

1.2.3.2 Fabrication of Low-k Dielectrics..........................11

1.2.3.3 Types of Low-k Dielectrics 13

1.3 Integration Challenges and reliability issues of PLK 18

1.3.1 Integration of PLK in Damascene processes 18

1.3.2 Integration challenges and reliability issues of PLK 22

1.3.2.1 Mechanical stability...22

1.3.2.2 Thermal stability...23

1.3.2.3 Chemical stability and Moisture contamination 23

1.3.2.4 Plasma Treatment induced damage 25

1.4 Thermo-Mechanical instability in Cu/Low-k interconnect 26

1.5 Research objectives and outline of the thesis 29

2. BACKGROUND: INDENTATION CREEP TEST.....................................32

2.1 The basic idea of the indentation test 32

2.2 Time dependent Plasticity: Creep 33

2.2.1 Creep Curve 34

2.2.2 Creep Characteristics 36

2.2.3 Mechanisms of Creep in Materials 38

2.3 Indentation Creep Test..41

2.3.1 Constitutive equations and Ball Indentation Creep process 42

2.3.2 Analysis of indentation creep test with a ball indenter......50

2.3.3 Indentation Creep in glassy materials...............................51

2.3.3.1 Viscosity of glasses..52

2.3.3.2 Investigation of plasticity of glasses by determination of viscosity using a ball indenter 54

3. EXPERIMENTAL and CHARACTERIZATION 58

3.1 Experimental samples 58

3.2 Equipment of Indentation Creep Test..61

3.3 Procedure 63

3.4 Sample Characterization 65

3.4.1 Optical (3D) surface Profilometer 65

3.4.1.1 Working Principle 66

3.4.1.2 Measurement of indentation depth in PLK............68

3.4.2 Fourier Transform Infrared Spectroscopy (FT-IR)............69

3.4.2.1 General Introduction and Fundamentals................69

3.4.2.2 FT-IR Techniques 72

3.4.2.3 FTIR Spectrum in PLK film 75

4. STUDY OF THERMO-MECHANICAL INSTABILITY OF POROUS LOW-K DIELECTRICS 78

4.1 Introduction...78

4.2 Experimental...81

4.3 Results and Discussions 83

4.3.1 Observation of viscoplastic deformation in PLK films 83

4.3.2 Kinetics model for the ball indentation creep test 85

4.3.3 Stress Dependence 88

4.3.4 Temperature Dependence 91

4.3.5 FT-IR Spectroscopy analysis 96

4.3.6 Proposed Mechanisms 101

4.4 Summary...107

5. EFFECT OF MOISTURE ABSORPTION AND INTEGRATION PROCESS STEPS ON THERMO-MECHANICAL INSTABILITY OF PLK..............109

5.1 Introduction...109

5.2 Experimental...111

5.3 Results and Discussions....114

5.3.1 Effect of moisture adsorption 114

5.3.2 Observation of viscoplastic deformation of PLK in moisture ambient 116

5.3.3 Kinetics of PLK exposed to moisture for the ball

indentation creep test 118

5.3.4 Temperature Dependence 119

5.3.4 The influence of integration process on thermo-mechanical PLK stability....122

5.4 Summary....125

6. CONCLUSIONS AND FUTURE WORKS....126

6.1 Conclusions....126

6.1.1 Detection of viscoplastic deformation in PLK 126

6.1.2 Study on viscoplasticity mechanism in PLK....127

6.1.3 Effect of contributing factors including porosity, plasma and moisture on thermo-mechanical instability of PLK...128

6.2 Future Works 130

6.2.1 Influence of Process Conditions on the Thermo-Mechanical Stability of PLK....130

6.2.1 Exploration of repair bond damage in PLK and strengthen resistance of PLK against viscoplasticity 131

REFERENCES 132

BIOGRAPHICAL INFORMATION....149

LIST OF ILLUSTRATIONS

Figure Page

1.1 The intrinsic gate delay and the interconnect (RC) delay as a function of feature size 5

1.2 (a) Scanning Electron Microscopy (SEM) images of interconnect architecture with six levels of Cu wires and vias, W contacts/local interconnects, and SiO_2 ILD and (b) without ILD 9

1.3 Schematic illustration of Si based dielectric material (a) A chemical structure of SSQ dielectrics: Cage structure (b) Ladder structure and (c) SiCOH 17

1.4 Schematic process flows to form a dual damascene structure with two metal Layers (M1,M2) and a via level between them 19

1.5 Cross-section of Hierarchical Cu/PLK interconnect structure 21

1.6 SEM image of Intel 32 nm interconnects from Metal-1 to Metal-8 21

1.7 SEM images showing (a) crack observed following CMP, (b) delamination by thermal stress developed from CTE mismatch during annealing 24

1.8 Cross-sectional TEM micrographs showing the Cu geometry and pore distribution annealed at 400°C. Note the elongation of Cu in the vertical direction and contraction in the horizontal direction with annealing, indicating time dependent plastic deformation at 400°C 28

2.1 Typical Creep Curve showing the 3 stages of Creep 35

2.2 Effect of applied stress on creep curves at constant temperature using tensile test .38

2.3 Scheme of the indentation creep under constant load (F) with a ball indenter....................44

2.4 Schematic depiction of how depth–time plots, obtained under constant load, can be used to determine values for the stress exponent, n using the ball indentation creep test. Pressure stress and strain rate are found using Equation (2.4) and (2.7) 49

3.1 Diagram of networked structure of cured SiCOH film deposited from a matrix precursor only 59

3.2 Porous cage networked structure of annealed SiCOH film deposited from a matrix precursor with organic precursor 59

3.3 Schematic illustration of PLK blanket film structure 60

3.4 (a) A picture of indentation testing setup and (b) a schematic illustration of the ball indentation creep apparatus 62

3.5 (a) Finite Element Mesh for ball indentation and (b) The maximum pressure stress on PLK with variation in ball loads at the elevated temperature (400˚C). The load is determined to produce 100 MPa ~ 200 MPa stress at PLK, which is actual stress level developed at real process 64

3.6 A schematic illustration of the working principle of the interferometric based WYKO® optical profiler 66

3.7 Optical microscope images showing the residual indentation regions in PLK films tested under 60gf at 400oC for 8 hours 68

3.8 (a) An observation of the indented area using the optical surface, (b) a 3D image showing the topography and the hollow area in the indented area (c) a cross section line profile of the same indent along the red dash line as in Figure 3.8 (a) 70

3.9 Schematic view of an FTIR system 71

3.10 A multiple reflection ATR system 73

3.11 A FTIR-ATR detector positioning on the indented and un-indented area on PLK films 75

3.12 Typical FTIR spectrum for PLK film showing various functional groups at specific wavenumbers 76

4.1 Surface topography images showing an indentation mark on a) as-prepared k=2.4, b) as-prepared k=2.2, c) the same film as b) but exposed to plasma. The indentation test is done at 400oC under 60g load on 20mm Alumina ball indenter 84

4.2 Indentation depth of films measured with time at 400C under 60g load, demonstrating (a) effect of porosity and (b) plasma damage on the viscoplasticity of PLK films....86

4.3 A plot showing $h^{3/2}$ vs. time of the data shown in Figure 4.2....................................87

4.4 A plot showing the determination of stress exponent from the indentation creep data for 3 different PLK films 90

4.5 Surface topography images showing variations in the indentation depth as a function of temperature for three different PLK films. The indentation test is done at the constant load of 60g for 8 hours 93

4.6 A plot showing the viscosity as a function of temperature for 3 different PLK films..94

4.7 FTIR spectra of A PLK film showing the difference in chemical bonds for the unindented and indented region after indentation creep test over the range 4000-750 cm^{-1} 97

4.8 Magnified FTIR spectra in Figure 4.7: (a) shows the Si-OH/H_2O area (3200-3700cm^{-1}) and CHx area (2850-3000cm^{-1}) and (b) exhibits the Si-CH_3 area (1090-1280 cm^{-1}) and Si-O-Si area (970–1250cm^{-1}) obtained from unindented and indented regions after indentation creep test 99

4.9 FTIR spectra of A PLK film showing the difference in chemical bonds as a function of time at the indented region after indentation creep test over the range 4000-750 cm^{-1} 101

4.10 Magnified FTIR spectra in Figure 4.9: (a) shows the Si-OH/H_2O area (3200-3700cm^{-1}) and CHx area (2850-3000cm^{-1}) and (b) exhibits the Si-CH_3 area (1090-1280 cm^{-1}) and Si-O-Si area (970–1250cm^{-1}) collected from the indented regions, respectively 102

4.11 Schematic diagram showing the proposed mechanism leading to viscoplasticity of PLK film 106

5.1 Optical microscope images showing the residual indentation regions in PLK films tested with different degassing processes under 60gf at 300°C for 4 hours 113

5.2 Optic and surface topography images presenting indentation regions with the absence/presence of moisture for B film and C film tested at 300°C with 60g loading for 8 hours, respectively 115

5.3 A plot showing indentation depth of B and C films with the absence/presence of moisture measured from the result of Figure 5.2...115

5.4 Surface topography images showing the residual indentation regions in (a) B film and (b) D film at 400°C under 60gf as a function of time......117

5.5 Plots showing the comparison of indentation depth as a function of time for B film without moisture and D film with moisture, respectively 117

5.6 Plots showing the indentation depth with a power of 3/2 as a function of time for B film without moisture and D film with moisture, respectively......119

5.7 Surface topography images showing variations in the indentation depth as a function of temperature for (a) B and (b) D films. The indentation test is done at the constant load of 60g for 8 hours......121

5.8 Viscosity in PLK film of D film exposed to moisture as a function of inverse temperature, showing Arrhenius-type behavior 121

5.9 Mean indentation depth in PLK films exposed to various integration processes after indentation testing at 400°C under 60gf for 4 hours......123

LIST OF TABLES

Table Page

1.1 Candidates metals for advanced interconnects 7

1.2 The International Technology Roadmap for Semiconductors 8

1.3 Candidates for Low-k dielectrics 14

3.1 Properties of porous SiCOH films with variation in porosity, plasma exposure and moisture absorption 61

3.2 FTIR assignment of the structures in low-k materials 77

5.1 Summary of the degree of deformation with different degassing procedures under 60gf at 300°C for 4 hours 113

5.2 Experimental splits of integration process steps 113

5.2 Mean indentation depth depending on the variations of process history 123

CHAPTER 1

INTRODUCTION

1.1 Research Motivation

With recent decision to replace Al/SiO_2 by Cu/porous low-k in the integrated circuit IC chips and package, the implementation of porous low-k dielectric (PLK) in Cu interconnect structures has become one of the key challenges in the microelectronics industry. The incorporation of PLK is necessary to preclude the interconnect RC delay from becoming the performance-limiting factor in the back-end-of-the-line (BEOL) interconnect, but has been suspended due to the reliability failure of interconnects integrated with PLK. While there is significant effort and continued concern for investigations on reliability failure mechanisms caused by characteristics of porous low-k dielectrics itself as well as the various integration processes such as annealing, plasma treatment for a photoresist removal ash process and chemical-mechanical polishing (CMP), where PLK can be exposed to chemicals and moisture, unfortunately, little is understood with respect to the relevance between intrinsic properties of PLK and failure mechanisms. During manufacturing process of interconnect structure, the dielectric constant of porous low-k material is determined by the introduction of pores into the already existing inter-layer material. Accordingly, it is a common belief that porous low-k dielectric layer is not only thermally stable, but also not deformed during the interconnect processing due to the stability of cross-linked bonding networks. However,

it is found from our previous study that the pores are not necessary stable based on the observations of diffusivity change of tracer ions after thermal annealing of interconnects with voltammetry technique, yet the exact mechanism of thermo-mechanical instability of PLK dielectrics behind such behaviors are not well understood. Therefore, it is essential to verify the existence of thermal and mechanical instability of PLK and understand the related mechanism behind the instability of PLK by the variation of PLK porosity, composition, absence/presence of plasma damage, and moisture and process conditions such as annealing with the temperature of around 400˚C and load conditions in real interconnects.

In this study, thermo-mechanical instability of PLK has been investigated. The primary focus of this study is to identify the mechanism leading to thermal and mechanical instability of porous low-k observed in Cu/PLK interconnects. For this, we have developed an indentation creep test technique that is designed to examine the thermal and mechanical instability of PLK film at relevant load and temperature conditions in the interconnect structure. Through this indentation creep test, viscoplastic deformation (Time-Dependent Plastic deformation) behavior of PLK has been explored, and the effect of porosity as an intrinsic factor and plasma damaged and moisture as extrinsic factors were investigated. Furthermore, in order to reveal the involved mechanism for viscoplastic deformation in PLK, the indentation creep testings at various temperature (300˚C~400˚C) and load (40gf ~100gf) conditions have been conducted. Based on the result of temperature and load dependence in PLK film, viscoplastic deformation mechanism of PLK was revealed.

Furthermore, the influence of integration process steps on thermo-mechanical instability of PLK was investigated. One of the obstacles in implementing PLK materials in a dual damascene structure is the degradation in its dielectric properties due to the various integration processes such as plasma etching/ashing, chemical-mechanical polishing and cure processes. While it has been well known that the introduction of porosity into the existing low-k film to generate further low-k makes the PLK sensitive to be damaged by the integration processes due to the lowering the density and mechanical strength of PLK films, there is still controversial issues that how much each process steps produces integration damage and little is known if cumulative damage occurs with individual process. Therefore, the purpose of this investigation is to examine the impact of each integration process steps to PLK stability. By using the ball indentation creep test, the damage to PLK stability was quantified with integration process steps and was found to be cumulative. Also, the most obstacle process induced damage for PLK stability was revealed. With the obtained results and understandings in this study, several damage repair methods have been proposed.

In this chapter, we will briefly review the technology of modern Cu/PLK interconnects and the integration challenges and reliability issues in relation to PLK.

1.2 Low-k dielectric materials in advanced microelectronics

1.2.1 RC time delay

The down-scaling of the device dimensions in integrated circuits (IC) leads to faster signal propagation across the transistor channels, resulting in the decrease of the intrinsic gate delay. However, more transistors have to be combined together due to the

increase of complexity in the structure of ICs. This compels the overall interconnect length to increase and makes cross section in IC to become smaller, which will lead to the increase of parasitic capacitance between adjacent wires as the distance between them decreases. These scaling effects have caused the signal propagation to be delayed through the intrinsic gate delay and interconnect delay. In the past, the transistor gate delay, which is proportional to the size of the transistor, limited the speed of logic devices. As shown in Figure 1.1, however, as the minimum device dimensions reduce beyond 0.18 μm, the increase in the interconnect signal delay, crosstalk noise, and power dissipation of the interconnect structure become performance limiting factors for ULSI of integrated circuits [1]. The interconnect delay can be estimated by the *RC* delay which is — the product of interconnect line resistance, *R*, and the parasitic capacitance coupling the interconnect to neighboring lines and underlying Si substrate, *C*.

The RC delay is given by:

$$RC \approx \frac{\rho}{t_M} \frac{L^2 \varepsilon_{ILD}}{t_{ILD}} \tag{1.1}$$

where ρ, L and t_M are the metal resistivity, the line length and thickness of the interconnect, and ε_{ILD} is usually cited in terms of the dielectric constant, k, defined as $\varepsilon/\varepsilon_0$ where ε_0 is the permittivity of free space and t_{ILD} is the thickness of interlayer dielectric (ILD)[2]. Equation (1.1) suggests that the decrease in feature size can lead to a sharp increase in the RC delay time, which for devices smaller than 250 nm, control

the overall on-chip cycle time. Consequently, by the inspection of the equation, in order to increase device speed (or reduce RC delay), it is obvious that the lower resistivity Cu

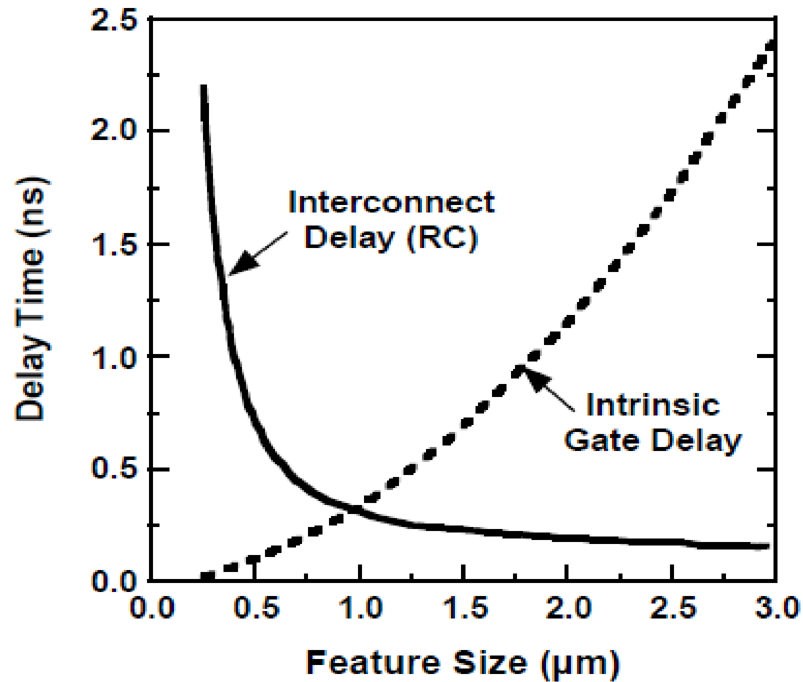

Figure 1.1 The intrinsic gate delay and the interconnect (RC) delay as a function of feature size [1].

is replacing Al, and the current ILD, SiO_2 is replaced by other dielectrics with a lower dielectric constant.

1.2.2 Copper metallization as interconnect Metal

Improvement of performance of the on-chip IC interconnection requires interconnect materials with lower resistivity. Aluminum (Al) and Al alloys, which is doped with about 1% copper (Cu) to improve its resistance *electromigration* (the transport of material caused by the momentum exchange between electrical charge carriers and diffusing metal atoms) have been used as traditional interconnect wires for

more than 30 years. Since then, several conductors have been aggressively studied as possible replacements for Al alloys. Only three elements exhibit lower resistivity than Al, namely gold (Au), silver (Ag), and copper (Cu). The material properties of these elements are listed in Table 1-1[3-6]. Among them, Au has the highest resistivity. Although Ag has the lowest resistivity, it has poor resistance against electromigration. Cu shows an excellent combination of good electrical and mechanical properties, offering a resistivity 40% better than that of Al. The self-diffusivity of Cu is also the lowest, compared to the four elements, resulting in improved reliability. At the same time, since the activation energies for grain boundary diffusion scale proportionally with the melting temperature [7], Cu with a higher melting point is less sensitive to electromigration, compared to Al [8-15]. Based on these comparisons, the use of Cu wiring thus enables higher IC chip speed, strengthens electromigration lifetime reliability, decreases power consumption, and eventually reduces manufacturing cost for IC chip [16]. In 1997, IBM and Motorola made their intensions known to adopt Cu as a new metal conductor in their CMOS logic technologies as seen in Figure 1.2(a) and (b)[17-18]. Since then, the performance improvement with Cu interconnect was demonstrated in high-speed microprocessors [19]. Semiconductor manufacturer worldwide have replaced Al by Cu as the new interconnect metal. To be used successfully as a new metal conductor in the IC chips, however, many challenges related to Cu integration need to be concerned, which are patterning Cu lines and preventing potential device contamination. These issues are overcome respectively by

using the Damascene process and by cladding the Cu interconnects with diffusion barriers, which will be discussed in Chapter 1.3.

Table 1.1 Candidates metals for advanced interconnects [3-6]

Properties		Al	Ag	Au	Cu
Resistivity (uΩ-cm)		2.66	1.59	2.35	1.67
Melting point (^{o}C)		660	962	1064	1084
Self- Diffusivity at 100ºC (cm^2/s)		$2.1x10^{-20}$	$1.1x10^{-26}$	$2.2x10^{-27}$	$2.1x10^{-30}$
Electromigration resistance		Low	Very low	High	high
Availability of deposition and etching process	Sputtering	o	o	o	o
	evaporation	o	o	o	o
	CVD	o	?	o	o
	plating	?	o	o	o
	Dry etching	o	o	o	o
	Wet etching	o	?	?	?

1.2.3 Low Dielectric constant materials

The technological solution for *RC* delay reduction is to replace the existing conductors and insulators that comprise the interconnect system with lower resistivity and the dielectric constant materials [20]. While Cu has replaced Al as the mainstream conductor material to reduce the resistivity, the introduction of low-k dielectrics in Cu interconnect structures has become one of the key challenges in the microelectronics industry. As seen in Table 1.2, the International Roadmap for Semiconductors (ITRS) suggests that, the interlayer dielectrics (ILD) with k lower than 2.4 are required to respond to the scaling down of device dimension beyond 32-nm technology node [21].

Accordingly, significant efforts have been made to reduce the dielectric constant of ILD, but the implementation of low-k dielectrics has been suspended due to the integration technical issues, as well as the reliability failure of interconnects in microelectronic community.

Table1.2 the International Technology Roadmap for Semiconductors [21]

Year of Production	2009	2010	2011	2012	2013	2014	2015
Technology node (nm)	52	45	40	36	32	28	25
Metal effective resistance (uΩ-cm)	3.70	4.08	4.48	5.00	5.63	6.00	6.61
ILD k_{bulk}	2.5~2.8	2.3~2.6	2.3~2.6	2.3~2.6	2.1~2.4	2.1~2.4	2.1~2.4
Interconnect RC delay (ps) for 1mm Cu metal 1 wire	1,439	2,100	3,234	5,068	7,457	10,059	14,474

1.2.3.1 How to lower a dielectric constant value

The reduction of the dielectric constants of ILD is achieved through the incorporation of atoms and bonds that have a lower polarizability, or else lowering the density of atoms and bonds in the material. In the case of the first effect, there are several mechanisms related to the polarization phenomenon that must be minimized in reducing the dielectric constant [22]. Among them, electronic polarization, atomic polarization, and orientational polarization are major components to be considered in dielectrics.

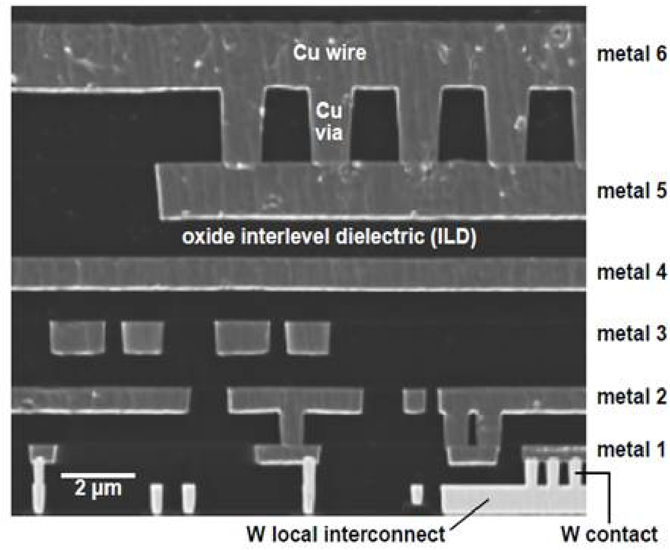

(a) interconnect with Cu wires and SiO_2 ILD

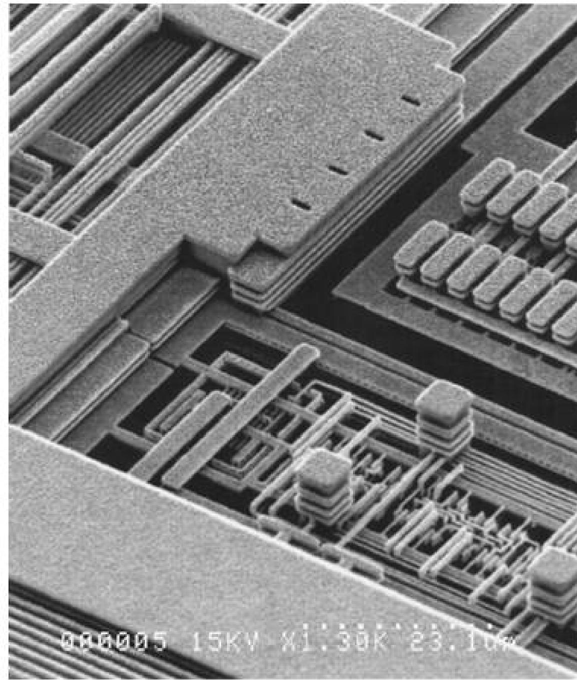

(b) interconnect with Cu wires without ILD

Figure 1.2(a) Scanning Electron Microscopy (SEM) images of interconnect architecture with six levels of Cu wires and vias, W contacts/local interconnects, and SiO_2 ILD and (b) without ILD [17-18].

Electronic polarization occurs when there is a displacement of the electronic cloud bound around the nuclei to electrical field. Ionic polarization occurs when there is a displacement of adjacent positive and negative ions relative to each other under the influence of an applied electric field. The orientation polarization results from permanent electric dipole moments. Depending on the signal frequency of the applied electrical field, the relative dominance of each polarization mechanism varies. The latter two polarization mechanisms contribute to polarization and are important at lower frequencies ($<10^{13}$Hz), while the electronic polarization dominates in dielectric permittivity at higher frequencies ($\sim10^{15}$Hz) [23]. At typical device operating frequencies, currently $<10^{9}$Hz, all three polarization mechanisms are important in the dielectric constant and should be minimized for optimum performance [24].

Among all the possible approaches for decreasing the dielectric constant of ILD, the most effective approaches is to reduce the volume density because the reduction of density indicates the decrease of the total number of electronic and ionic dipoles per unit volume. The density can be reduced by using lighter atoms such as C and H atoms and/or by introducing more free space around the atoms. Accordingly, introduction of pores into the existing SiO_2 is a natural approach to increase the free space and decrease the ILD density. There are two methods for adding pores into existing low-k materials-constitutive and subtractive [23,24]. The constitutive method for fabricating low-k materials is the porogenless structural approach. The porosity in the film can be obtained by using particular precursors that contain molecular pores when the film cross-links during annealing, leaving behind pores [25-29]. In the subtractive method, a

skeleton precursor mixed with a porogen precursor is introduced by using the PECVD. During curing of the dielectric, the porogen precursors burn out of the dielectric, leaving nano-sized pores[30]. The effect of porosity on dielectric constant can be predicted by using the Bruggeman effective medium approximation model [31, 32]:

$$f_1 \frac{k_1 - k_e}{k_1 + 2k_e} + f_2 \frac{k_2 - k_e}{k_2 + 2k_e} = 0 \qquad (1.2)$$

where $f_{1,2}$ represents the fraction of the two components, $k_{1,2}$ the dielectric constant of the components, and k_e is the effective dielectric constant of the material. The model assumes two components to the film: the solid dielectric material and pores. Since the dielectric constant of free space is unit, the introduction of pores reduces the dielectric constant by lowering the density of the ILD. However, the drawback of incorporating pores in a material is to reduce the mechanical strength and degrade thermal properties, which leading to potential reliability issues as well as significant integration challenges in advanced Cu/PLK interconnects. Such reliability issues and integration challenges will be reviewed in more details in section 1.3.

1.2.3.2 Fabrication of Low-k Dielectrics

Low-k or porous low-k films can be categorized to two, based on the methods to obtain these materials. The two methods are spin-on and chemical vapor deposition (CVD). Both the deposition techniques have their advantages and disadvantages and there is very little agreement that which of the two techniques is best suitable for future technology.

For the spin-on deposition, the dielectric precursors mainly consist of organic or inorganic polymer matrixes mixed with solvent along with porogen precursors to make porous films. There are several steps involved in spin coating: first the substrate on which the low-k film has to be coated is placed on the spinner and the precursors are dispensed onto the center of the substrate at room temperature and ambient pressure. The second step is to rotate the spinner to produce a uniform distribution of material on the substrate by the creation of centrifugal force [23]. The thickness and uniformity of the coated film are dependent on the viscosity of the film, the spinning rate and the evaporation rate of the solvent. The coating is subsequently cured to at temperatures typically around 200 ºC to remove the solvent and induce polymerization and cross-linking of the precursors. Lastly, heating to temperatures typically around 400 ºC, or using e-beam technology is required to remove organics and porogens. This baking and curing steps result in the final cross-linking of polymer chains which gives desirable mechanical strength to the film.

Chemical vapor deposition has widely gained importance in depositing thin films [53]. The CVD is a process in which chemical components from a gas phase absorb and react on the surface of substrate in a vacuum environment. There are several methods of CVD deposition such as APCVD, done at atmospheric pressure, LPCVD, done at low pressure and PECVD which is a plasma-enhanced CVD process. Recently, most of the low-k films have been deposited by a subtractive PECVD technique. In the subtractive technique, precursor materials such as diethoxymethylsilane(DEMS), octamethylcy-clotetrasiloxane (OMCTS) and tetramethylcyclotetrasiloxane (TMCTS)

can be introduced into the PECVD reactor and deposited on the substrate. During the deposition of the precursor, a volatile organic species or porogen material is mixed with the precursor, creating a dual phase material like SiCOH-CH*x* material. The organic species (the labile CH*x* fraction) or porogen is removed by either annealing the film for four hours at temperatures below 400ºC or annealing it with energetic species such as electrons(EB cure) or photons(UV cure) at 350-400ºC. By the removal of the porogen during curing process, the decomposed precursor forms a porous low-k film (pSiCOH) with a silicon dioxide skeleton and terminating organic groups, consisting of hydrogen or methyl groups (-CH_3) [30]. Such materials are called porous low-k dielectrics (PLK), and hence make it possible to further reduce dielectric constant of low-k materials by the reduction in film density due to the fact that the methyl group is substituted for oxygen in SiO_2.

1.2.3.3 Types of Low-k Dielectrics

Low-k materials can be categorized from different perspectives. The most well-known approach is based on basic compositional and structural properties [33]. Also, low-k materials can be grouped with the method of pore generation as stated in previous section: constitutive porous material and subtractive porous material [23,24], or according to the method of film deposition such as Chemical Vapor Deposition(CVD) or Spin-on Deposition. Table 1.3 summarizes recognized dielectric material candidates for ILD integration [34,35]. The first generation of low-k materials were fluorinated silicates glasses (FSG), in which the Si-O bonds are replaced with less polarizable Si-F bonds. The disadvantage of these FSGs has a limit of k ~3.6 due to chemical instability

when fluorine loadings exceed a certain percentage. However, FSG has been the material of choice for both the 180 and the 130 nm technology nodes [36–40].

Table1.3 Candidates for Low-k dielectrics [34,35]

Materials	K value	Deposition Methods
SiO_2	3.9 – 4.2	CVD
Fluorosilicate glass (FSG)	3.2 – 4.0	CVD
Diamond-like Carbon (DLC)	2.7 – 3.4	CVD
Fluorinated DLC	2.4 – 2.8	CVD
Black Diamond ™ (SiCOH)	2.7 – 3.3	CVD
Parylene-F	2.4 – 2.5	CVD
Parylene-N	2.7	CVD
Hydrogen silsesquioxane(HSQ)	2.9 – 3.2	Spin-on
Methyl silsesquioxane(MSQ)	2.6 – 2.8	Spin-on
B-staged Polymers (CYCLOTENE and SiLK)	2.6 – 2.7	Spin-on
Fluorinated Polyimides	2.5 – 2.9	Spin-on
Polyimides	3.1 – 3.4	Spin-on
Poly(arylene ether)(PAE)	2.6 – 2.8	Spin-on
PTFE	1.9	Spin-on
Porous HSQ	1.7 – 2.2	Spin-on
Porous SiLK	1.5 – 2.0	Spin-on
Porous MSQ	1.8 – 2.2	Spin-on
Porous PAE	1.8 – 2.2	Spin-on
Aerogels/Xerogels(Porous Silica)	1.1 – 2.2	Spin-on
Air Gaps	1.0	?

The next generation of low-k ILD materials has been organosilicate glasses (OSG) or carbon-doped low-k materials, termed as SiCOH. In this material, part of oxygen atoms in SiO_2 structure is replaced by $-CH_x$ organic molecules, resulting in the terminal Si-H or Si-R (where R is an organic group such as CH_3) into a silica network. Since the Si-R or Si-C bonds have less polarizability than the Si-O bond and a lower density of SiCOH compared to SiO_2, OSGs have a lower k ~2.7-3.0 than SiO_2 [41,42].

OSGs use silsesquioxane(SSQ) precursors, which have organic- inorganic polymers with the empirical formula $(RSiO_{3/2})_n$ [43,44]. The lower dielectric constant is also attributed to the three factors : 1) the typical cage structures with more free space as shown in Figure 1.3(a); 2) the organic molecules which provide a lower density matrix material; and, 3) the lower polarizability of the Si–R bond in comparison with the Si-O bond in SiO_2[45-48]. The most common SSQ based materials are Hydrogen silsesquioxane (HSQ) which results when R=H, and methyl silsesquioxane (MSQ) when $R=CH_3$. The main difference between HSQ and MSQ is that MSQ is thermally stable even at temperatures above 400˚C, but HSQ is not thermally stable at a given temperature, >400˚C due to the oxidation of Si-H bonds to Si-O [49]. In addition, MSQ materials have a lower dielectric constant as compared to HSQ because of the larger size of the CH_3 group and lower polarizability of the Si–CH_3 bond as compared to Si–H[23]. The chemical structures of HSQ and MSQ are depicted in Figure 1.3(a) and (b) [53]. Most of the initial candidate low-*k* materials, organic polymers or hybrids, OSG, were prepared by spin-on techniques. In the 90nm node technology, however, OSGs by using Chemical Vapor Deposition (CVD) have become the main candidates as ILD materials, and have been typically deposited by plasma enhanced CVD (PECVD). For pure thermal CVD processes, the film densities are lower than desired and films often contain substantial amounts of moisture and/or SiOH(Silianol), which require additional film treatment or additional depositions [50-52]. Such being case, common OSGs such as Aurora™ (k = 2.9, ASM), Coral™ (k = 2.85, Novellus), and Black Diamond™ (k = 2.0-3.0, Applied Materials) have been deposited by plasma enhanced CVD (PECVD)

processes, which have become increasingly popular. The elementary units of these films are presented in Figure 1.3(c) [23].

Also, several organic polymer low-k materials have been developed and reported as ILD materials [54-56]. Some of them are deposited by CVD method including parylene-N, parylene-F, polynaphthalene and polytetrafluorethylene (Teflon™). Others are deposited by spin-on method using polyarylene ethers, derivatives of cyclobutane, polynorbornenes, amorphous Teflon™, and phase-separated inorganic-organic hybrids [57]. Polymers include fluorinated polymers, such as PTFE (k = 2.2), and aromatic polymers, such as SiLK™ (k = 2.65, Dow Chemicals). Due to the low polarizability of the bonds and the light atoms, these materials have an inherently low k. However, these types of materials generally suffer from low thermal developed for SiO_2 based dielectrics. Moreover, it is difficult to further decrease their k-value by only changing the chemical structure and/or chemical composition.

In order to achieve dielectric constants with $K < 2.5$, two-phase film deposition techniques have been developed whereby a labile or unstable organic phase is removed to leave a discrete pore structure in the existing backbone or skeleton phase. A variety of chemical precursors such as tetramethylcyclotetrasiloxane (TMCTS), octamethylcyclotetrasiloxane (OMCTS), decamethylcyclopentasiloxane (DMCPS), and diethoxymethylsilane (DEMS) can be used for preparing OSG thin films by PECVD or by sol-gel chemistry [58-65]. So far, only OSG films (or SiCOH films) prepared by PECVD have been successfully implemented in volume production and widely used in the new generations of Cu interconnects [66, 67]. In comparison to PECVD, integration

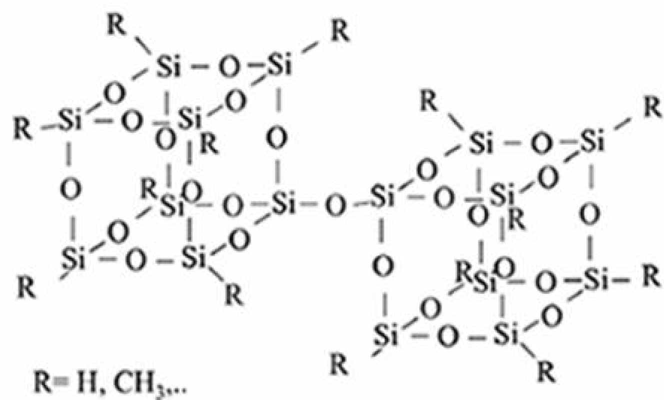

(a) SSQ dielectrics: Cage structure

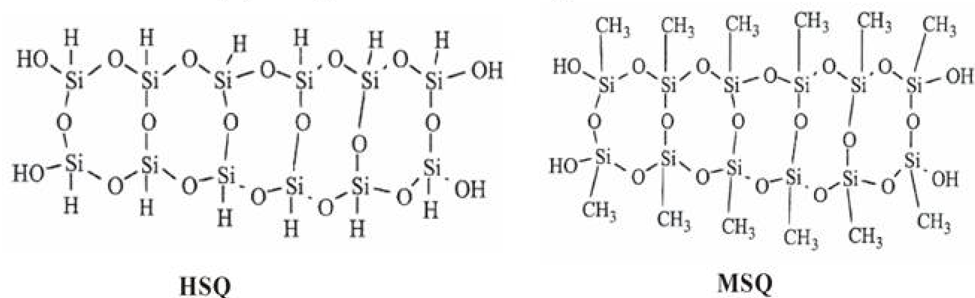

(b) SSQ dielectrics: ladder structure

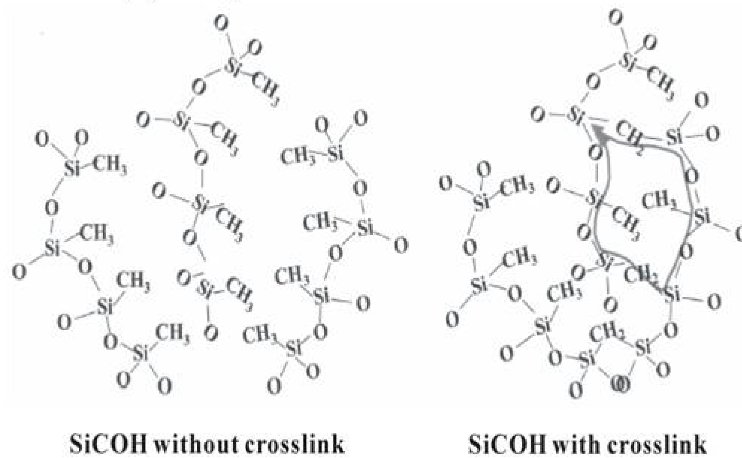

(c) SiCOH

Figure 1.3 Schematic illustration of Si based dielectric material (a) A chemical structure of SSQ dielectrics: Cage structure (b) Ladder structure and (c) SiCOH [53].

of OSG films synthesized using spin-on dielectrics has proved to be challenging because these materials have inferior mechanical and thermal reliability at equivalent dielectric constant, and need to be further improved for new Cu/PLK interconnect. While porous OSG low-k materials are also widely regarded as the most promising low-k dielectrics, it is still required to further lower the dielectric constant for future integrated circuit technologies. Accordingly, implementation of porous OSG low-k dielectrics becomes increasingly more difficult with decreasing device scale. In the next section, we will briefly review the integration challenges and reliability issues relative to porous low-k materials.

1.3 Integration Challenges and reliability issues of Porous Low-k dielectrics

1.3.1 Integration of PLK in Damascene processes

There are a number of technical challenges associated with the integration of porous low-k dielectrics with Cu metallization. In the past, Al interconnect was formed with a subtractive patterning technique using reactive ion etching (RIE). Aluminum is deposited as a blanket film, patterned using photoresist, and then unwanted portion of Al is etched away. A dielectric material is then deposited to fill the openings between the exposed isolated wires. For Cu interconnects, the subtractive patterning technology is not applicable due to the fact that Cu is lacking of volatile reactive by-products at low temperature and thus acceptable etching rate cannot be achieved [68, 69]. Instead, Cu dual damascene process has been developed and employed as manufacturing process as shown in Figure 1.4 [70, 71]: A dielectric film is first deposited on a substrate and patterned and etched, leaving holes termed as trenches or vias, by subsequent litho/etch

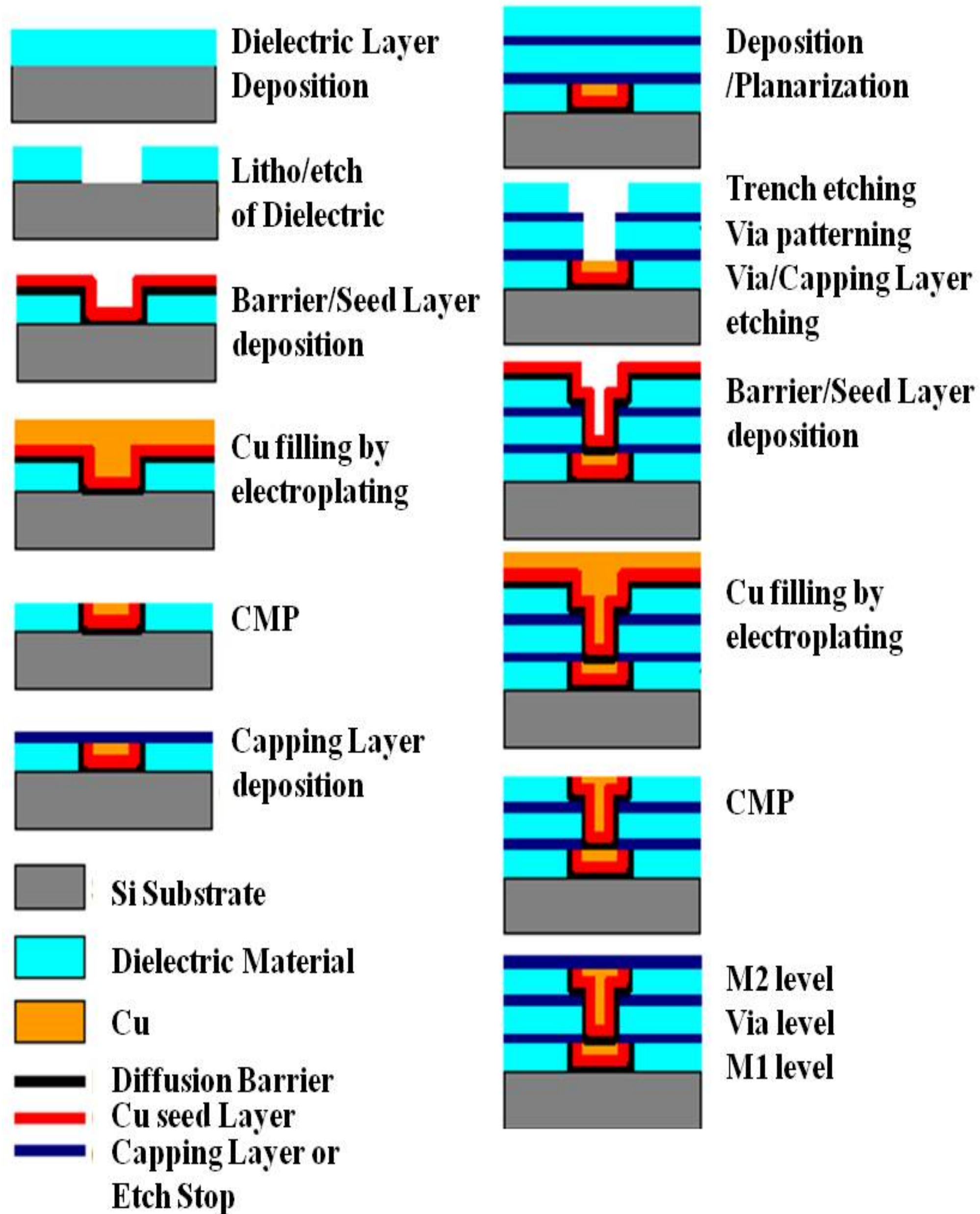

Figure 1.4 Schematic process flows to form a dual damascene structure with two metal-layers (M1,M2) and a via level between them.

process, followed by diffusion barrier/seed layer deposition. Cu is filled into the holes with an electrochemical plating (ECP) technique on the seed layers and diffusion barriers. After thermal annealing of Cu, its grains begin to grow and stabilize. This is followed by chemical mechanical polishing (CMP) to remove overburden Cu and seed layers/diffusion barriers, leading to the deposition of capping layers (SiN_x or SiC_xN_y). In the single damascene process, vias and the upper metal level (*i.e.* the M2 level) are fabricated separately. In comparison, the dual damascene process achieves vias and the M2 level processing simultaneously. As a result, the common advantage of dual damascene process compared to RIE Al patterning is at the lower cost due to the reduced number of process steps by which trenches and vias are manufactured separately but filled with metals together [72]. Accordingly, the dual damascene process is preferred to the single damascene approach in multi-level interconnect structures. Figure 1.5 shows a cross-section of a typical hierarchical interconnect organization which uses Cu as conductor material [73]. In Figure 1.6, a SEM micrograph of Intel 32nm Cu/PLK interconnect structure is shown [93]. The implementation and integration of low-k dielectrics keeps being delayed due to a series of reliability challenges [74]. In order for porous low-k materials to be successfully implemented into the interconnect structure, there are a number of stringent requirements on their mechanical properties, thermal properties, chemical properties, electrical properties, and compatibility with other materials. While the incorporation of pores into the existing dielectric is effectively helpful in reducing the dielectric constant, it also causes numerous integration challenges resulting from the properties of the low-k materials associated

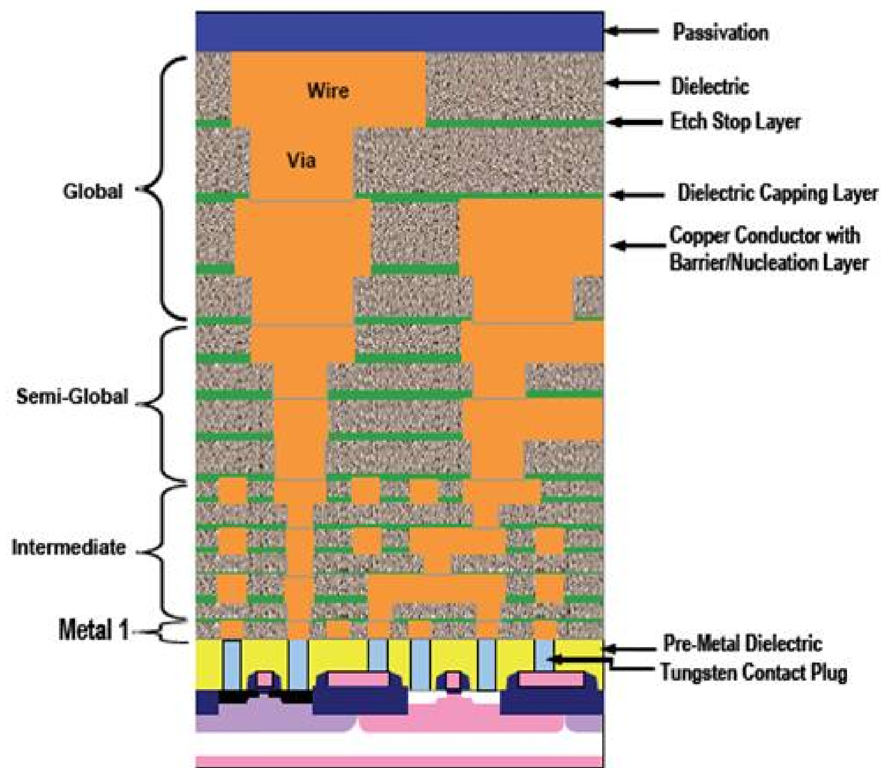

Figure 1.5 Cross-section of Hierarchical Cu/PLK interconnect structure[73].

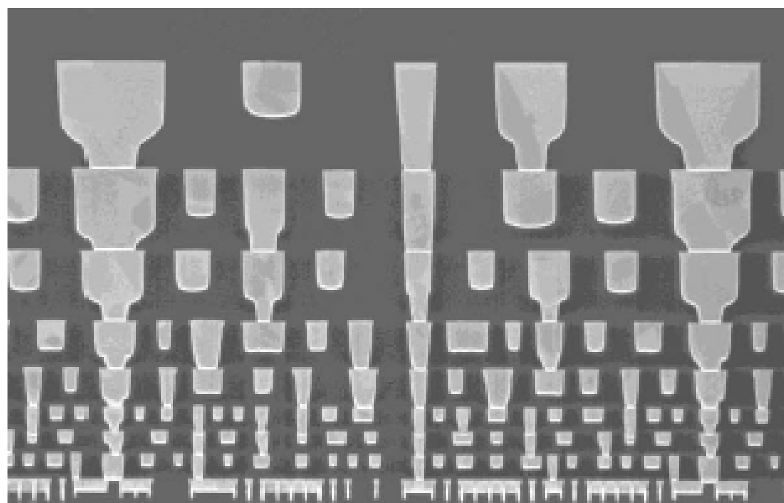

Figure 1.6 SEM image of Intel 32 nm interconnects from Metal-1 to Metal-8[93].

with the integration. In this section, we will briefly review the integration challenges related to the properties of PLK and reliability concerns in Cu/PLK interconnect.

1.3.2 Integration challenges and reliability issues of PLK

1.3.2.1Mechanical stability

There are a number of technical challenges for integration of porous low-k materials as ILDs. One concern is the mechanical stability of PLK, since the incorporation of pores into the dielectrics makes PLK films intrinsically weak [75]. The mechanical reliability of the devices with multi-layer Cu/PLK interconnect structure is profoundly linked to mechanical strength of PLK including adhesion between adjacent layers, and the ability to withstand mechanical stress during Cu Chemical Mechanical Polishing (CMP) process and assembly or packaging processes when fully processed devices are connected to the outside. The low-K materials with weak mechanical strength can be highly sensitive to damage by the CMP processes, as depicted in Figure 1.7(a)[80], because the PLK is exposed to highest mechanical stress during the CMP.

Also, the mechanical reliability can be affected by flaws or defects in the low-K material itself or at the various interfaces [76,77]. The elastic, or Young's, modulus (E) of the dielectric material is also an important material parameter as an indication of mechanical stability for low-k candidate materials. The Young's modulus of most organic and inorganic low-k candidate materials is at least an order of magnitude lower than that of standard SiO_2 films(~59GPa) [78]. As a result, sufficient mechanical strength is required for the low-k or porous low-k materials to withstand the stresses caused by the integration process, leading to a structural integrity of interconnect.

1.3.2.2Thermal stability

Most of the candidate PLK materials have poor thermal conductivity because of the introduction of pores into the matrix material. The poor thermal conductivity of the porous low-k materials severely reduces the thermal conduction in the dual-damascene stack interconnect structures, and thus makes joule heating worse and increases EM reliability concern. In addition, the dielectric materials are supposed to go through various thermal cycles around 400ºC during the manufacture of multilevel interconnect structures, which induce thermal stresses resulting from thermal expansion coefficient (CTE) mismatch between different materials in the interconnect structure. For instance, the CTE of Cu is 16.5 ppm/°C, while the CTE of many organic low-κ materials is higher than 50 ppm/°C [79]. Such large thermal stresses induced by the thermal loading in the integration processes can lead to delamination or cracks at the weak low-k interfaces as shown in Figure 1.7(b) [81]. Therefore, the candidate low-k materials must have sufficient thermal stability to withstand the elevated processing temperatures.

1.3.2.3 Chemical stability and Moisture contamination

With respect to chemical reliability issues, the pore structure makes the low-k materials prone to the penetration of moisture and other chemicals during the integration process such as CMP, plasma-based etching and ashing. It has been reported that low-k materials are vulnerable to moisture contamination even though they are usually hydrophobic [82, 57, 83-90]. In order to remove the absorbed moisture in the low-k films, annealing or curing process is usually carried out at high temperatures within the

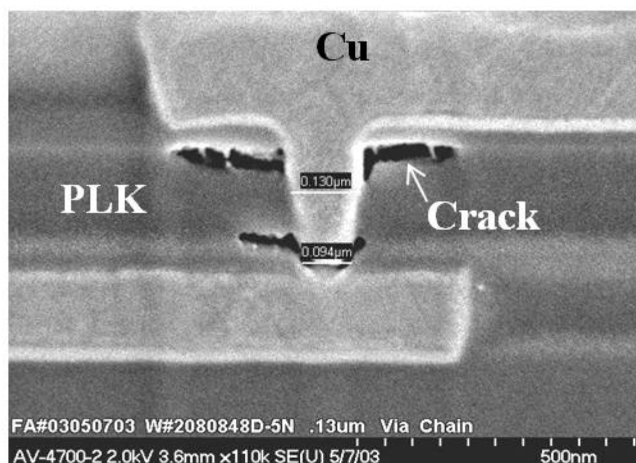

(a) crack observed following CMP

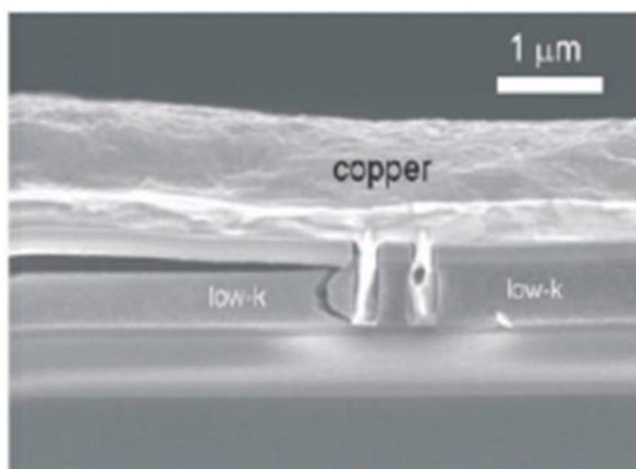

(b) delamination by thermal stress

Figure 1.7 SEM images showing (a) crack observed following CMP [80],(b) delamination by thermal stress developed from CTE mismatch during annealing [81].

range that the low-k material can tolerate. However, a portion of chemisorbed and/or trapped moisture in low-k materials typically is not removed thoroughly. Moreover, when the low-k samples are exposed to a moisture-rich environmental again, re-adsorption of moisture may occur [85]. The existence of moisture in low-k films can have a negative influence on electrical reliability of interconnect structure and their

mechanical integrity. With regard to electrical reliability, the dielectric constant value of water or moisture is as high as 80 due to the polar O-H bonds, so that even a small amount of water intrusion into the low-k films can significantly raise the dielectric constant of porous low-k films.

Water also impacts the leakage current of the dielectrics adversely. From the mechanical point of view, the presence of water deteriorates interface-adhesion properties between dielectrics and cap layers [91, 92]. Such a moisture uptake is especially important for porous low-k materials because they have a large surface area per unit volume, where moisture could potentially be adsorbed, resulting in even more severe and problematic reliability issues in Cu/PLK interconnects.

1.3.2.4 Plasma Treatment induced damage

A low-k material must have compatibility with a variety of integration processes, especially etching and cleaning or ashing. Since plasma etching can be highly directional and selective, compare to wet etching, it is widely used for the small physical size of trench and via lines in advanced Cu/PLK interconnects. For plasma-based ashing that is also used to remove the residues after photoresist(PR) strip and etching , it has advantage over wet chemical cleaning because it is a dry cleaning process which is less prone to moisture uptake in PLK. However, many studies have been made on the adverse effect of plasma-based treatments on the properties of PLK due to physical ionic bombardment and possible chemical reactions between ionized species and PLK film [94-104]. O_2 plasma is generally used in plasma etching PLK or ashing of PR residues, but tends to degrade low-k materials through removing CH_3

groups. The more pores are introduced into the existing low-k materials, the larger plasma species are penetrated, leading to more damage. If the plasma energy is high, Si-O-Si backbone may even be broken due to physical bombardment. As a result, when PLKs are exposed to plasmas, it can break Si-H, Si-C, and Si-CH_3 bonds, replacing them with Si-O, resulting in which methyl(CH_3) groups are depleted (Carbon depletion region), pores collapse, the density of film is increased, and the dielectric constant increases. More seriously, the PLK surface is transformed from hydrophobic to hydrophilic by introducing the higher polar silanol group(Si-OH) after the O_2 plasma etching/ashing, which makes PLK vulnerable to moisture adsorption in the subsequent processes when directly exposed to humid environment [103, 104]. The moisture uptake into the low-k material further increases dielectric constant, and the higher polar group silianol (Si-OH) degrades interconnect reliability such as current leakage [105,106].

When the technology approaches 45 nm or lower, low-k materials have more methyl groups and pores to further reduce dielectric constant. In such a case, the plasma damaging effect is more pronounced for highly porous low-k materials, causing reliability issues and yield loss in Cu/PLK interconnects.

1.4 Thermo-Mechanical instability in Cu/Low-k interconnect

A recent decision to implement Porous low-k dielectrics (PLK) to advanced interconnect structure has spurred various material/process developments as well as investigations on characteristics of porous low-k dielectrics. Among many research interests in terms of integration challenges and reliability concerns in Cu/PLK interconnects [6, 11, 107-112], thermo-mechanical stability of PLK has attracted a

particular interest not only because it is critical to the successful integration of PLK dielectrics to interconnect structure but also it is the area that is least understood. PLK dielectrics achieve low dielectric constant through the use of pores as integral part of dielectric materials, and therefore its thermo-mechanical stability (size and distribution) is believed to be critical to the structural and performance reliability of PLK dielectrics especially during processing of interconnect structure. It is a customary belief that PLK dielectric layer is relatively stable, so that their instability may not be of practical concern [113]. However, it is found from our previous study that the pores are not necessary stable based on the investigation where pore size (and density) was indirectly measured using voltammetry technique [114, 115]. From the findings of diffusivity change of tracer ions after thermal annealing of interconnects, it was concluded that the pores may coalesce and/or collapse depending on pattern density.

While this study suggests thermo-mechanical instability of pores and its variation with pattern density (stress condition), confirmation through direct observation and understanding of the mechanism is lacking. For this reason, we have conducted a series of investigations to better characterize the PLK instability through the use of HRTEM characterization and FEM stress simulation. It is found that the PLK instability is indeed active and is triggered by thermo-mechanical stresses developed into the dielectric layers due to the CTE mismatch between inter-layer PLK dielectrics and Cu [116]. The evidence of PLK instability showing time dependent plastic deformation of low-k is described in Figure 1.8, where TEM micrographs taken after 14 hours of the heat treatment at 400°C are shown. Upon annealing, both Cu and PLK layers are

subjected to pressure stress due to thermal expansion. The relaxation of such stress in PLK layer takes place by redistributing pores in the direction of least stressed points. For Cu, stress relaxation in Cu interconnects must take place by creep process, resulting in the elongation along the vertical direction and the generation of compressive stress in the lateral direction as seen in Figure 1.8. Even though our previous investigation indicates that PLK become unstable under thermal and mechanical stresses and undergo reconfiguration, the exact mechanism of thermo-mechanical instability of PLK dielectrics behind such behaviors is not well understood and still elusive. Therefore, it is necessary to verify the existence of thermal and mechanical instability of PLK and understand the related mechanism behind the instability of PLK so as to bring its implementation forward to real interconnect.

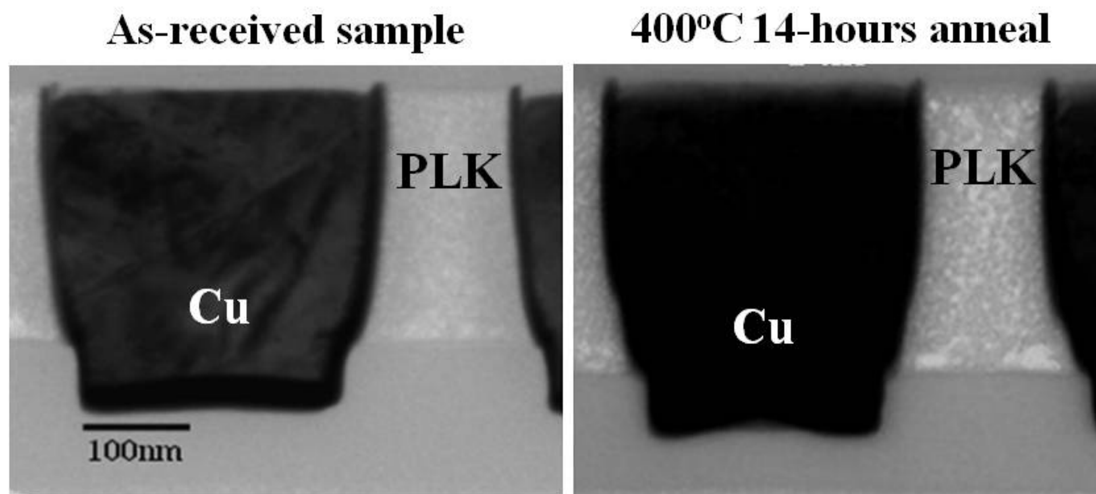

Figure 1.8 Cross-sectional TEM micrographs showing the Cu geometry and pore distribution annealed at 400°C. Note the elongation of Cu in the vertical direction and contraction in the horizontal direction with annealing, indicating time dependent plastic deformation at 400°C [116].

1.5 Research objectives and outline of the thesis

One of the key advances in microelectronics technology is the implementation of porous low-k dielectrics (PLK) in interconnect structures. The use of PLK is necessary to increase the device operation speed, yet its implementation has been seriously delayed due mainly to the reliability failure of interconnects integrated with PLK. As reviewed in the previous section, there is a significant growing concern of thermal and mechanical instability of PLK in relation to the reliability issues that are anticipated to become worse with the increase of porosity. While several reliability failure mechanisms instigated by PLK have been identified, the linkage between those mechanisms and properties of PLK itself has been elusive.

The primary objective of this research is thus to identify the mechanism leading to thermo-mechanical instability of PLK dielectrics observed in Cu/PLK interconnects. For this, we have developed an indentation creep test technique that is designed to examine the thermal and mechanical instability of PLK film at relevant temperature and load conditions in the interconnect structure.

In addition, in order to properly cope with the reliability problems of PLK, it is also important to understand the impact of intrinsic factors such as porosity and extrinsic factors like plasma damage and moisture uptake on thermal and mechanical instability of PLK. As a result, the second objective, which is also the primary focus of this study, is to investigate the influence of such intrinsic and extrinsic factors on thermal and mechanical instability of PLK and reveal the associated mechanism. Although this dissertation is focused on investigation of thermo-mechanical instability

of PLK, the results will also be useful in finding a practical method of strengthening PLK.

The dissertation is organized into six chapters.

In chapter 1, the advanced technology of modern Cu/PLK interconnects is briefly introduced and some fundamental properties of low dielectric constant material are reviewed. The integration challenges and reliability issues due to the material properties of Cu and PLK are discussed. Among them, thermo-mechanical instability of PLK in relation to reliability concerns is emphasized.

In chapter 2, some background information of indentation creep test will be reviewed. A ball indentation creep test for the examination of thermo-mechanical instability of PLK has been introduced. The indentation depth with time can be measured by using this test method. From the indentation depth-time curve, we can suggest the associated mechanism for creep deformation of PLK through the introduction of established theory on the ball indentation.

In chapter 3, the experimental details will be summarized. First, selected experimental PLK samples will be explained. Then, the indentation creep test method used in this study will be overviewed. At last, the analytical techniques used for sample evaluation will be briefly introduced.

In chapter 4, it is devoted to the investigation of viscoplasticity mechanism of PLK using indentation creep test. Understanding viscoplastic deformation mechanism of PLK and exploring the influence of porosity as intrinsic factor and plasma damage as

an extrinsic factor on thermo-mechanical instability of PLK are the major foci in this chapter.

In chapter 5, with the understanding of the proposed mechanism on viscoplasticity of PLK, the effect of moisture absorption as one of extrinsic factors on thermo-mechanical instability of PLK and the associated mechanisms will be investigated. Moreover, the influence of integration process steps on thermo-mechanical stability of PLK will be discussed.

In chapter 6, the summary of the thesis and future research will be presented.

CHAPTER 2

BACKGROUND: INDENTATION CREEP TEST

2.1 The basic idea of the indentation test

Most of the indentation (impression) tests are applied for the determination of static plastic properties of materials (e.g. hardness, yield stress) [117]. For the investigation of the time-dependent properties of materials, the indentation tests with various indenters such as ball(spherical), pyramidal, conical and cylindrical indenters have been largely used due to the simplicity of operation, involving relatively little demand on the sample preparation and the small volumes related to the deformation during indentation process in comparison with the tensile tests which are generally applied to examine the time dependent mechanical properties of materials(e.g. creep, viscous flow)[118,119]. In our study, among various types of indentation tests the ball (or spherical) indentation creep test is employed to investigate the existence of thermo-mechanical instability of PLK dielectrics at relevant load and temperature conditions in the interconnect structure. The primary advantage of the ball indenter is that it is less sensitive to alignment between the indenter and material surface, which is essential to obtain precise geometries in hard materials, thereby making experiments are easy to perform. Another advantage of using ball indenters is that indentation contact begins elastically as the load is first applied, but then changes to elastic-plastic at steadily increasing the load, which can theoretically be used to examine yielding and associated

phenomena (e.g. strain-hardening behavior) in a single test[120]. In this chapter, the theoretical background of indentation creep, especially a ball indentation creep test, will be reviewed including characteristics of time dependent plastic deformation, i.e. creep deformation.

2.2 Time dependent Plasticity : Creep

Several types of solids can be distinguished according to their mechanical behavior. In the simple but common case when a solid material is loaded at a sufficiently low temperature or short time scale, and with sufficiently limited stress magnitude, its deformation is fully recovered upon unloading. The material is then said to be elastic. But materials can also deform permanently, so that not all of the deformation is recovered. When the permanent deformation is not so much a consequence of longtime loading at sufficiently high temperature but more a consequence of subjecting the material to large stresses (above the yield stress), the permanent deformation is described as a plastic deformation and the material is called elastic-plastic. In the case when permanent deformation depends mainly on time of exposure to a stress and tends to increase significantly with time of exposure, such a permanent deformation is called viscous, or creep deformation, and materials that exhibit those characteristics for elastic response, are called viscoelastic materials (or sometimes viscoplastic materials, when the permanent strain is emphasized rather than the tendency for partial recovery of strain upon unloading) because time-dependent deformations are usually denoted by the prefix *visco*-. According to the facts mentioned above, creep is thus defined as the time-dependent plastic deformation of materials at

elevated temperatures over prolonged periods of time and is *viscoplastic* deformation. In the context of polymers, the time-dependent elastic deformation is frequently denoted as creep as well so that creep can be used as more comprehensive concept in terms of time-dependent deformation. Also, the historical method of evaluating the creep deformation of engineering materials is called the creep test. Creep is not an intrinsic materials property but rather a performance based behavior that is highly dependent on the operating temperature and stress. At temperature exceeding half the melting point of the material (Homologus temperature : T/Tm > 0.5, where T: operating temperature, Tm : Melting temperature), creep deformation is of significant concern.

2.2.1 Creep Curve

When a constant load is applied to a tensile specimen at a constant temperature (usually greater than 0.4-0.5 of the absolute melting temperature of the specimen), the strain of the specimen is determined as a function of time. A typical variation of creep strain with time in a specimen at a constant load is schematically shown as curve A in Figure 2.1. The slope of this curve is the creep rate. There are three distinct regions in the creep curve which can be differentiated by the underlying mechanism of deformation [121]. Stage I of curve I follows after an initial instantaneous strain, which includes elastic and plastic deformations. During stage I, the creep rate decreases with time. This is termed primary creep. Stage II of curve A, during which the creep rate approaches a stable minimum value, relatively constant over time, is secondary creep or steady-state creep. The creep rate in the secondary creep stage is an important engineering property, because most deformations involve this stage. In stage III, termed

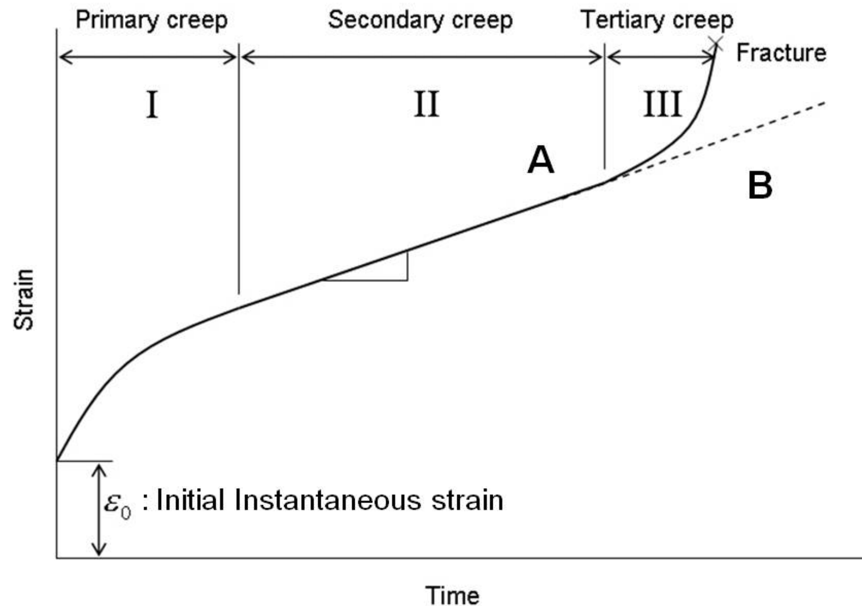

Figure 2.1 Typical Creep Curve showing the 3 stages of Creep for tensile test
(A: Constant-Load test, B: Constant –Stress test)

tertiary creep, the creep rate accelerates with time and usually leads to failure by creep rupture. Curve B in Figure 2.1 is different from curve A and indicates a creep test with a constant stress. Under a constant load, the uniaxial stress increases with time because the specimen decreases in cross-sectional area. The increasing stress thus accelerates creep and causes strains in the tertiary phase, as shown in curve A. In most engineering creep tests, it is often easier to maintain a constant load during the test because of instrumentation limitations. But constant-stress conditions are preferred to study the fundamental mechanism of creep. Under constant-stress, as shown in curve B, steady-state creep dominates over a much longer time period and thus greatly postpones tertiary creep.

2.2.2 Creep Characteristics

Creep characteristics are dependent on several factors such as time, temperature, stress (or load), and micro-structure. For example, a time scale is always involved in a creep test. For most engineering materials tested at low temperatures, measured tensile properties are relatively independent of the test time. In contrast, if time dependence is observed in a creep test, the material is creeping. The main reason for the time dependence of creep is the involvement of thermally activated time-dependent processes. The overall creep rate during creep deformation is usually controlled by a single dominant thermally activated process.

With regard to temperature dependence of creep behavior, since creep is strongly temperature dependent, a measurement of the temperature dependence of creep is important. At high temperature, the mobility of atoms or vacancies increases rapidly with temperature so that they can diffuse through the lattice of the materials along the direction of the hydrostatic stress gradient, which is called self-diffusion. The self-diffusion of atoms or vacancies can also help dislocations climb toward the direction perpendicular to its slip plane [122]. Given that at temperatures above $0.5T_m$, the diffusion creep in crystalline materials is thought to be controlled by an Arrenius-type rate model as follows:

$$\dot{\varepsilon} = \frac{d\varepsilon}{dt} = A\sigma^n \exp(\frac{-Q}{RT}) \tag{2.1}$$

where $\dot{\varepsilon}$ is the strain-rate, σ is the applied stress, A is the constant for a given temperature and material, Q is the apparent activation energy for creep, n is the stress exponent that represents which mechanism of creep is operating, R is the gas constant

and T is the absolute temperature. Creep occurs faster at higher temperatures. However, what constitutes a high temperature is different for different materials. When considering creep, the concept of a homologous temperature is useful. The homologous temperature is the actual temperature divided by the melting point of the material, with both being expressed in K. In general, creep tends to occur at a significant rate when the homologous temperature is 0.4 or higher. At low temperatures, creep becomes less diffusion-controlled. Diffusion can occur, but is limited in local areas such as grain boundaries and phase interfaces, which are called grain-boundary diffusion.

Creep rate is also very sensitive to the applied stress level and stress state. Figure 2.2 schematically shows how the applied stress level affects creep rate at constant temperature [123]. As the applied stress increases, the primary and secondary (steady-state) stages are shortened or even eliminated.

Creep properties of materials are intrinsically determined by the microstructure of the materials. Grain size affects creep rate in all three creep stages. Precipitations and impurity particles initiate creep cavities. These microstructural effects can be superimposed and can affect creep properties of materials in various complex ways. At constant stress and constant temperature, for example, the increase of grain size increases the steady-state creep rate of copper, but decreases that of lead. Porosity due to sintering is another microstructural effect, particularly in ceramic materials. Both volume percentage and shape of pores directly influence the creep property of ceramic materials.

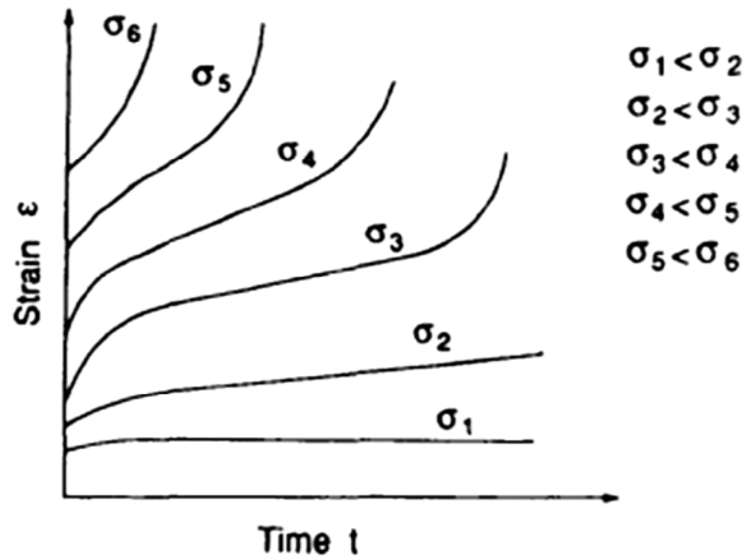

Figure 2.2 Effect of applied stress on creep curves at constant temperature using tensile test [123].

2.2.3 Mechanisms of Creep in materials

The mechanism of creep in a material can either be classified as diffusional creep or dislocation creep. At low stress, diffusion creep occurs by transport of material via diffusion of atoms in a material that may involve interstitial or vacancy diffusion, grain boundary diffusion and dislocation core diffusion. There are two types of diffusion creep, depending on whether the diffusion paths are predominantly through the grain boundaries, termed Coble creep (favored at lower temperatures) or through the grains themselves, termed Nabarro-Herring creep (favored at higher temperatures).

Dislocation creep is a mechanism involving motion of dislocations. This mechanism of creep tends to dominate at high stresses and relatively low temperatures. Dislocations can move by gliding in a slip plane, a process requiring little thermal

activation. However, the rate-determining step for their motion is often a climb process, which requires diffusion and is thus time-dependent and favored by higher temperatures. Obstacles in the slip plane, such as other dislocations, precipitates or grain boundaries, can lead to such situations.

As it was suggested earlier [124,125], the value of the activation energy, Q, and that of the stress exponent, n, is very important to investigate the mechanism of high temperature creep. The activation energy Q can be determined by plotting the natural log of creep rate against the reciprocal of temperature experimentally. In the case of the stress exponent, its value can be obtained by plotting the natural log of creep rate as a function of the applied stress. When considering certain pure metals and ceramics under appropriate conditions, due to the presence of crystalline phases, the value of the stress exponent of diffusion creep is approximately one, while its value for dislocation creep is generally found to range from three to five [118]. In some ceramic materials which contain glassy phases, it is found that the deformation process at a high temperature is governed by the deformation of the glassy phases, which highly enhances the plasticity of the material, therefore the value of the stress exponent decreases to about two [126].

Creep can take place viscoelastic materials such as polymer, glass, and even metals. Viscoelastic materials have molecules in which the load-deformation relationship is time-dependent. If a load is suddenly applied to such a material and then kept constant, the resulting deformation is not achieved immediately. Rather, the solid gradually deforms and attains its steady-state deformation only after a significant period of time. This behavior is also called creep in viscoelastic materials.

As for amorphous materials (or glass materials), creep occurs at temperatures around or above glass transition temperature (T_g) of the material. For this case at elevated temperatures and low stresses (or low strain rates), the range of stress exponent values (n) is $1 \leq n < 10$, indicating that the flow which often occurs with deformation is more viscous and become homogeneous (in the case of n=1, the flow would be Newtonian viscous). At high stress levels and low temperatures (room temperature or far below T_g), a condition of $n > 10$ is given, implying that the flow becomes inhomogeneous or non-Newtonian viscous. In other words, plastic deformation occurs by the rearrangement of a particularly oriented cluster of molecules (or atoms) at localized sites, and the plastic flow is concentrated into a few such particularly oriented clusters, and thus the flow is more inhomogeneous [127-131].

While most oxide glasses are Newtonian, at least for the typical low strain rates (or low stresses) and high temperatures, polymers or organic materials have typically exhibited shear thinning (or pseudoplastic behavior)[132]. For this shear thinning fluids, n is less than one ($n < 1$). This behavior can occur in the polymer melts such as molten polystyrene, polymer solutions such as polyethylene oxide in water, and some paints. For instances, when paint is sheared with a brush, it flows comfortably, but when the shear stress is removed, its viscosity increases so that it no longer flows easily. Of course, the solvent evaporates soon and then the paint sticks to the surface. The behavior of paint is a bit more complex than this, because the viscosity changes with time at a given shear rate. The deformation mechanism for this fluids has less been known so that it has been generally surmised that the non-Newtonian behavior is a

result of complex molecular chain kinetics such as unfolding, stretching, cross linking, etc. Similarly, when silicate glasses are subjected to high strain rates or high compressive stresses and low temperatures, they have typically showed densification [133]. The densified glasses are retained even after unloading. For this densification behavior, n is also less than one ($n < 1$) [134,135].

Moreover, it is well known that the value of the activation energy, Q, is closely related with the bonds keeping the material in solid state. During the deformation of metal alloys, for instance, since most of metals exhibit metallic bonding, the value of the activation energy is usually comparable with that of the self-diffusion of the base metal (~130 kJ/mol or ~1.4 eV)[136]. In the case of glasses, glass-ceramics and ceramics, the activation energy can be very high (>400 kJ/mol or > 4 eV) due to stable and strong ionic or covalent bonds [137].

2.3 Indentation Creep Test

The goal of our study in relation to PLK's stability is to verify the existence of viscoplastic deformation (or creep deformation) leading to thermal and mechanical instabilities and understand the related the mechanism. However, with lack of proper characterization techniques, the possibility and mechanism of plasticity in PLK films have not been properly assessed. For this, the indentation creep test, especially a ball indentation creep test, is introduced to investigate the thermo-mechanical instability of PLK in this work.

Indentation testing of materials has been conducted in order to determine the static plastic properties of materials such as hardness, yield stress, etc. These types of

measurements are well-understood and applied widely. However, the instrumented indentation method for measuring the temperature and strain rate-dependent properties of materials is less well-known as compared with its importance [138-152]. These properties are helpful in understanding the kinetics of plastic deformation and the associated mechanisms in materials. In this section, in order to better understand time, temperature and stress dependent properties of PLK films measured by means of the ball indentation creep method, a review of the fundamentals of a ball (spherical) indentation creep test and model that is used for the measurement of viscosity of glass will be entailed. In particular, since the PLK material is an amorphous material based on silicon oxide, the creep properties and the kinetics of deformation in PLK films can be compared and related to those same properties and the kinetics in glass using the ball indentation creep test for both materials.

2.3.1 Constitutive equations and Ball Indentation Creep process

One equation used to describe the flow behavior of materials which depends on the material's structure, temperature, and stress state under creep states is

$$\dot{\varepsilon} = A\sigma^{n} \tag{2.2}$$

where $\dot{\varepsilon}$ and σ are the uniaxial strain-rate and uniaxial stress, respectively. A is a constant for a given material and temperature, and the quantity n is known as the stress exponent for creep. This equation has been used by many researchers to describe indentation creep for materials from metals to oxide glasses [153,154].

There are two primary types of indentation creep tests: the constant load test and the constant displacement test. In the case of the constant load test, the indentation depth (*h*) is recorded as a function of the elapsed time (*t*) at a given temperature while the load is constant (*F*) [141, 152-159]. Measured indentation depth with time can be converted to stress (s) or hardness (*Hv*), or strain rate for metals [144,156,158], glasses [154] and organic compounds [155]. During creep time, the indenter continues to displace into the surface of the deforming specimen. The constant displacement test (or the relaxation test) reverses the roles of the displacement and the load; the indenter is pushed into the specimen and held at some fixed depth, while the reducing load is measured [149]. In our study, the fixed load test has been used because it can simplify measurement and analysis, and facilitate rapid data collection. Besides, it has been reported that a number of researchers have found good correlations between experiment and literature values for stress exponent (n) and activation energy (Q) in various materials using this constant load method [162-164].

The analysis of indentation creep data is more complicated than that of conventional creep tests. In Equations (2.1) and (2.2),   and σ are typically defined with regard to uniaxial experiments. In an indentation experiment, the material beneath the indenter exists in a complicated state of multiaxial compressive stress. Figure 2.3 shows the geometry of the ball indentation, where R is the ball indenter radius, a is the contact radius at a given indentation depth, *h*. With a ball indenter the pressure distribution varies along the contact radius, a , under the ball indenter during the indentation performed at the constant load.

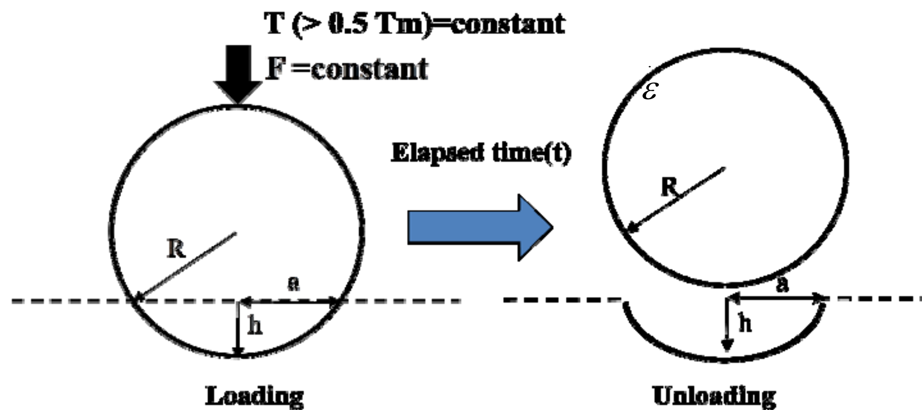

Figure.2.3 Scheme of the indentation creep under constant load (F) with a ball indenter

In general, indentation creep is measured by holding constant load on the material and monitoring changes in indentation size with time (t). It is very difficult to determine the accurate radius of contacting bodies using a ball indenter owing to pile-up or sink-in at around the residual indentation after unloading stage and the development of low load indentation enabling the indentation depth to be continuously monitored with time, the use of indentation depth is more likely to be applicable to obtain creep properties of materials for instrumented ball indentation techniques, where the indentation depth as a function of time is measured.

During loading, as shown in Figure 2.3, the deformation beneath the ball indenter is the combination of instantaneous elastic and plastic deformation processes, and the indenter conforms perfectly to the ball shape of the pressure indentation. For the vertical indentation depth (h) of the ball indenter, one can write $h=h_{elastic} + h_{plastic}$. When there is substantial elastic recovery, such as in ceramic materials where elastic modulus is low or at the beginning of indentation experiment, the elastic recovery process can be

pronounced upon unloading, which mainly influences the indentation depth. Accordingly, both the elastic and plastic (or flow) components of the deformation beneath the indenter have to be taken into account to analyze the indentation print. However, when the plastic deformation process is fully developed for a sufficiently long time period the elastic recovery is very small. Many researchers [144,165] have confirmed this with experimental results for various materials such as aluminium, brass and selenium as a viscoelastic material. The results indicated that the portion of the elastic recovery in the fully plastic contact regime is about 1~3% of the total indentation depth. Based on this fact, it is reasonable to assume that the elastic recovery is negligible at a condition of a fully developed plastic zone. Hence, in our study, since all PLK films deformed plastically in the indentation creep test (refer to chapter 4 and 5), it can be assumed that the PLK films being indented have negligible elastic recovery. That means that the plastic depth of indentation ($h_{plastic}$) is equal to the total depth of indentation (h).

During indentation creep test the indentation pressure, p_s, under the ball indenter can be expressed as a function of the indentation depth:

$$p_s = \frac{F}{\pi a^2} = \frac{F}{\pi h(D-h)} \tag{2.3}$$

Assuming that D >> h, where D (=2R) is the diameter of the ball indenter, Equation (2.3) can be expressed in the following form:

$$p_s = \frac{F}{\pi h D} \tag{2.4}$$

For the ball indenter, Tabor et al. [166] assumed that the strain rate (or equivalent strain rate) at any stage in the indentation process was

$$\dot{\varepsilon} = \frac{1}{D}\frac{da}{dt} \tag{2.5}$$

However, instead of measuring a contact radius a, it is possible to use the indentation depth (h) with time using this relation: $a^2 = h(2R - h)$, if R>>h, $a^2 = 2Rh$ and $ada = Rdh$.

In this case, the strain rate can be defined as the ratio of the indentation rate and the radius of the contact at the given indentation depth. Applying the same approach as in Equation (2.3) we achieve:

$$\dot{\varepsilon} = \frac{1}{D}\frac{da}{dt} = \frac{1}{2a}\frac{dh}{dt} = \frac{1}{2\sqrt{h(D-h)}}\frac{dh}{dt} \tag{2.6}$$

Supposing that D>>h, Equation (2.6) can be rewritten in the following form:

$$\dot{\varepsilon} = \frac{1}{2\sqrt{hD}}\frac{dh}{dt} \tag{2.7}$$

Equation (2.7) reflects the strain-rate of materials underneath the ball indenter, which can be used to investigate the time dependent plasticity of PLK.

Results from hardness tests of Tabor [197] indicated that indentation hardness behavior and strain associated with a spherical (ball) indenter closely correlated to the results in uniaxial tensile test. These correlations are based on three premises: (i) monotonic true stress–true plastic strain curves obtained from tension and compression testing are reasonably similar; (ii) indentation strain correlates with true plastic strain in

a uniaxial tensile test; and (iii) mean ball indentation pressure correlates with true flow stress in uniaxial tensile test. These three premises were found to be well established for several materials [167]. In addition, according to Mulhearn and Tabor [166], it was found that the value of stress exponent (n) and activation energy for conventional tensile creep and indentation creep test with a spherical indenter were similar for pure metals such as lead and indium. Therefore, these results indicate that the indentation test conducted with ball indenters enables the exploration of the time dependent plasticity of metallic materials to be properly investigated.

Since the contact area changes as the ball indenter penetrates the material while the load is held constant, the pressure stress changes as the creep test proceeds. This means that indentation creep tests using the ball indenter including conical, pyramidal indenters do not show a steady state creep at constant load, meaning that the strain rate under the ball indentation creep testing deceases continuously with time. Thus, indentation test method using the ball indenter is preferred to determine the viscosity of amorphous materials due to the fact that there is no work hardening or dynamic recovery which is the main cause of transient creep following the steady state creep in the amorphous materials such as glasses and non crystalline materials. Accordingly, from this point of view, two approaches can be used to determine the stress exponent with the ball indentation creep testing. The first approach is that indentation tests are conducted for different several loads at the same creep time. By using Equations (2.4) and (2.7) to obtain the strain rate and the applied stress (or pressure) from the indentation data, the stress exponent n, which reveals the creep properties and

mechanisms of the given materials, can be extrapolated from the slope of logarithm $\dot{\varepsilon}$ of *versus* logarithm of σ curve [log($\dot{\varepsilon}$) - log(σ)] plotted from equation (2.2). The other approach is that indentation test is performed for the fixed load as a function of time. Due to the geometry of the ball indenter, the pressure (or stress) changes with time because the contact area also changes with time. The applied stress changes under the ball indenter, meaning that several stress-strain rate pairs from one indentation testing can be obtained. Accordingly, as shown Figure 2.4, the value of stress exponent can be determined from the slope of a plot of several log pressure stress-log strain rate data which can be obtained from the measured creep curves by using Equation (2.4) and (2.7) [168]. If the indentation depth with time is continuously recorded by using automated depth sensing indentation system, the second approach is useful in the determination of the stress exponent because this indentation creep test under constant load involves multiple indentations by the ball indenter at a single penetration location.

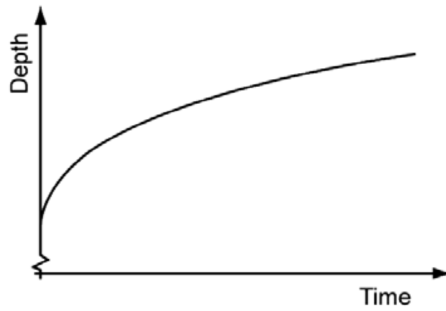

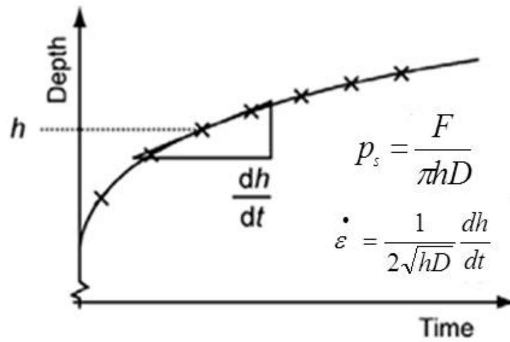

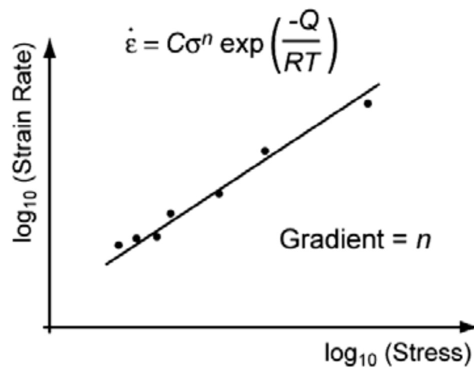

Figure 2.4 Schematic depiction of how depth–time plots, obtained under constant load, can be used to determine values for the stress exponent, n using the ball indentation creep test. Pressure stress and strain rate are found using Equation (2.4) and (2.7) [168].

2.3.2 Analysis of indentation creep test with a ball indenter

Generally, it is thought that Equation (2.2) describes the relation between the strain rate and pressure stress at any moment during indentation experiment with the ball indenter. This means that the momentary strain rate and pressure stress obtained by Equation (2.4) and (2.7) obey the constitutive equation. Accordingly, in order to analyze the creep curves measured with a ball indentation test, Equation (2.2) can be regarded as a differential equation, which contains the indentation depth, h, and the elapsed time, *t*:

$$\frac{1}{2\sqrt{hD}}\frac{dh}{dt} = A\left(\frac{CF}{\pi hD}\right)^n \tag{2.8}$$

By rearranging and integrating the Equation (2.8), it can be described in the following form:

$$\int_0^{h(t)} h^{n-\frac{1}{2}} dh = \int_0^t \left(\frac{2AC^n F^n}{\pi^n D^{n-\frac{1}{2}}}\right) dt \tag{2.9}$$

where C is constant(not depending on material, strain rate and temperature). Since it is assumed that the threshold stress is zero in the case of pure metals or glasses, Equation (2.9) can be simplified to the following form:

$$h^{n+\frac{1}{2}} = (n+\frac{1}{2})\frac{2AC^n F^n}{\pi^n D^{n-\frac{1}{2}}} t \tag{2.10}$$

The indentation creep curves with the ball indenter can be described by an equation derived from the power law constitutive equation for the creep behavior at the high temperature. Equation (2.10) can be fitted numerically to the measured creep curves from a single indentation experiment. Also, it is worth noting that if fitting the

Equation (2.10) to measured indentation creep curves yields n=1 value, the value of $h^{3/2}$ varies linearly as a function of time under the ball indenter, indicating that tested material is characterized as Newtonian viscous flow material.

2.3.3 Indentation Creep in glassy materials

The creep behavior of crystalline materials at high temperatures has been traditionally investigated in tensile or compressive test [169]. Also, indentation testing has been successfully applied in exploring time-dependent plastic deformation of different crystalline materials and non-crystalline materials like glasses [137,154,155,170,171]. Due to the fact that it has been known that the PLK material is amorphous material based on silicon dioxide(SiO_2), the knowledge of creep properties and kinetics of deformation in glasses (or glassy materials) is indispensable to better understand the creep mechanism leading to thermo-mechanical instability of PLK dielectrics observed in Cu/PLK interconnect. Furthermore, it is found from our study that the kinetic model established by Douglas et al. [172] fits well to our measurement of indentation depth as a function of time. Since this model is applied for viscous flow materials in a ball indenter, this finding may indicate that the viscous flow is the mechanism of viscoplastic deformation in PLK films.

Therefore, in this section, the necessary theoretical background on the ball indentation creep for viscous flow materials such as amorphous materials and glasses will be provided to allow for the correct interpretation of the experimental results presented in the subsequent chapter 4 and 5.

2.3.3.1 Viscosity of glasses

Viscosity is defined as the resistance to flow or the ratio of shear stress to shear strain rate. The relationship is:

$$\eta = \frac{\tau}{\dot{\gamma}} \qquad (2.11)$$

where η is the shear viscosity, τ is the shear stress, and $\dot{\gamma}$ is the shear strain rate. The ease of flow in liquid is characterized by its viscosity. The viscosity is the result of the diffusion of atoms or molecules in an amorphous material, which is related to viscous flow. In physics, viscous flow is defined as transport phenomenon involving the movement of various entities, such as mass, momentum, or energy, through a medium, fluid or solid, by virtue of nonuniform conditions existing within the medium. For example, first, variations of concentration in a medium lead to the relative motion of the various chemical species, and this mass transport is generally referred to as diffusion. Second, variations of velocity within a fluid result in the transport of momentum, which is normally referred to as viscous flow. Lastly, variations in temperature result in the transport of energy, a process usually called heat conduction. There are many similarities in the mathematical descriptions of these three phenomena; and the three often occur together physically. In glassy materials such as silicates, amorphous, alloys, glassy polymers etc, the knowledge of viscosity is thus of importance for investigating their creep behaviors at elevated temperatures [173,174]. The viscosity gives some powerful insight into the physical nature of glasses, including their structure (short range order) and the thermodynamics of flow (activation energies and volumes). The

range of viscosity is very wide and it is not possible to make measurements over the whole range by any one method.

In fact, the viscosity of glasses depends strongly on temperature and can be generally described by the formula:

$$\eta = \eta_0 \exp(\frac{Q}{kT}) \tag{2.12}$$

where η_0 is a constant, k is the Boltzmann constant and Q is the activation energy of the process controlling the viscous flow. Substituting Equation (2.12) into Equation (2.11) and the shear strain rate ($\dot{\gamma}$) can be described by:

$$\dot{\gamma} = \frac{1}{\eta_0} \tau \exp(-\frac{Q}{kT}) \tag{2.13}$$

This formula can be regarded as a particular case of the equation:

$$\dot{\gamma} = A \tau^n \exp(-\frac{Q}{kT}) \tag{2.14}$$

$$(\dot{\varepsilon} = A \sigma^n \exp(-\frac{Q}{kT}) \text{ (For uniaxial or indentation test)})$$

which is generally used for the interpretation of the steady state creep of metals and ceramics at high temperatures. In Equation (2.14) A is a material specific constant, Q and n are the activation energy and the stress exponent of the activation process, respectively. For a Newtonian viscous flow material, the value of stress exponent is exactly 1 and then the equation (2.14) goes back to Equation (2.13). From the viscosity values at different temperatures, the activation energy for the creep process can be calculated according to the Equation (2.12) or the following Equation:

$$\frac{\partial \ln \eta}{\partial (1/T)} = \frac{Q}{k} \quad (2.15)$$

The calculated viscosity values at different temperatures can be plotted against inverse absolute temperature and then the slope by the plotting $\ln \eta$ versus 1/T gives the activation energy for viscous flow of materials.

2.3.3.2 Iinvestigation of the plasticity of glasses by determination of viscosity using a ball indenter

The viscosity can be determined by a variety of methods, but three of the most common methods are the rotation viscosimeter in the high temperature [175], fiber extension [176] and beam bending [177] for low temperature measurement. The phenomenological interpretation of these tests is relatively simple because the stress field is macroscopically uniaxial and homogenous in the sample during the test. However, for some glasses, these methods suffer from the fact that the sample has to be withdrawn from the furnace and cooled prior to the measurement of the indentation depth. In the case of advanced structural ceramics, it is very difficult to prepare samples for tensile testing. For this reason, indentation techniques have been introduced and used as an alternative method for the determination of the viscosity of glasses as well as the exploration of the high temperature plasticity of amorphous materials [172,178].

The contact problem for a viscoelastic body and an indenter can be analyzed by the use of the appropriate solution for the case of an elastic material, where the shear modulus (G) is substituted by the viscosity (η) and the displacement (u) is replaced by the displacement rate or strain rate ($u' = du/dt$) [179].

The Hertz contact solution for the displacement (u) of the two spheres at a distance r from the center of contact area in elastic contact is [180]

$$u = (k_1 + k_2)\frac{p_{\max}\pi^2}{4a}(2a^2 - r^2) \tag{2.16}$$

where

$$k_1 = \frac{1-\nu_1^{\ 2}}{E_1},\ k_2 = \frac{1-\nu_2^{\ 2}}{E_2} \tag{2.17}$$

and P_{max} is the maximum pressure, $P_{\max} = 3F / 2\pi a^2$, where F is the applied load and a is the radius of contact, and E is the elastic(Young's) modulus, ν is the Poisson's ratio. If the spheres are incompressible (i.e. ν=1/2) and one is rigid (i.e. $E_1=\infty$), k_1=0 and $k_2 = 3/(4\pi E_2)$ and also, $P=P_{max}$ at r=0. Therefore,

$$u = \frac{9P}{16aE_2} \tag{2.18}$$

According to Goodier[182], Equation (2.18) is applicable for a viscous body if du/dt is substituted for u, and η for $E_2/3$. Thus,

$$\frac{du}{dt} = \frac{3P}{16a\eta} \tag{2.19}$$

If the radius of the sphere is large compared with the radius of indentation, then $a^2 \approx 2Ru$ and $du \approx ada/R$. Substituting into Equation (2.19) gives

$$16\eta a^2 da = 3PR\,dt \tag{2.20}$$

Integrating and rearranging,

$$\eta = \frac{9PR}{16a^3}t \qquad (2.21)$$

where t is the time for a to grow from 0 to a.

Douglas et al.[172] started from the same equations for the displacement of two elastic spheres, but considered the indentation depth (h) rather than the indentation radius (a). If the indentation depth is considered, then $a^2 = h(2R-h)$ and Equation (2.19) can be written in the following:

$$\frac{dh}{dt} = \frac{3F}{16\eta}\frac{1}{\sqrt{h(2R-h)}} \qquad (2.22)$$

If R>>h, Equation (2.22) can be rewritten in the following simpler form:

$$\frac{dh}{dt} = \frac{3F}{16\eta}\frac{1}{\sqrt{h(2R)}} \qquad (2.23)$$

After integrating and rearranging

$$\eta = \frac{9}{32(\sqrt{2R})}\frac{F}{h^{3/2}}t \qquad (2.24)$$

And then (for D=2R, where D is the diameter of sphere)

$$h(t)^{3/2} = \frac{9}{32\eta(D)^{1/2}}Ft \qquad (2.25)$$

Equation (2.21) and (2.24) are equivalent, except that one relates viscosity to the size of indentation and the other to the depth of the indentation. Equation (2.24) is more likely to be applicable for instrumented indentation techniques, where the displacement as a function of time is measured. Cox [181] compared the viscosity of a glass determined by Equation (2.18) to that obtained by fiber extension. It was found that there was good

agreement between these methods over the common temperatures ranges. Douglas *et al*.[172] compared the viscosity achieved with their apparatus to that of previously published viscosity of a glass and found good agreement. These results imply that the indentation method with the ball indenter can be used to determine the viscosity of materials from the indentation depth as a function of creep time.

CHAPTER 3

EXPERIMENTAL AND CHARACTERIZATION

3.1 Experimental samples

The PLK films (termed as SiCOH, carbon-doped oxides, or organosilicate glasses (OSG)) used in our study were prepared using industry standard PECVD processes. The various PLK films were obtained from Globalfoundaries. The grown PLK films by PECVD are the main characterization target. PLK films incorporate carbon as $Si–CH_3$. The methyl (CH_3) groups lower the film's density, polarizability and make the film hydrophobic, resulting in the decrease of the dielectric constant (k) of the film, and PLK films typically have a k of about 2.5–3.0. As shown in Figure 3.1, the structure of PLK film fabricated by PECVD is highly complicated by a variety of different crosslinked networks [183]. The introduction of additional porosity in PLK films is used to further lower the k. Porosity is created by incorporating an organic precursor (porogen), which is mixed with PLK matrix (skeleton) precursor during deposition. The organic precursor is thermally decomposed and removed from the film during the subsequent curing, leaving behind pores. The structure of the resulting porous cage networked PLK film which is deposited from the mixture of a matrix precursor and the organic precursor can be described by the schematic diagram shown in Figure 3.2. It has been reported that PLK film with k value as low as 2.2 and rather large pores of 4nm is obtained by this approach, subtractive fabrication by molecular

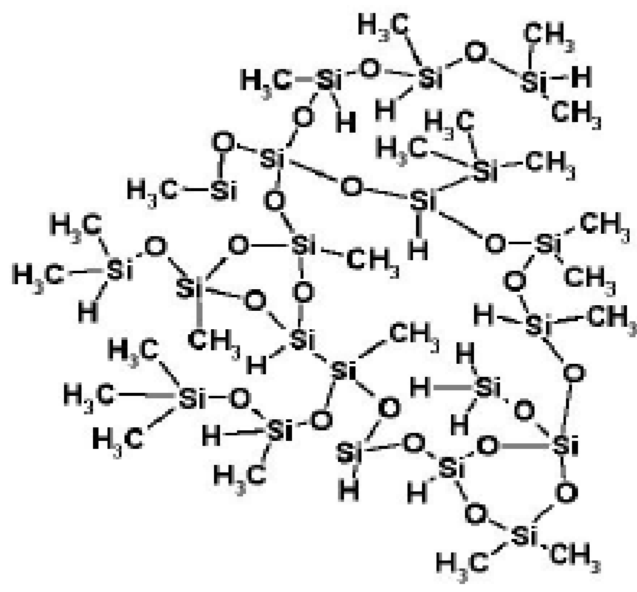

Figure 3.1 Diagram of networked structure of cured SiCOH film deposited from a matrix precursor only [183].

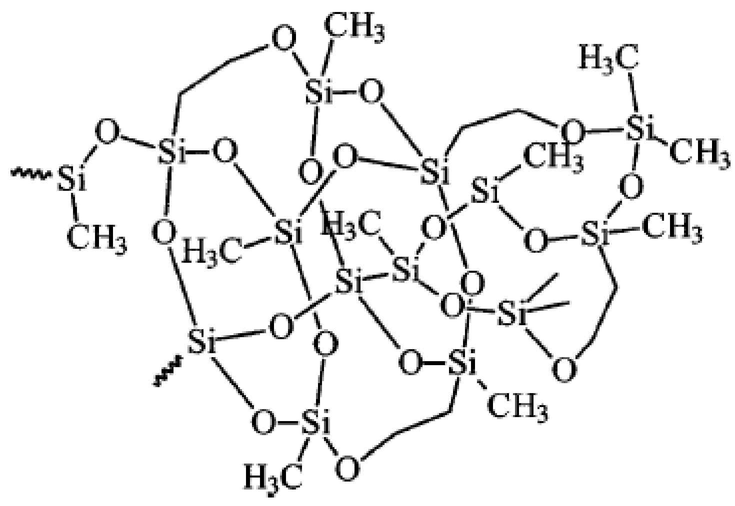

Figure 3.2 Porous cage networked structure of annealed SiCOH film deposited from a matrix precursor with organic precursor [183].

porogens, using proper precursors and plasma conditions [184]. The optimization of the network structure is extremely momentous in lowering polarity and thus dielectric constant.

The optical micrograph image and the schematic illustration of the PLK film cross section are displayed in Fig. 3.3. The PLKs used in our study are the 400nm-thick SiCOH films PECVD deposited on top of a SiO_2 coated Si wafer. After PLK deposition, a 25nm thick SiCN layer was deposited to provide protection of PLK during characterization process.

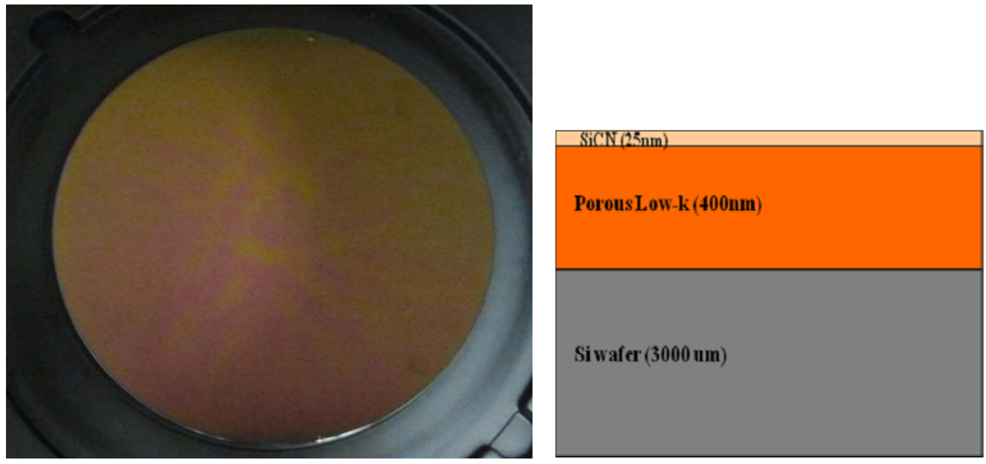

Figure 3.3 Schematic illustration of PLK blanket film structure.

These films do have variation in porosity (effective k~2.4, 2.2), controlled plasma exposure and moisture uptake, A film: PLK film with lower porosity (k=2.4), B film: PLK film with higher porosity (k=2.2), C film: PLK film with higher porosity exposed to plasma, D film: PLK film with higher porosity (k=2.2) in the presence of moisture. Table 3.1 summarizes the properties of used porous SiCOH films in our study. These films allow us to examine the effect of intrinsic (porosity) and extrinsic (plasma damage

and moisture) on the mechanism of viscoplasticity in PLK dielectrics.

Table 3.1 Properties of porous SiCOH films with variation in porosity, plasma exposure and moisture absorption.

Wafer ID	Composition	Dielectric constant : k	Porosity (%)	Carbon Contents	Plasma Exposure	Moisture Absorption
A	pSiOC:H	2.4	25	-	No	No
B	pSiOC:H	2.2	30	Low	No	No
C	pSiOC:H	2.2	30	Low	Yes	No
D	pSiOC:H	2.2	30	Low	No	Yes

3.2 Equipment of Indentation Creep Test

The method of a ball indentation creep test we developed is very simple but helpful in revealing the thermo-mechanical instability of porous low-k dielectrics. It relies on an application of a constant load on top of porous low-k film and measures the penetration depth (*h*) as a function of time (*t*). Figure 3.4 display the ball indentation creep test setup and a schematic illustration showing the testing arrangement. A spherical aluminum oxide indenter with a diameter of 20mm was used for indentation creep test. The ball indenter is fixed in the loading rod which is connected to weight holder plate. The loading rod is allowed to move vertically freely, and the axis of the ball indenter is perpendicular to the surface of the PLK sample. The holder plate, in which weights can be placed providing the constant load, is fixed. The temperature of the sample is continuously monitored with a type K thermocouple and maintained to within ±0.1°C.

(a) indentation testing setup

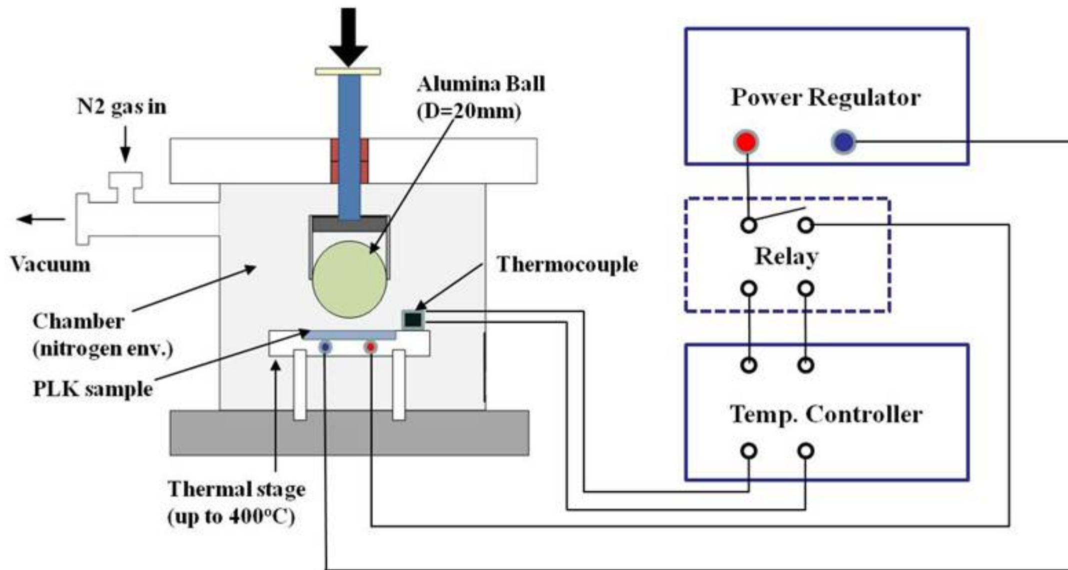

(b) ball indentation creep apparatus

Figure 3.4 (a) A picture of indentation testing setup and (b) a schematic illustration of the ball indentation creep apparatus.

3.3 Procedure

The experimental procedure consisted of the following steps: Since the temperatures used for annealing process which is one of current integration processes, can be as high as 400˚C, the indentation creep experiments were performed at different temperatures (300 ˚C ~ 400 ˚C) for all PLK films using a wide range of loading time from 1hr to 8hr in N_2 atmosphere. Note that all PLK films were evacuated and purged with N_2 alternately to remove external factors including water from the films, indicating that all PLK films were dried before the indentation creep testing. Also, N_2 gas was kept flowing to protect the PLK film against water. Since the annealing process of wafer in the current integration process is necessary after the completion of the interconnect layer [185], compressive stress is developed into PLK dielectrics due to a thermal expansion mismatch between the inter-layer PLK dielectrics and Cu. It has been reported that the stresses generated during the interconnect fabrication process and functioning can be as high as several hundreds of MPa [186]. The simulation is based on solely elastic behavior assumption. First, thermal stress in the interconnect structure was calculate from the elastic model. The indentation load level creating similar stress levels in the Cu interconnect was calculated from FEM. Even though the low-k exhibits plasticity behavior, the approach is correct as the stress-strain is a state function (yielding at plastic flow will be same as they are under same mechanical state). According to our simulations for thermal stress development in PLK, the range of pressure stress was between 100MPa and 200MPa at pitch size from 0.06um to 0.15um.

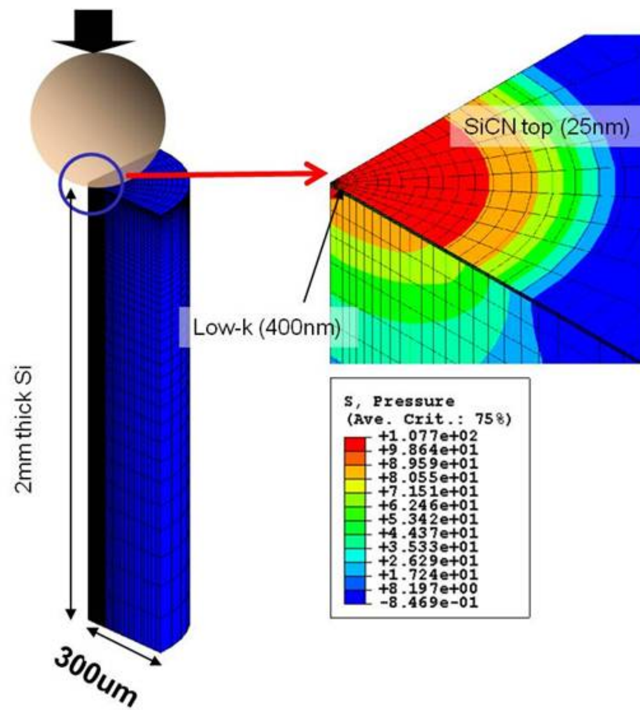

(a) Finite Element Mesh for ball indentation

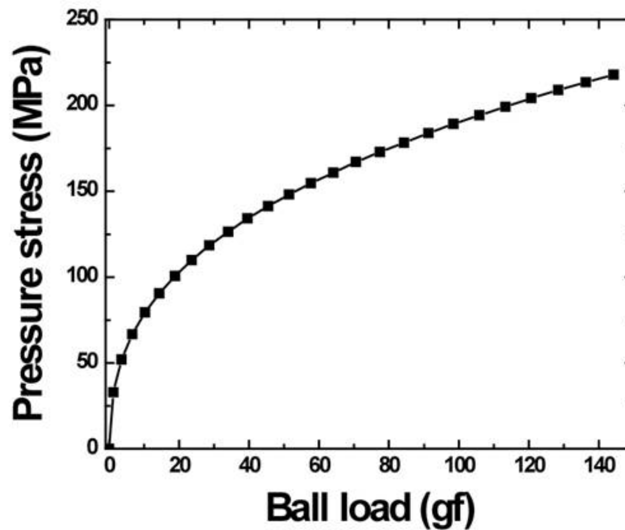

(b) The maximum pressure stress on PLK with ball loads

Figure 3.5 (a) Finite Element Mesh for ball indentation and (b) The maximum pressure stress on PLK with variation in ball loads at the elevated temperature (400˚C). The load is determined to produce 100 MPa ~ 200 MPa stress at PLK, which is actual stress level developed at real process.

Accordingly, as shown in Figure 3.5, the loads that we apply in our study were less than 100gf, corresponding to 120MPa~200MPa developed at real process.

The indentation surfaces were observed after each experiment using an optical microscope and using a Wyko model NT9100 optical profilometer equipped with Vision software. The mean of the residual indentation depths were measured by examination of at least 5 separate regions around the center of indented area on each specimen.

3.4 Sample Characterization

A lot of characterization techniques have been established to be able to obtain useful information with regards to the properties of low-*k* materials. These properties are of much importance because they determine the distinctiveness and hence the application of these PLK materials. The techniques that are used to characterize the films are: optical surface profilometer and Fourier transform infrared spectroscopy (FTIR). After indentation creep testing is completed, PLK samples are chosen for determination of indentation depth with optical surface profilometer as well as characterization of the change of chemical compositions using FT-IR.

3.4.1 Optical (3D) surface Profiler Meter

In order to determine the indentation depth of PLK films after the indentation creep testing, the measurements of the depth of indentation were conducted under a WYKO® optical profiler NT9100™. The WYKO® NT9100™ optical profiler combines non-contact interferometry with advanced automation for highly accurate, 3D surface topography measurements.

3.4.1.1 Working Principle

The working principle of the WYKO® optical profiler is shown in Figure 3.6 [187]. Light from the illuminator travels through the IMOA (Integrated Modular Optics Assembly) and downs to the objective (2.5X Michelson, etc.). A beamsplitter inside the

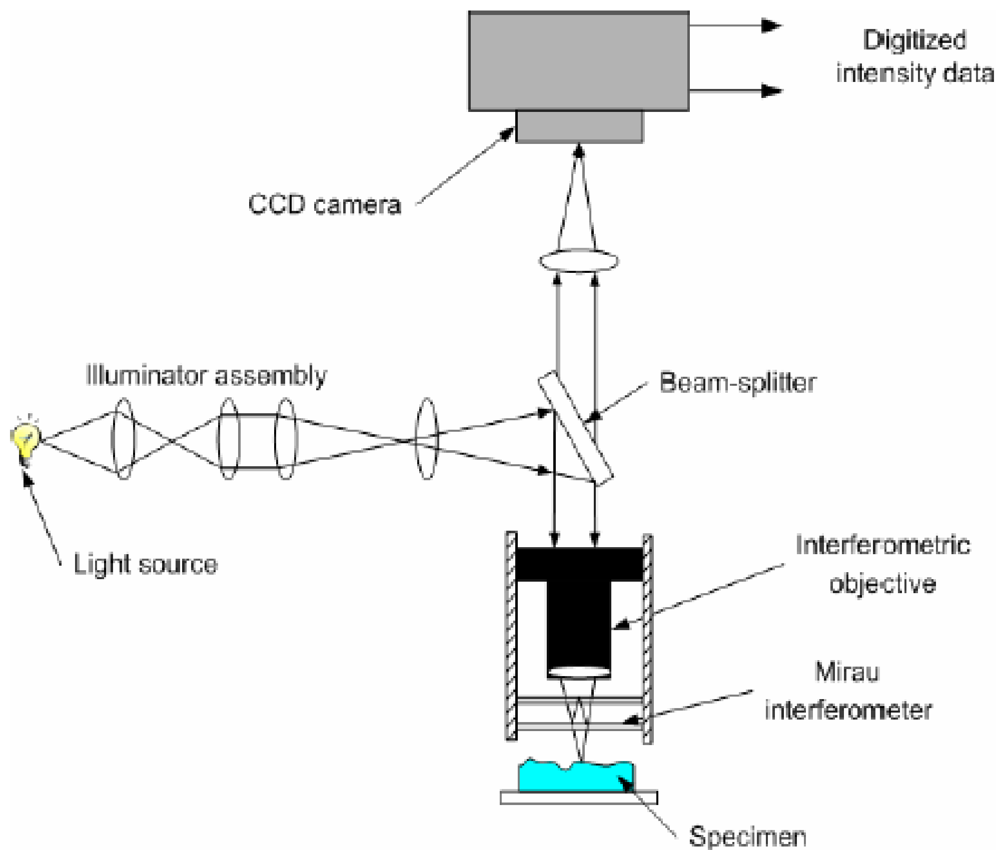

Figure 3.6 A schematic illustration of the working principle of the interferometric based WYKO® optical profiler [187].

objective splits the light into two beams. One beam, called reference beam, reflects from a super smooth reference mirror inside the objective. The other beam, called the test beam, reflects from the sample and back to the objective. When these two lights

recombine, an interference pattern is received by the camera, and the signal is transferred to the computer, where it is processed by Vision software. Vision then computes and produces a graphical representation of the sample surface. In our study, VSI (Vertical scanning-interferometry) mode was used to measure indentation depth and surface roughness. Vertical scanning-interferometry is a newer technique than phase-shifting interferometry. The basic interferometric principles are similar in both techniques: light reflected from a reference mirror combines with light reflected from a sample to produce interference fringes, where the best-contrast fringe occurs at best focus. However, in VSI mode, the white-light source is not filtered, and the system measures the degree of fringe modulation, or coherence, instead of the phase of the interference fringes. In vertical-scanning interferometry, a white-light beam passes through a microscope objective to the sample surface. A beam splitter reflects half of the incident beam to the reference surface. The beams reflected from the sample and the reference surfaces recombine at the beam splitter to form interference fringes. During the measurement, the objective moves vertically to scan the surface at varying heights. A stepper motor precisely controls the motion. Because white light has a short coherence length, interference fringes are present only over a very shallow depth for each focus position. Fringe contrast at a single sample point reaches a peak as the sample is translated through focus.

The system scans through the focus (starting above focus) at evenly-spaced intervals as the camera captures frames of interference data. As the system scans downward, an interference signal for each point on the surface is recorded. The system

uses a series of advanced computer algorithms to demodulate the envelope of the fringe signal. Finally the vertical position corresponding to the peak of the interference signal is extracted for each point on the surface.

3.4.1.2 Measurement of indentation depth in PLK with optical profiler

The indentation surfaces in PLK films were measured after each experiment using an optical microscope and using a Wyko model NT9100 optical profilometer equipped with Vision software.

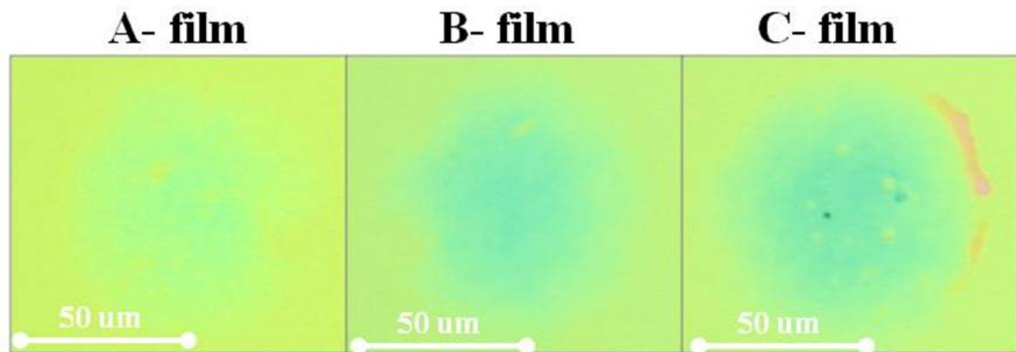

Figure 3.7 Optical microscope images showing the residual indentation regions in PLK films tested under 60gf at 400°C for 8 hours.

The profiler recorded the z-displacement for each point (x,y) on the surface of indented area. The vertical resolution (i.e. in z - displacement) of the measurement was ±0.1nm [187]. The magnification objective used was 20X, which has an optical resolution of ±0.38 um min. The mean of the residual indentation depths was measured by examining at least 5 separate regions around the center of the indented area on each specimen. Figure 3.7 shows the fractography images obtained by using an optical microscope in the PLK films tested under 60gf at 400°C for 8 hours. It can be seen that the PLK films are found to exhibit the residual indentation regions after test.

Figure 3.8(a) shows the observations of the indented area using the optical surface profiler in the PLK film exposed to plasma at the temperature of 400 ^{o}C under the constant load of 60gf for 8 hours in N_2 ambient. It can be seen that the surface of the PLK film is found to exhibit the change of color from its own color to blue in the indented area, inferring that the indentation depth of the PLK film has changed due to the plastic deformation with time during the ball indentation. Figure 3.8 (b) is a 3D image showing the topography and the hollow area after the indentation on the PLK film. Figure 3.8 (c) demonstrates a cross section line profile of the same indent as in Figure3.8 (a).

3.4.2 Fourier Transform Infrared Spectroscopy (FT-IR)

3.4.2.1 General Introduction and Fundamentals

Fourier Transform Infrared Spectroscopy (FTIR) is one of the most common spectroscopic techniques. Currently, this infrared spectroscopic technique has been employed for the identification and characterization of functional groups, as well as its molecular structure [188]. The main purpose of infrared (IR) spectroscopy analysis is thus to determine the chemical composition (functional group) of many organic and inorganic chemicals in the sample. The technique is based on the absorbance of IR radiation and is sensitive to bulk changes in the rotational, bending, and stretching vibrational modes of the molecules in the film.

When an infrared source with a broad band of different wavelengths of infrared radiation is focused on the sample, there is an interaction between IR radiation and molecules consisting of atoms and bonds in the sample. If the frequency (or energy) of

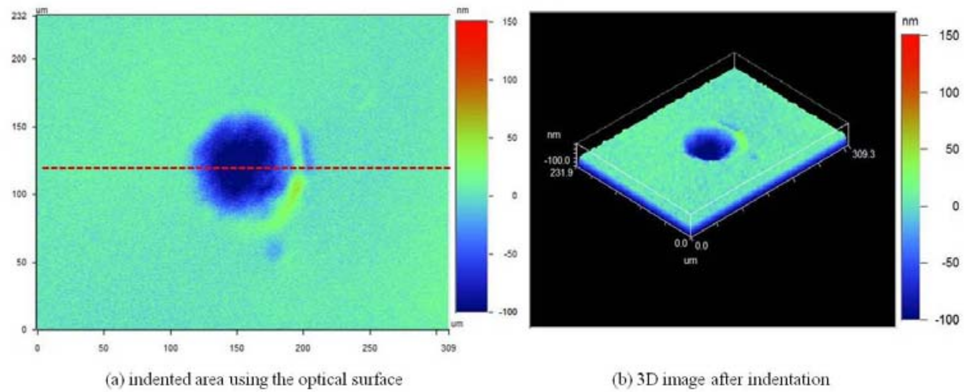

(a) indented area using the optical surface (b) 3D image after indentation

(c) demonstrates a cross section line profile

Figure 3.8 (a) A observation of the indented area using the optical surface, (b) a 3D image showing the topography and the hollow area in the indented area (c) a cross section line profile of the same indent along the red dash line as in Figure 3.8 (a).

the radiation matches the vibrational frequency (or energy) of the bonds between the atoms, radiation will be absorbed, causing a change in the amplitude of bond vibration. As a result, different functional groups absorb characteristic frequencies of IR radiation, and then identification of the composition can be made from the pattern of IR absorbed.

Figure 3.9 is a schematic view of an FTIR system. Its optical part is the Michelson Interferometer which is the common interferometer. It is comprised of three main parts: a moving mirror, a fixed mirror and a beam splitter as shown in Figure 3.8. The two mirrors are placed perpendicular to each other. The beam splitter is a semi-reflecting device which is typically made of KBr.

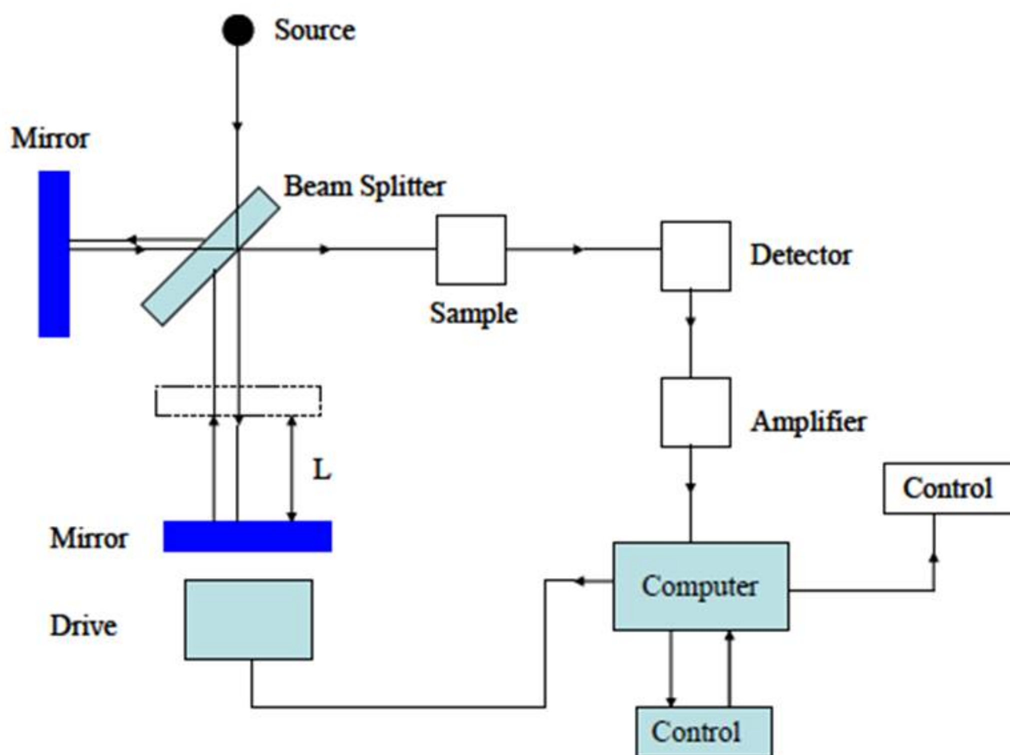

Figure 3.9 Schematic view of an FTIR system

The beam splitter splits the incident beam into two beams: half of the IR beam goes towards the fixed mirror and the other half towards the movable mirror. After reflectance upon the two mirrors, the split beam recombines at the beam splitter. If two paths are the same or different by an integral number of wavelengths for a given frequency, they add up together and result in constructive interference. Otherwise, they

result in destructive interference. As the movable mirror changes it positions relative to a fixed mirror, an interference pattern is generated. The computer collects the interferogram and performs Fourier transformation to obtain a spectrum with wavelength or wavenumber as the x-axis and absorption intensity or percent transmittance as the y-axis. The instrument used in this research was a Bruker Optics FT-IR spectrometers coupled with HYPERION Series FT-IR Microscopes. The spectrometer was purged with nitrogen to maintain a dry and clean environment during experiments. A 10 um IR beam spot size was available. MCT/A detector and KBr beam splitter were used for mid-IR (4000–400 cm^{-1}) data collection with a resolution of 4 cm^{-1}. The attenuated total reflectance (ATR) collection mode was used in our study. In addition, the sample spectrum was obtained by subtracting the background spectrum. OPUS software is frequently used to process the FTIR spectra. Depending on the materials that are characterized, peaks at certain positions should be zero. Baseline correction is a first and important step before fitting the FTIR data. In order to compare the FTIR spectra, the baseline must be consistent for all spectra.

3.4.2.2 FT-IR Techniques

Infrared spectroscopy has two modes: transmission mode and reflectance mode (or FTIR- Attenuated Total Reflectance (ATR) mode). At the transmission mode, the infrared beam penetrates the whole sample and the photon detector measures the light intensity for each wavenumber. Accordingly, the transmittance is calculated by the ratio of the transmitted and incident light intensities

$$T = \frac{I}{I_0} \tag{3.1}$$

where T is the transmittance, I_0 is the light intensity measured with no sample in the infrared beam (background spectrum) and I is the light intensity with a sample in the infrared beam (sample spectrum). According to Beer's Law, the absorbance is directly proportional to the concentration of molecules and the thickness of the film.

$$A = -\log(T) = a \cdot c \cdot t \tag{3.2}$$

where a is the absorbance, c is the molecular concentration, and t is the film thickness [189]. In the case of the absorbance, there are no standard tables so that we can only look at relative trends in the data without knowledge of the absorbance. Usually, a ratio of the intensity of spectral components is used to characterize the functional groups. This eliminates the need to know the thickness of the material.

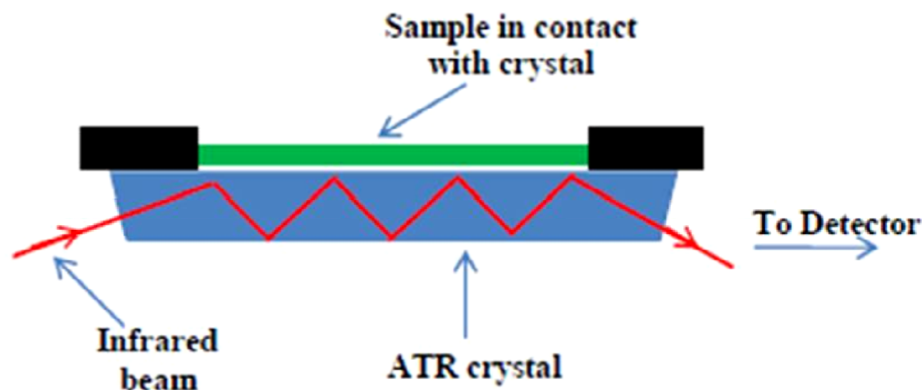

Figure 3.10 A multiple reflection ATR system.

For the ATR mode, as shown in Figure 3.10, it is an internal reflectance method which measures the alterations that occur in a totally internally reflected infrared beam when

the beam comes in contact with a sample. Also, the ATR mode is used in analysis of surfaces, powders, liquids, bulk materials, and samples that do not transmit sufficient light [188]. In Figure 3.9, an infrared beam is directed onto an IR transparent medium with high refractive index, normally Si or Ge, and if the angle of incidence is greater than the critical angle, the radiation will experience total internal reflection [188,190,191]. This creates an evanescent wave that can extend beyond the surface of the crystal into the sample with a penetration depth of only a micron (0.5 ~ 1 μm). The evanescent wave then will interact with the sample, which will absorb (Fig. 5.3a). Therefore the evanescent wave will lose energy at the absorption point and it will be attenuated. This is why it is called attenuated total reflectance (ATR). To optimize the contact between the sample and the ATR prism pressure has to be applied. Due to the small indented area of the PLK film after indentation creep testing, the transmission mode will be very challenging and a detailed analysis is needed to extract PLK dielectric signals from the indented area. In our study, the attenuated total reflectance (ATR) mode has been employed to characterize the indented area as well as the un-indented area in the same PLK film.

In Figure 3.11, the FTIR-ATR detector and optical image of the indented area are introduced. The ATR detector with the diameter of ~50μm can be placed directly onto the indented area for measuring because the diameter of the indented area is usually around 100μm.

3.4.2.3 FTIR Spectrum in PLK film

For porous low-k dielectrics, FTIR is also a popular technique for studying a chemical

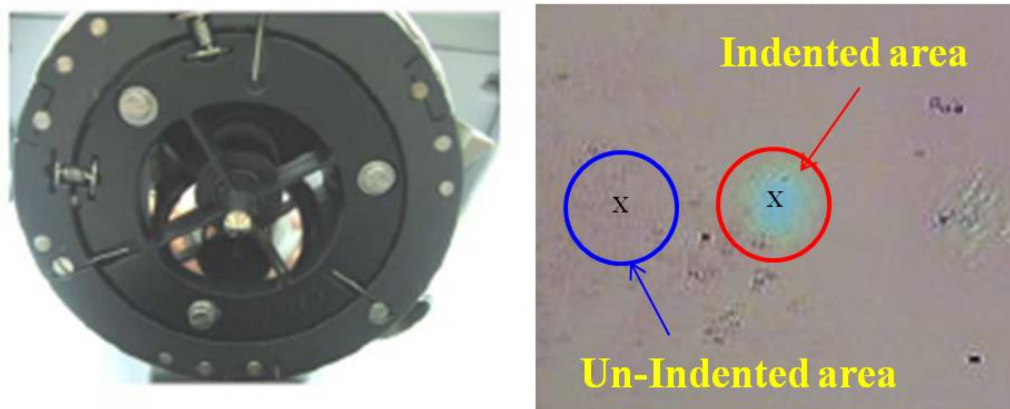

Figure 3.11 A FTIR-ATR detector positioning on the indented and un-indented area on PLK films.

composition and structure of porous low-k dielectrics [23]. Typical absorbance spectra of PLK films processed by PECVD are shown in Figure 3.12. A major fraction of the PLK skeleton is composed of Si-O-Si bonds, and their FTIR absorption is reflected in the band at 970–1250cm^{-1}. The vibrational frequencies of the broad anti-symmetrical stretch of Si-O-Si are dependent on the bond angle of Si-O-Si. The anti-symmetric stretch region for the Si-O-Si bond can be decomposed to find three distinct molecular units. These units are cage, sub-oxide, and network and the three individual peaks are 1135 cm^{-1}, 1063 cm^{-1}, and 1023 cm^{-1}, respectively. The absorbance peak around 2250 cm^{-1} is attributed to the H–functional group. CH_x terminating groups give rise to stretch bands in the region 2900–3100 cm^{-1}, the band around 1270 cm^{-1} is attributed to -CH_3 groups, and those at 750 –870 cm^{-1} are from the Si–CH_3 rocking mode. A broad band can be observed at about 3200 and 3700 cm^{-1}, which is attributed to the vibration of -OH groups in the form of Si-bonded OH group.

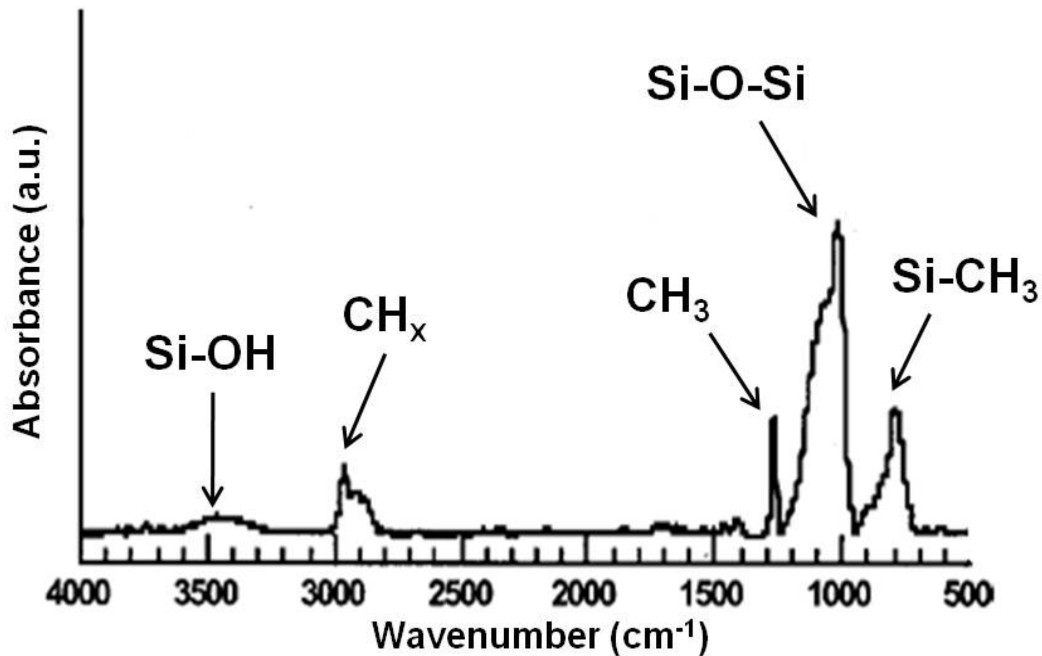

Figure 3.12: Typical FTIR spectrum for PLK film showing various functional groups at specific wavenumbers [192].

This broad peak is usually a result of moisture adsorption/formation of –OH group and is due to the vibration of silanol groups (Si–OH) and H_2O molecules. This is especially important because H_2O (around 3600 cm-1) is a polar molecule and is detrimental to both the real and imaginary part of the *k* value. Table 3.2, shown below, contains the FTIR peak assignments for low-k films. It was taken from Grill and Neumayer [61].

Table 3.2 FTIR assignment of the structures in low-k materials [61]

TABLE II. FTIR peak assignments. Major contributors are listed first for each vibration. ν=stretching, δ=bending, ρ=rocking, a=antisymmetric, and s=symmetric.

TMCTS	$k=2.8$	$k=2.05$	Mode	Comment	References
2968	2969	2968	ν^a C–H_3	sp^3 CH_3	15–18, 32
2906			ν^s C–H_3	sp^3 CH_3	15–18, 32
	2916	2932	ν^a C–H_2	sp^3 CH_2	15–18, 32
	2880	2875	ν^s C–H_2	sp^3 CH_2	15–18, 32
	2232		ν^s Si–H	H–SiO_3	8–14
	2178		ν^s Si–H	H–SiO_2Si	8
2165			ν^s Si–H	H–SiOSi	8
		1740, 1714	ν C=O	As deposited only	15
		1461	δ C–H_2	CH_2 isolated from Si	15, 35
1405	1412	1412	δ^a C–H_3	$SiMe_x$	15–19, 32
	1358	1379	δ C–H_2	Si–CH_2–Si	15–19
1259	1273	1274	δ^s C–H_3	$SiMe_x$	15–19, 26, 32, 36
	1135	1140	ν^a Si–O–Si	Cage	9–10
				Si–O–Si angle ~150°	11–13, 20
			ν C–O	Si–O–C	16, 24, 25
1063	1063	1065	ν^a Si–O–Si	Network (network)	9, 10
				Si–O–Si angle ~144°	
	1023	1035	ν^a Si–O–Si	Silicon suboxide,	21, 22, 23
				Si–O–Si angle <144°	
				D_{3h} ring structure	16, 17
	890		δ H–Si–O	H–SiO_3	8–14
			ν Si–C, ρ^s CH_3	$SiMe_2$	15–18, 19, 24, 33
865			δ H–Si–O	H–SiO_2Si	8
	848	843	δ H–Si–O	Network smaller angle	10, 12–14, 35
			ν Si–C, ρ^a CH_3	$SiMe_3$	15–19, 24, 26, 33
	802	800	ν Si–C, ρ^a CH_3	$SiMe_2$	15–19, 24, 33
754			ν Si–C, ρ Si–CH_3	$SiMe_1$	
	773	779	ν Si–C, ρ CH_3	$SiMe_1$	18, 24, 36
			ν Si–C, ρ^s CH_3	$SiMe_3$	15–19, 24, 33
710	730	720	ν^s Si–O–Si		11, 12, 13
	440	440	δ of O–Si–O	Network and ring opening vibrations	11, 12, 13

CHAPTER 4

STUDY OF THERMAL-MECHANICAL INSTABILITY OF POROUS LOW-K DIELECTRICS

4.1 Introduction

Successful integration of porous low-k dielectrics (PLK) in Cu interconnect structures is considered to be one of the key technical advancements in microelectronics [23,193]. The incorporation of PLK is necessary to preclude interconnect RC delay from becoming the performance-limiting factor in the back-end-of-the-line (BEOL) interconnect [21]. While there is a significant research effort to develop successful PLK technology, the progress has been slow with various reliability failures with unforeseen nature. Among many concerned properties of PLK in relation to the reliability is the thermal and mechanical stability of PLK film itself. During manufacturing process of interconnect structure, the dielectric constant of porous low-k material is determined by the introduction of pores into the already existing inter-layer material. Accordingly, it is a prevailing belief that PLK exhibits sufficient stability against thermal and mechanical load during the interconnect processing owing to the strength provided by the cross-linked bond networks [113]. The high degree of cross-linked networks in PLK film are generated by plasma-enhanced chemical vapor deposition (PECVD) and crosslinking usually occurs through Si–Si, Si–O–Si, Si–CH_2–Si, and Si–CH_2–O–Si by rearranging their chemical bond structure during curing the as-deposited films. However, it is found

from our previous study that the pores are not necessary stable based on the observations of diffusivity change of tracer ions after thermal annealing of interconnects with voltammetry technique [114], and that the PLK instability is indeed active and is triggered by thermo-mechanical stresses developed into the dielectric layers due to the CTE mismatch between inter-layer PLK dielectrics and Cu [116], yet the exact mechanism of thermo-mechanical instability of PLK dielectrics behind such behaviors are not well understood.

The primary objective of this chapter is thus to identify the mechanism leading to thermo-mechanical instability of PLK dielectrics observed in Cu/PLK interconnects. Since the low-k materials with k lower than 2.3 are required to respond to the scaling down of device dimension beyond 32-nm technology node [21], pores must be introduced into these existing low-k matrices to effectively achieve this dielectric constant values. However, porosity in a material reduces its mechanical strength and increases its active surface area, thus, making these films vulnerable to plasma damage and to moisture adsorption when the property of film is changed to hydrophilic.
Also, a low-k material must have compatibility with a variety of integration processes, especially plasma-based processes such as etching, cleaning and ashing because they are widely used for the small physical size of trench and via lines in advanced Cu/PLK interconnects, as well as the removal of the residues after photoresist(PR) strip and etching. However, many studies have made on the plasma-induced damage when PLK is exposed to plasma [94-104]. The plasma treatment tends to degrade the PLK by removing methyl(CH_3) groups, resulting in silanol(Si-OH) formation, film densification

and dangling bonds defects, increase of the dielectric constant values of low-k materials [194].

In order to properly cope with the reliability problems of PLK, it is also important to understand the impact of porosity as an intrinsic factor and extrinsic factor such as plasma damage on thermal and mechanical instability of PLK. As a result, the second objective, which is also the primary focus of this study, is to investigate the influence of such intrinsic and extrinsic factors on thermal and mechanical instability of PLK and reveal the associated mechanism. However, with lack of proper characterization techniques, the possibility and mechanism of plasticity in PLK films has not been properly accessed. For this, we introduce indentation creep test that examines the existence of thermo-mechanical instability in PLK dielectrics. Our study with the indentation creep test finds that PLK films indeed plastically deforms with time and that the viscoplasticity of PLK dielectrics varies significantly with porosity (intrinsic factor), plasma damage (extrinsic factor). Furthermore, testing at various relevant load (40gf ~100gf) and temperature (300˚C~400˚C) conditions of PLK processing reveals that all investigated PLK films deform by viscous flow, and that the deformation occurs with unexpectedly low activation energy (1.27eV to 1.5eV). This suggests that the viscous flow of PLK is controlled by chemical reaction happening in PLK matrix. Based on the FT-IR characterization, it is found that Si-OH or Si-H is acting as catalysis. From these findings, we believe that such thermo-mechanical instability is fundamentally driven by viscous flow but influenced significantly by the existence of incomplete bond-networks, silanol(Si-OH) or Si-H, within porous low-k

dielectrics. This chemically assisted viscous flow mechanism may explain the low activation energy of viscoplstic deformation and an extreme dependence of the deformation kinetics on extrinsic factors. This chapter displays experimental and characterization data supporting of our findings.

4.2 Experimental

The PLK samples used in our study were made using industry standard PECVD processes, SiCOH films deposited by PECVD on the Si wafer with the thickness of 400nm. PLK films of three types described in chapter 2 were used in this study. These films do have variation in porosity (effective k~2.4, 2.2), controlled plasma exposure. These films allow us to examine the effect of intrinsic (porosity) and extrinsic (plasma damage) factors on the mechanism of viscoplasticity. The method of a ball indentation creep test we developed is very simple but helpful in revealing the thermo-mechanical instability of porous low-k dielectrics. In our technique, 20mm diameter Alumina ball with static weight is placed on top of 400nm PLK films. The weight is controlled to produce 100-150MPa pressure stress on the film in order to simulate the stress that PLK/Cu interconnect (with PLK width smaller than 100nm) experiences during integration process. The whole test assembly, the ball with weight and PLK film on Si substrate, is in a chamber where temperature and environmental conditions can be controlled. Our test routine is to 1) evacuate with N_2 gas purge cycle at room temperature without making contact between the ball and substrate, 2) raise the temperature of Si substrate to 300 ˚C - 400 ˚C, and 3) apply load to PLK film by bringing the ball into contact with the film. The indentation surfaces in PLK films were

observed after each experiment using an optical microscope and then, the depth of indentation was determined by using a Wyko model NT9100 optical profilometer equipped with Vision software. The mean of the residual indentation depths were measured by examination of at least 5 separate regions around the center of indented area on each specimen.

FTIR spectra were measured on Bruker Optics FT-IR spectrometers coupled with HYPERION Series FT-IR Microscopes to examine the chemical bonds reconfiguration of PLK films. The spectrometer was purged with nitrogen to maintain a dry and clean environment during experiments. A 10 um IR beam spot size was available. MCT/A detector and KBr beam splitter were used for mid-IR (4000–400 cm^{-1}) data collection with a resolution of 4 cm^{-1}. Due to the small indented area of the PLK film after indentation creep testing, the transmission mode will be very challenging and a detailed analysis is needed to extract PLK dielectric signals from the indented area. In our study, the attenuated total reflectance (ATR) mode has been employed to characterize the indented area as well as the un-indented area in the same PLK film.

4.3 Results and Discussions

4.3.1 Observation of viscoplastic deformation in PLK films

With the availability of this simple yet helpful ball indentation method in revealing the thermo-mechanical instability of porous low-k dielectrics, various investigations are possible. A series of topography images shown in Figure 4.1 presents the highlights of our investigation and clearly evidences the occurrence of viscoplastic deformation (or time-dependent plastic deformation) in PLK films and its sensitive dependence on PLK conditions. It can be seen that all PLK films are found to exhibit the change of color from their own color to green or blue in the indented area, inferring that the indentation depth of films is changed due to the plastic deformation of PLK films during a ball indentation. Also noteworthy is the fact that the same PLK films but having a lot less porosity (k=2.7) do not show any viscoplasticity when tested at the identical condition. Many similar indentation tests are conducted at various load and temperature conditions and principle behavior shown in Figure 4.1 is found to be maintained.

In order to make more quantitative measure of viscoplasticity, the indentation depth is measured, as it is the reflection of true vioscoplastic deformation. Figure 4.2 shows example results. It can be seen that the indentation depth result is consistent with the basic behavior shown in Figure 4.1. Notice that the rate of indentation depth increase is not linear with time but shows saturation behavior. Also, it is found that an increase of porosity results in the larger indentation depth compared to PLK film (A film) with lower porosity, confirming that the stability of PLK film is strongly dependent on the porosity associated with intrinsic strength of the PLK film.

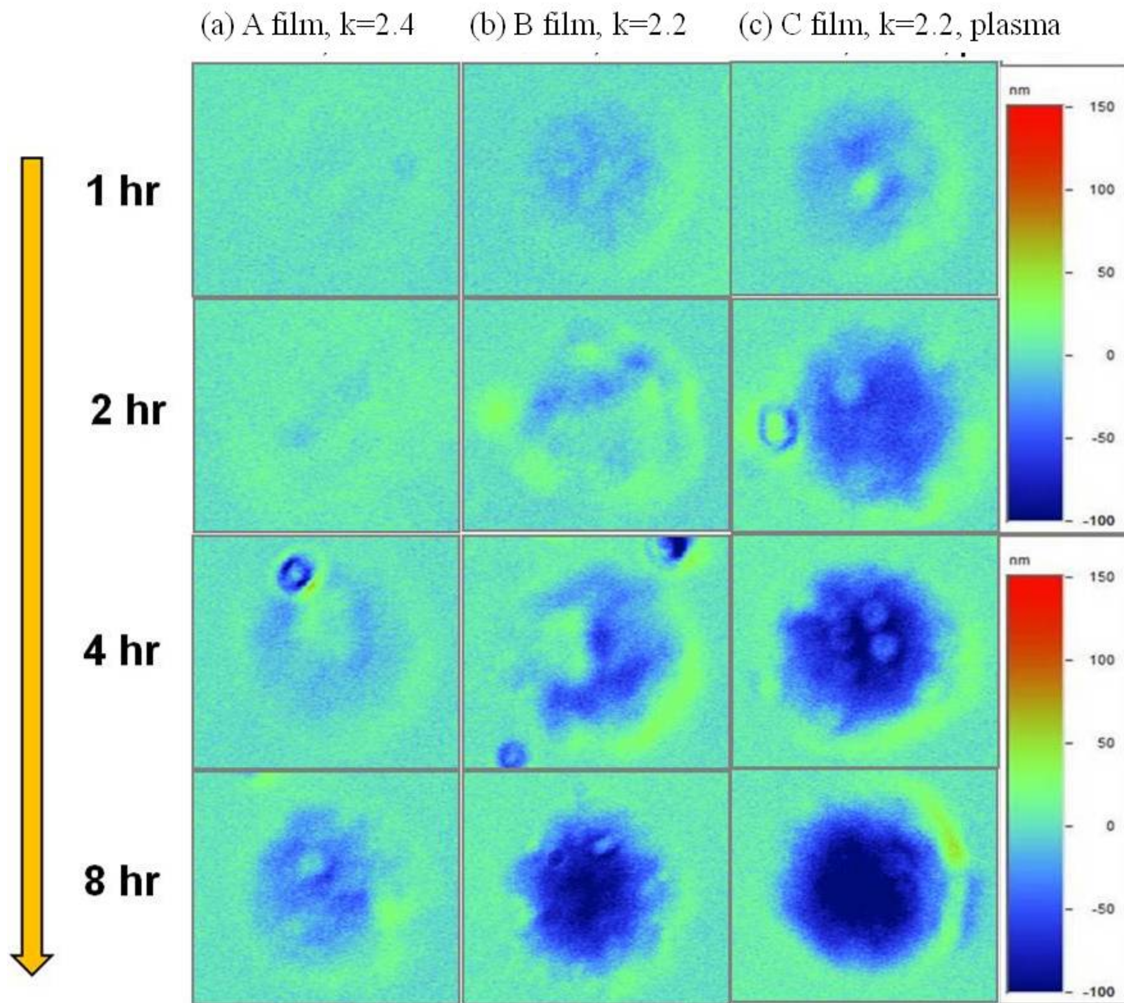

Figure 4.1 Surface topography images showing an indentation mark on a) as-prepared k=2.4, b) as-prepared k=2.2, c) the same film as b) but exposed to plasma. The indentation test is done at 400°C under 60 g loads on 20mm Alumina ball indenter.

Notice also that as shown in Figure 4.2 (b), the considerable increase of indentation depth in the PLK film exposed to plasma(C film) is observed while the B PLK film without exposure to plasma exhibits a smaller deformation at an identical porosity and composition. It is clearly pointed out that plasma damage makes PLK films to be more sensitive to viscoplasticity. This is consistent with current understanding of the fact that plasma exposure can significant damage in PLK materials due to the loss of carbon content and/or hydrophilization, resulting in the increase of dielectric constant k values. Therefore, on the basis of results shown in Figure 4.1 and 4.2 through the ball indentation creep test, it is reasonable to conclude that viscoplastic deformation does occur, resulting in the thermo-mechanical instability in PLK films. Furthermore, it is our belief that the PLK instability is significantly affected by the content of porosity and plasma treatment as an intrinsic and extrinsic factor, respectively.

4.3.2 Kinetics model for the ball indentation creep test

According to established theory on the ball indentation (viscous flow of glass), the indentation depth (h) increases with time (t) following kinetic relation [172]:

$$h(t)^{3/2} = \frac{9}{32\eta(D)^{1/2}} Ft \qquad (4.1)$$

where F, η, and D denote the load, viscosity, and ball diameter respectively. It is found that this kinetic equation fits to our data exceptionally well as shown in Figure 4.3.

This result may indicate that the viscoplastic deformation in PLK films occurs by the mechanism of viscous flow at the given temperature and load conditions.

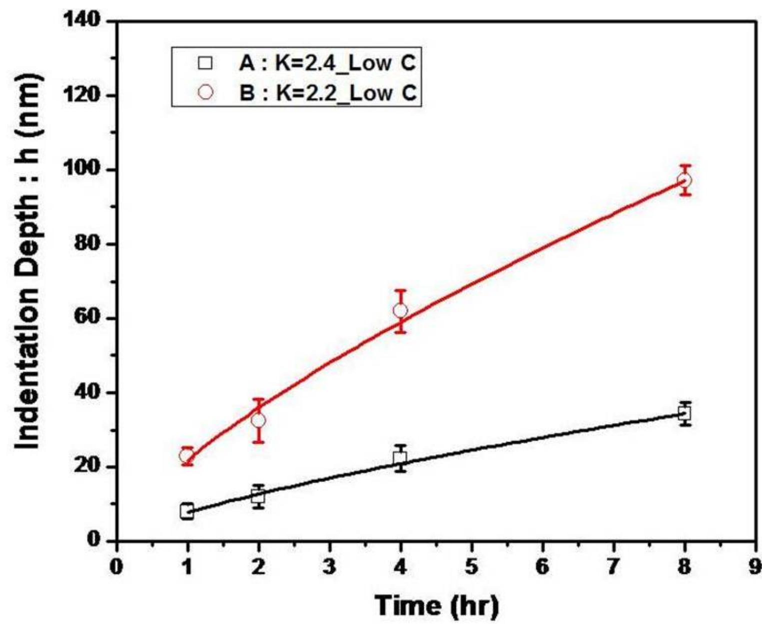

(a) effect of porosity

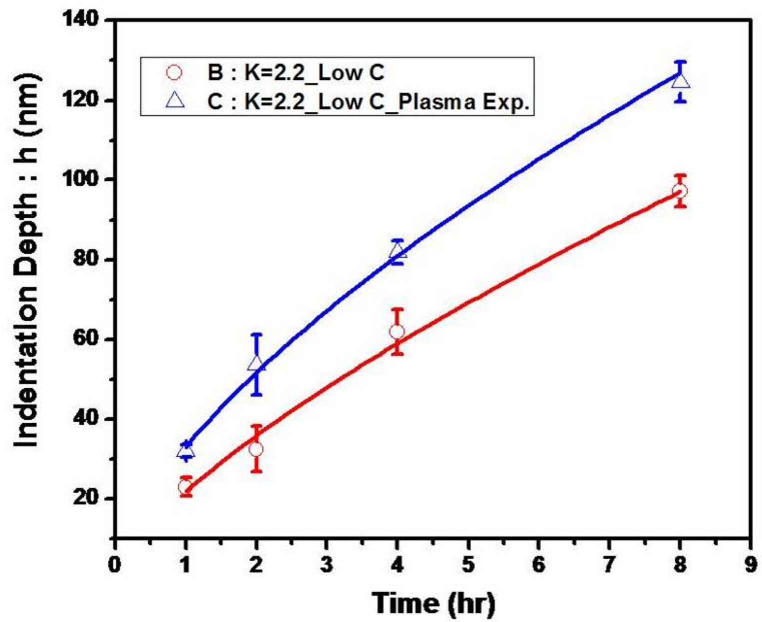

(b) effect of plasma damage

Figure 4.2 Indentation depth of films measured with time at 400C under 60g load, demonstrating (a) effect of porosity and (b) plasma damage on the viscoplasticity of PLK films.

Considering the fact that PLK material is amorphous material based on silicate backbone and the kinetic theory is developed specifically for the viscous flow of glass material in a ball indentation, the viscoplasticity by the viscous flow appears to be reasonable. Additional supporting evidence is found from the deformation behavior of PLK itself. Close inspection of PLK after ball indentation reveals the existence of build-up mass around the indentation mark (yellow ring around indentation mark in Figure 4.1). This is the area where mass of PLK is extruded while indentation proceeds. This behavior is very much in consistent with the deformation mechanics of Newtonian fluid by viscous flow.

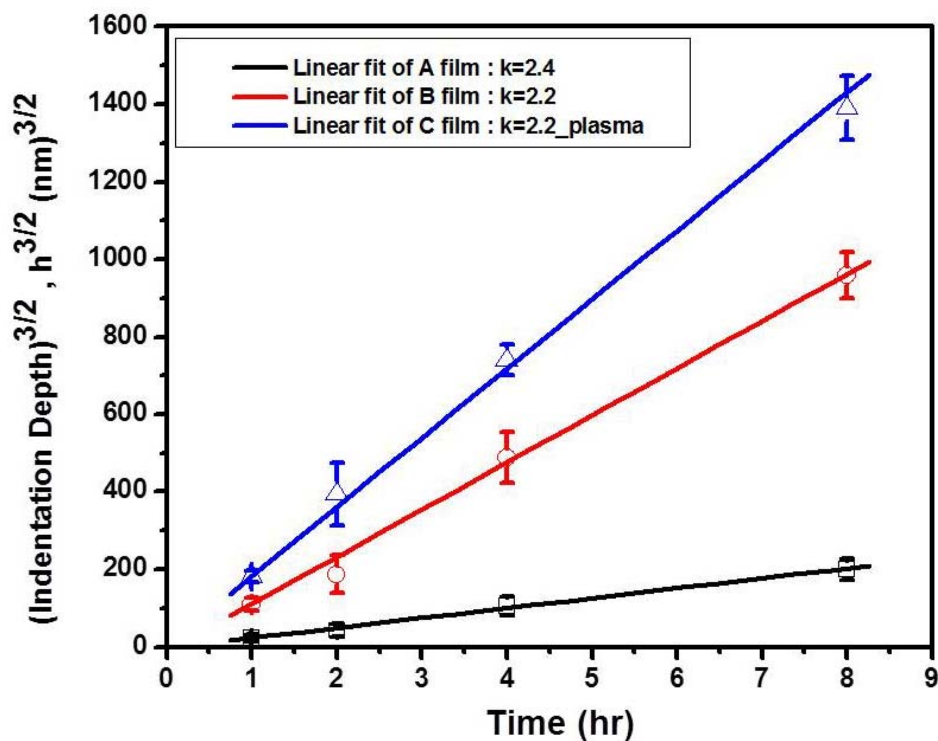

Figure 4.3 A plot showing $h^{3/2}$ vs. time of the data shown in Figure 4.2.

4.3.3 Stress dependence

For given PLK materials, different creep (or viscoplastic deformation) mechanisms may be operative at different temperatures and stress levels. In order to identify more insights into the time-dependent properties of the sample materials, it is desirable to achieve the relationship between the strain rate and the applied stress during creep time. In the uniaxial tests, the steady-state behavior of a wide range of materials can be expressed by

$$\dot{\varepsilon} = A\sigma^{n} \tag{4.1}$$

where $\dot{\varepsilon}$ and σ are the uniaxial strain-rate and uniaxial stress, respectively. A is a constant for a given material and temperature, and the quantity n is known as the stress exponent for creep.

In the conventional uniaxial creep tests, either the stresses or the strain rates are kept constant. Indentation creep tests, however, are different with traditional uniaxial tests in several ways. First, the developed stresses in an indentation test include multiaxial compressive stress. The strain rates experienced in an indentation test are also much more complex and may cover a wide range, especially at the beginning of the indentation [144]. Despite all the differences, The Equation (4.1) can be equally valid for the indentation creep test with a self-similar indenter (Ball indenter in this study) in which the strain rate and applied stress obey equivalent relations that have been verified by a number of previous theoretical and experimental studies [141,166,195,196]. Tabor [166,197] first proposed an empirical equivalent strain concept, which was validated by

Bower *et al* [141] through both theoretical modeling and finite element analysis. Storåkers and Larsson [195] extended the work of Hill [196] on the contact mechanics of the indentation process and also determined that the indentation creep could be defined by an equivalent indentation strain rate. For a ball indenter, the strain rate in Equation (4.1) can be substitute by an equivalent strain rate defined as

$$\dot{\varepsilon} = \frac{1}{D}\frac{da}{dt} \tag{4.2}$$

where D(=2R) is the diameter (radius) of the ball indenter, a is the contact radius and t is indentation creep time. However, instead of measuring a contact radius a, it is possible to use the indentation depth (h) with time using this relation: $a^2 = h(2R-h)$, if R>>h, $a^2 = 2Rh$ and $ada = Rdh$ (refer to chapter 2). Equation (4.2) can be rewritten in the following form in the ball indenter:

$$\dot{\varepsilon} = \frac{1}{2\sqrt{hD}}\frac{dh}{dt} \tag{4.3}$$

During indentation creep test the indentation pressure, p_s, under the ball indenter, can be expressed as a function of the indentation depth (h) at the constant load (F):

$$p_s = \frac{F}{\pi a^2} = \frac{F}{\pi h(D-h)} \tag{4.4}$$

Supposing that D >> h, where D (=2R) is the diameter of the ball indenter, Equation (4.4) can be expressed in the following form:

$$p_s = \frac{F}{\pi hD} \tag{4.5}$$

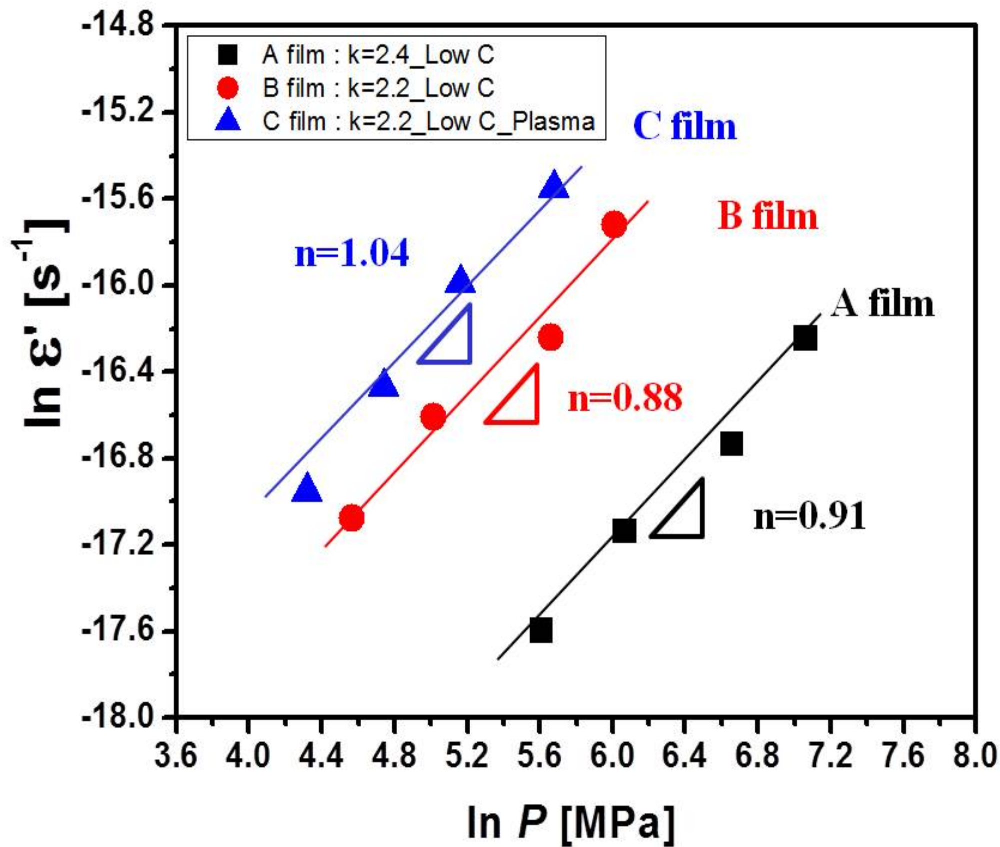

Figure 4.4 A plot showing the determination of stress exponent from the indentation creep data for 3 different PLK films.

Equation (4.3) and (4.5) reflect the strain-rate of materials and applied pressure, respectively, underneath the ball indenter, which can be used to investigate the behavior of plasticity with time, especially stress exponent (n), of PLK. Due to the geometry of the ball indenter, the pressure (or stress) changes with time because the contact area also changes with time. The applied stress changes under the ball indenter, meaning that several stress-strain rate pairs from one indentation testing can be obtained in the case when the indentation depth can be recorded continuously. Accordingly, in order to

determine the stress exponent in given PLK films, the indentation test was conducted for different creep times (1~8 hours) under constant load of 60gf and temperature of 400°C. By obtaining the strain rate and the pressure stress from the indentation data by using Equations (4.3) and (4.5), the stress exponent *n*, which reveals the creep properties and mechanisms of the given PLK materials, can be extrapolated from the slope of log (pressure stress)-log (strain rate) data plotted from equation (4.1). As shown in Figure 4.4, the evaluated stress exponent for 3 different PLK films is found to be very close to unity. This result indicates that PLK films deform by Newtonian viscous flow at the given load and temperature conditions, confirming that the plastic deformation behavior with time in PLK films fits well to the kinetic model developed for viscous flow materials under the ball indentation.

4.3.4 Temperature dependence

Since the temperature used in our experiment may be far lower than the glass-transition temperature which has not been reported yet for PLK materials, it is difficult to explain the data solely based on the viscous flow mechanism. For this reason, further consideration of plasticity with the related viscosity at these temperatures is necessary to explore the mechanism leading to the time dependent plastic deformation of PLK films behind the viscous flow as state above.

To investigate the temperature dependence on the instability of PLK films, the indentation creep test was conducted at various temperatures (300°C ~400°C) under the constant load of 60gf. If the viscous flow of PLK films is considered as a thermally

activated phenomenon, the temperature dependence can be described by an Arrhenius relation defined by the subsequent equation:

$$\frac{\partial \ln \eta}{\partial (1/T)} = \frac{Q}{R} \tag{4.6}$$

where η is the viscosity, Q is the activation energy of viscous flow, R is the ideal gas constant, and T is the temperature. By using the kinetic Equation (4.1) for the determination of viscosity from the penetration of a ball indenter under constant load, the viscosity of PLK films can be also easily determined. Based on the experimental data acquired through a ball indentation test, the activation energy of the viscous flow of PLK materials is calculated from the values of viscosity at different temperatures.

Figure 4.5 exhibits the topography images observed for PLK films after indentation creep testing with variations in temperature for 8 hours under the constant load of 60gf. It can be clearly seen that all PLK films do show film instability at temperature above 300°C. It is also observed that C film exposed to plasma presents the worst stability, while A film with lower porosity shows the best stability among the tested PLK films. This observation suggests the extreme dependence of PLK film stability on temperature, as well as PLK film conditions.

Figure 4.6 shows a logarithmic plot of viscosity of dense, porous and plasma-damaged PLK samples as a function of inverse temperature. The activation energies extracted in our study exhibit from 1.27 to 1.45eV in the range of 300 ^{o}C ~400 ^{o}C. According to research on glass materials, its activation energy of viscosity is usually above 4.0eV due to the existence of stable and strong ionic or covalent bonds.

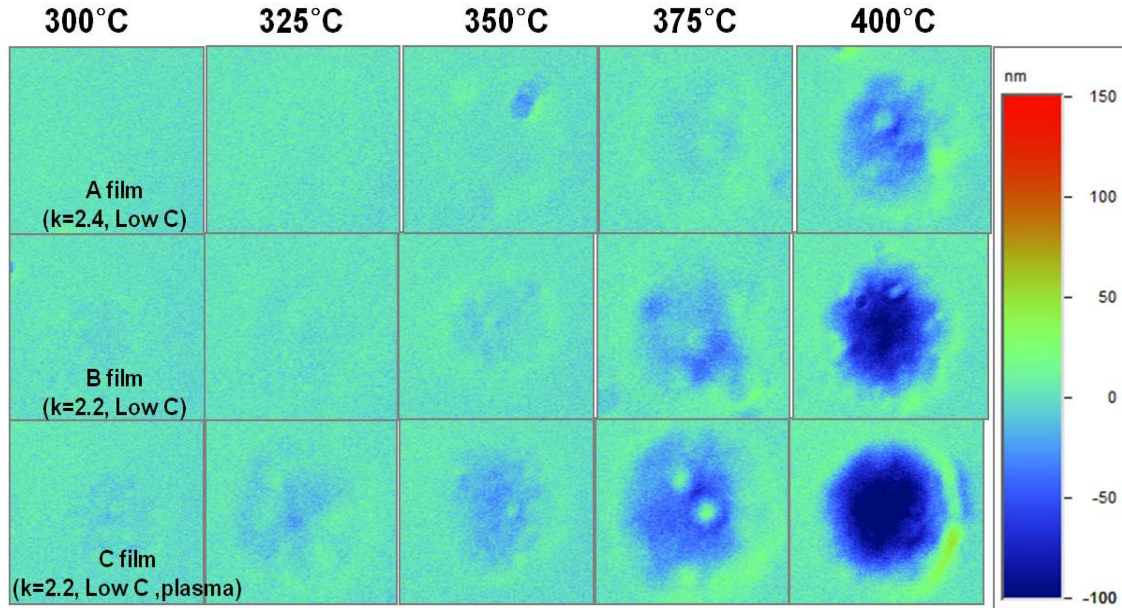

Figure 4.5 Surface topography images showing variations in the indentation depth as a function of temperature for three different PLK films. The indentation test is done at the constant load of 60g for 8 hours.

However, in the case of PLK films, the activation energy of the viscosity that is calculated back from the kinetic equation is too low. The fact that the activation energy of PLK's viscosity is far lower suggests that the viscoplasticity of PLK films is not pure viscous flow but assisted by some other mechanisms. The extracted activation energies for PLK films are similar to that of the energy barrier, which is about 1.5eV [199], combining H_2O molecules diffusion with an activation energy of 0.8~0.9eV [198] and Si-OH (silanol) formation with 0.3~0.7eV by reaction between water molecules and Si-O-Si bonds in amorphous SiO_2 [199]. It is also important to note that water molecules can form from the condensation reaction with Si-OH groups resulting from PLK film itself during the post annealing process [192, 200], despite efforts of vacuum and

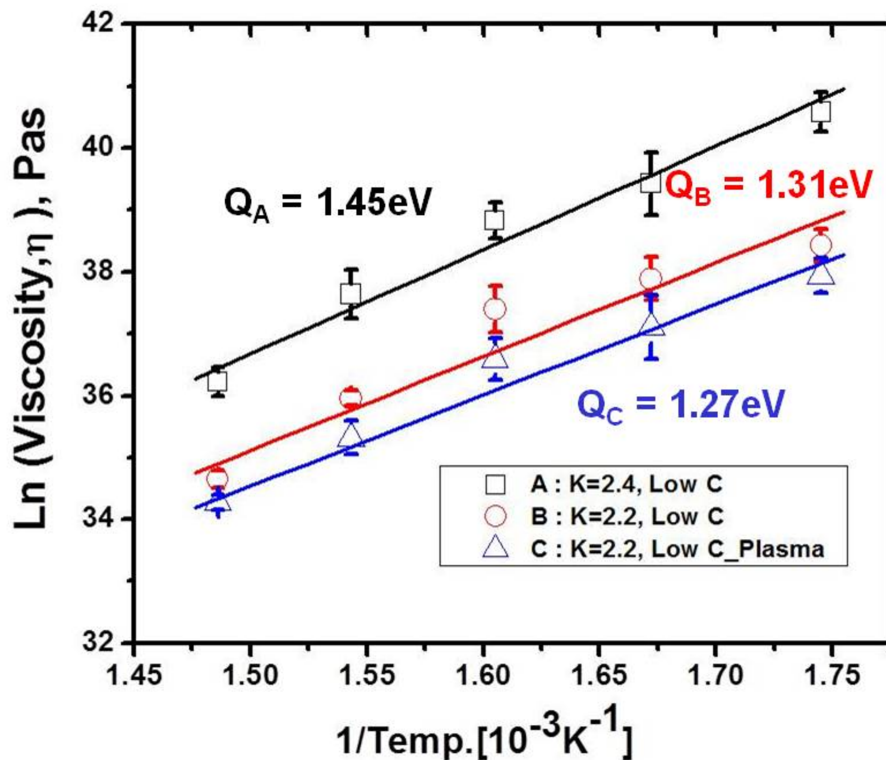

Figure 4.6 A plot showing the viscosity as a function of temperature for 3 different PLK films.

degassing which are conducted in our study, as well as the water absorption from integration processes. This is due to the fact that the formation of Si-OH groups already occurs, mainly as terminal bonds in PLK films, afterPECVD and annealing process. As a result, even if it is assumed that the existing water molecules are completely removed by evacuation and purging process, since thermal annealing process produces a certain amount of hydroxyl groups as by-product, the formation of water molecules is considered to be inevitable by condensation of proximal Si-OH groups during subsequent annealing of PLK film. Moreover, trapped moisture may be remaining due to Si-OH buried deep inside in the film that the N_2 purging gas cannot reach.

Accordingly, it is possible that the diffusion of water and reaction with siloxane bonds (Si-O-Si) with energy barrier of 1.5 eV, generate new two silanol groups even at low temperature(~400 ^{o}C)[201]. Since the concentration of Si-O-Si bonds cross-linked with the covalent bonds has a significant role in determination of creep occurrence, the formation of Si-OH responsible for the breakage of Si-O-Si bonds due to the reaction with water can be brought to deformation even under relatively low temperature and applied load. Furthermore, T. Bakos et al.[199] suggested that the continuing diffusion-reaction process for long time to reach equilibrium would make the silanol groups considerable because of the low formation energy with 0.3~0.7 eV, indicating that the deformation of PLK film can keep occurring until reaching an equilibrium state.

In addition, it should be noteworthy that an increase in Si-OH groups at the surface of films would be able to give a rise to a significant degradation of the thermo-mechanical properties due to the facts that the reconfiguration of bond network chains by the formation of silanol groups results in the transition of chemical nature from hydrophobicity to hydrophilicity, as well as the collapse/coalescence of the existing pores in the PLK film. Therefore, based on the result of temperature dependence in PLK films, we believe that such viscoplasticity is catalyzed by the chemical evolution in incomplete bond-networks, especially Si-OH groups, within PLK structure in the given relatively low temperature.

At elevated temperature where PLK structure become very weak, however, it should be noted that the activation energy for viscoplastic deformation and other constitute parameters, especially pre-exponential factor (η_0) representing the vibration

frequency of atoms, will become similar between PLK and SiO_2 because they have very similar base structure. According to creep kinetics theory [202], there are two theorem explaining creep kinetics, parallel and serial. In parallel theorem, the fastest deformation mechanism determines the creep kinetics. In serial theorem, the slowest mechanism determines the kinetics. In our study, since our suggestion is that the viscoplastic deformation is assisted by the chemical evolution due to the formation of Si–OH from H_2O present in the PLK film, the bond reconfiguration generated by the chemical reaction between H_2O and Si-O-Si bonds will determine the creep rate, which is serial. But at elevated temperature where silicate backbone structure is very weak, therefore, the resulting Si-OH formation created by the chemical reaction between H_2O and Si-O-Si bonds is not necessary for its viscoplastic deformation, which is parallel.

4.3.5 FT-IR (Fourier Transforms Infra-Red) Spectroscopy analysis

Although our investigation finds that PLK dielectrics shows the considerable viscoplastic deformation and it occurs by the viscous flow which is enhanced by the chemical evolution, further investigation is necessary to provide complementary evidence supporting the mechanism. In particular, identifying the chemical bond changes using FT-IR (Fourier Transforms Infra-Red Spectroscopy) is required to explain the details of bond reconfiguration which is responsible for the viscous flow.

Figure 4.7 shows the variation of the absorbance spectra collected from the unindented and indented areas over the range of 4000–750 $cm^{-1}$of PLK films after indentation creep test for 8 hours.

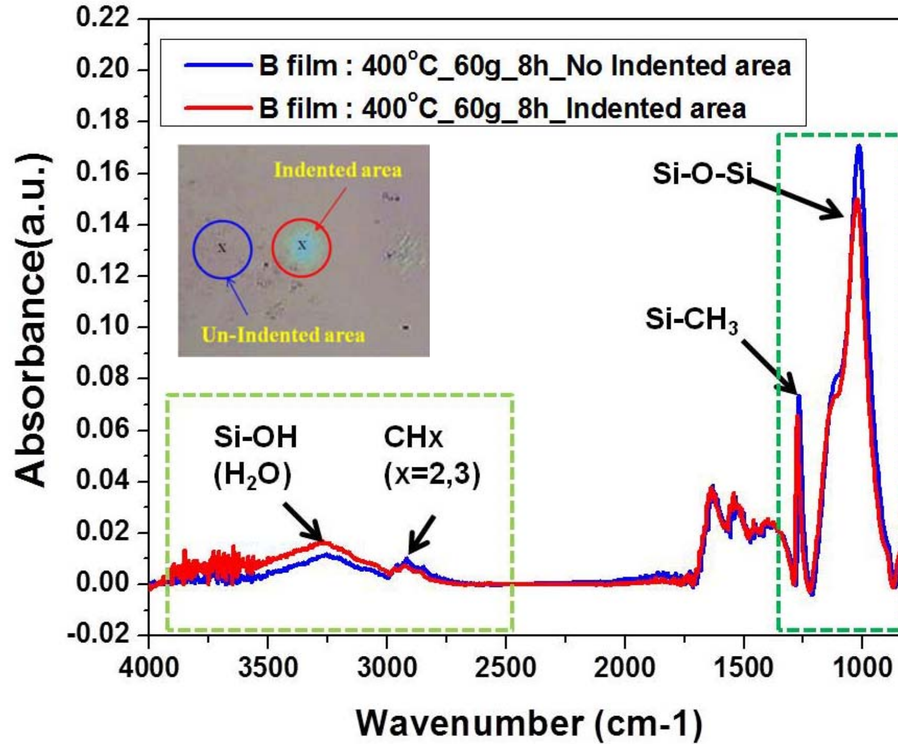

Figure 4.7 FTIR spectra of A PLK film showing the difference in chemical bonds for the unindented and indented region after indentation creep test over the range 4000-750 cm^{-1}.

A major fraction of the PLK skeleton is composed of Si-O-Si bonds, and their FTIR absorption is reflected in the band at 970–1250cm^{-1}. The absorbance peak around 2250 cm^{-1} is attributed to the H (hydrogen) group. The stretch bands in the region 2850–3000 cm^{-1} are from CHx (x=2,3) bending vibration, which signifies the presence of methyl groups in the PLK film. The adsorption peak at approximately 1090-1280 cm^{-1} is from symmetric deformation vibration of CH_3 in Si-CH_3 groups. A broad band can be observed, with two components at about 3200 - 3700 cm^{-1}, which is attributed to the vibration of -OH groups in the form of Si-bonded OH group. This broad peak is usually a result of moisture adsorption/formation of –OH group and is due to the vibration of

silanol groups (Si–OH) and H_2O molecules. In four areas a significant change in the FT-IR spectrum is observed after indentation creep test: (1) the Si-OH/H_2O area (3200-3700cm^{-1}), (2) CHx area (2850-3000cm^{-1}), (3) the Si-CH_3 area (1090-1280 cm^{-1}) and (4) Si-O-Si area (970–1250cm^{-1}).

Figure 4.8(a) and 4.8(b) show the magnified FTIR spectra in Figure 4.7 for the Si-OH/H_2O /CHx areas and the Si-CH_3 / Si-O-Si areas obtained from unindented and indented regions, respectively, after indentation creep test. For the unindented area, the peak of Si-OH/H_2O bond is detected within 3200-3700cm^{-1}, meaning that the formation of Si-OH bonds is taken place even by solely thermal effect, corresponding to the mechanism that we suggested in the previous section. In Figure 4.8 (a), the comparison of FTIR absorbance shows that the indented area in the film yields a significant increase in the intensity of Si-OH bonds while the intensity of CHx bond is smaller in the indented region than in the unindented area. Figure 4.8(b) shows the decrease of CH_3 bonds in Si-CH_3 groups at around 1090-1280 cm^{-1} and clear evidence of bond-breaking in Si-O-Si bonds at around 970–1250cm^{-1}. The fact that clear differences of FTIR spectra are found between the indented and unindented areas suggests that mechanical load can make Si-CH_3 to be disintegrated, leading to the generation of Si dangling bond able to absorb H_2O to form Si-OH and cause further breakage of Si-O-Si bonds which can react with H molecules in the broken CH_3, resulting in additional Si-OH formation. Therefore, it is reasonable to suppose that the additional Si-OH bonds are generated by chemical reaction related to the

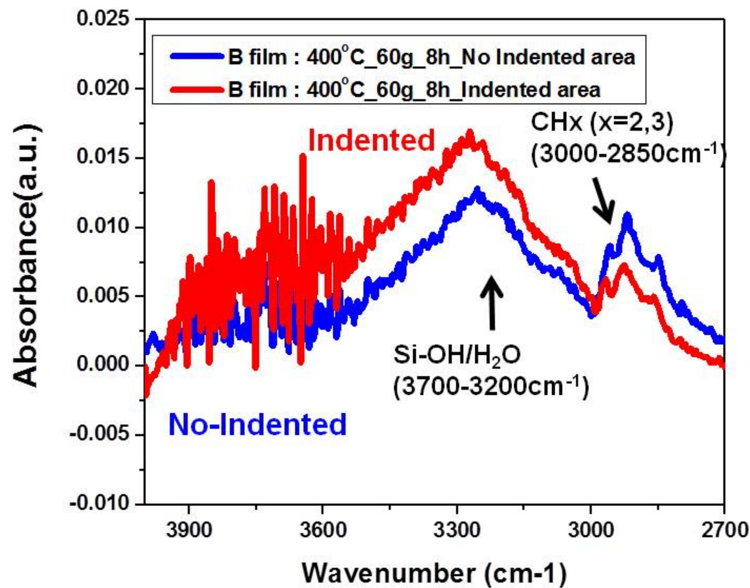

(a) Magnified FTIR spectra of the Si-OH/H_2O and CHx area

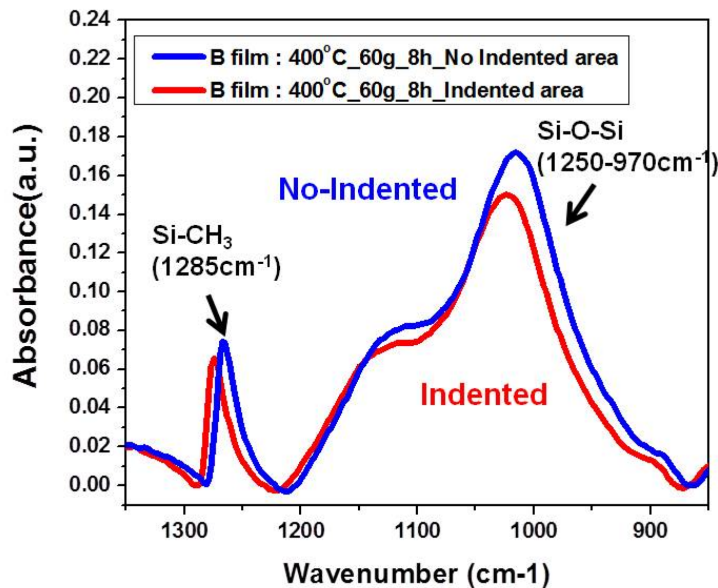

(b) Magnified FTIR spectra of the the Si-CH_3 and Si-O-Si area

Figure 4.8 Magnified FTIR spectra in Figure 4.7: (a) shows the Si-OH/H_2O area (3200-3700cm^{-1}) and CHx area (2850-3000cm^{-1}) and (b) exhibits the Si-CH_3 area (1090-1280 cm^{-1}) and Si-O-Si area (970–1250cm^{-1}) obtained from unindented and indented regions after indentation creep test.

decrease in $CHx/Si-CH_3$ bonds and Si-O-Si bonds due to mechanical load beyond the thermal effect. It is thought that C (carbon) atom in broken CH_3 bonds is not only removed from the film, but also become integrated into the Si-O network ($Si-CH_2-O$) [203]. This can lead to an increase in the PLK density, resulting in the increase of dielectric constant value.

Fig. 4.9 shows the FTIR spectra of A PLK film as a function of time at the indented region after indentation creep test in the wavelength range between 750 and 4000 cm^{-1}. The peaks of interest are the absorption by Si-OH stretching vibration at approximately 3200-3700 cm^{-1} and CH*x* stretch at approximately 2850-3000 cm^{-1} and $Si-CH_3$ and Si-O-Si located at around 970-1280 cm^{-1}.

Figure 4.10 (a) and (b), where FTIR measurement is conducted at the indented area, show that the intensity of Si-OH bond increases significantly, but that of CH*x*, $Si-CH_3$ and Si-O-Si bonds decrease in FTIR spectrum as indentation creep time increases, which is consistent with the FT-IR comparison of the unindented and indented areas.

It can be seen that, the increase in the FTIR peaks for Si-OH bonds correlates well with the increase in the degree of deformation with time noted earlier in Figure 4.1. This result clearly evidence the fact that presence of Si-OH bond or production of Si-OH bond by decomposition of $CHx/Si-CH_3$ and Si-O-Si bonds and their subsequent evolution to H_2O is responsible for viscoplasticity. Based on the FT-IR measurements, thus, it is believed that the formation of Si-OH bonds can be considerable by the mechanical load, as well as the thermal load and the Si-OH bond is acting as catalysis

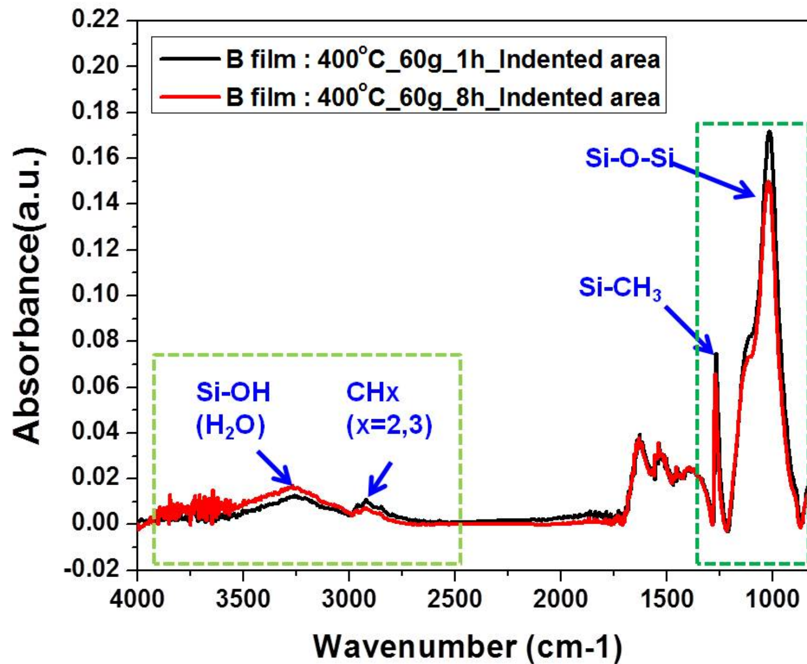

Figure 4.9 FTIR spectra of A PLK film showing the difference in chemical with time at the indented region after indentation creep test over the range 4000-750 cm^{-1}.

so that the generation of Si-OH bonds is responsible for the lowering activation energy for viscous flow, leading to the occurrence of viscoplasticity observed in all PLK films.

4.3.6 Proposed Mechanisms

In order to find the mechanism behind the PLK instability, the ball indentation creep tests and FTIR characterization were conducted at various load and temperature conditions with variation in PLK porosity and plasma-exposure. This study leads us to four main findings and they are 1) viscoplastic deformation does occur under a relevant load and temperature conditions of PLK processing, 2) all investigated PLK films deform by viscous flow, 3) the activation energy of the viscosity back calculated from

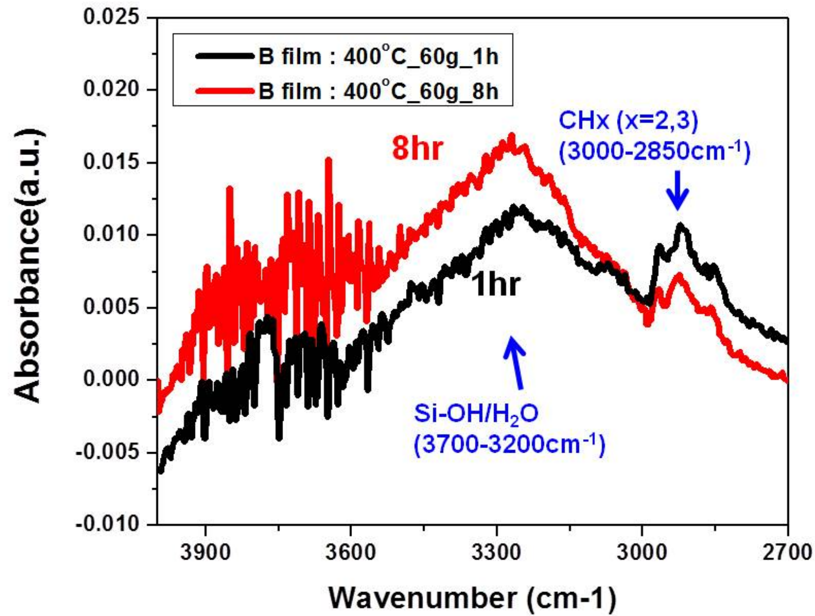

(a) Magnified FTIR spectra of the Si-OH/H2O and CHx area

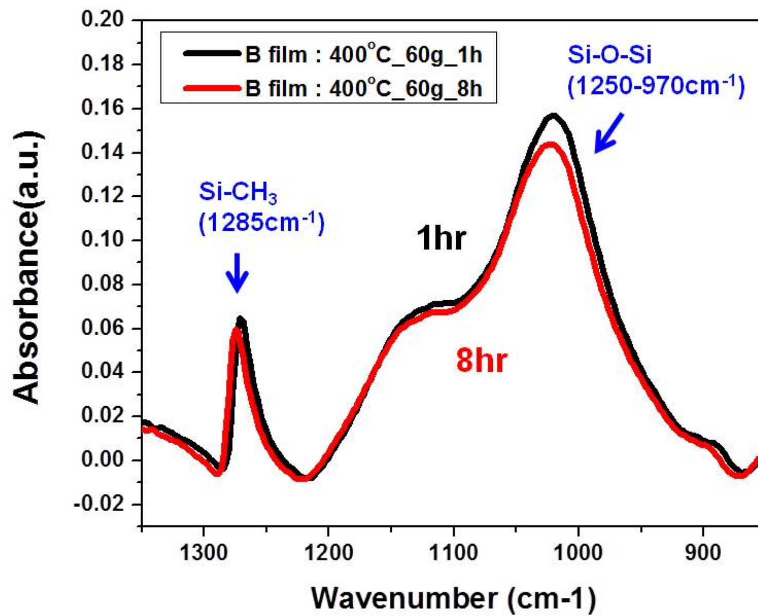

(b) Magnified FTIR spectra of the the Si-CH3 and Si-O-Si area

Figure 4.10 Magnified FTIR spectra in Figure 4.9: (a) shows the Si-OH/H_2O area (3200-3700cm^{-1}) and CHx area (2850-3000cm^{-1}) and (b) exhibits the Si-CH_3 area (1090-1280 cm^{-1}) and Si-O-Si area (970–1250cm^{-1}) collected from the indented regions, respectively.

the experimental value of the kinetics is found to be much smaller than that of a pure glass, and that 4) the degree of deformation is greatly influenced by PLK's intrinsic (porosity) and extrinsic (plasma damage) factors. Even though further analysis of microstructures under indentation area and mass build-up around indented regions are required to explain the details of bond reconfiguration which is followed by pores structure change behind the apparent thermo-mechanical instability of PLK dielectrics, based on the findings made in our study, we propose the mechanism leading to viscoplasticity of PLK dielectrics as follows. The flow diagram schematically illustrating this mechanism is shown in Figure 4.11. Considering the activation energy that we obtained as the result of temperature dependence, two mechanisms are involved [199]: 1) water molecules diffuse through interconnected network with the activation energy of 0.8-0.9eV and, 2) the water molecules react with Si-O-Si bonds, resulting in the formation of Si-OH bonds with the activation energy of 0.3-0.7eV in amorphous SiO_2. Note that the existence of water can be attributed to the condensation reaction of the existing Si-OH groups as by-product during deposition and deeply trapped moisture inside in the film that the N_2 purging gas cannot reach.

Compared to dense PLK of A film with lower porosity, as shown in Figure 4.6, the presence of higher porosity in PLK of B film seems to favor this time-dependent plastic deformation. Since B film has larger open structure, water molecules can diffuse more easily through the bond-networks, leading to further reaction with Si-O-Si bonds and larger deformation. The fact that the activation energy of the viscous flow is somewhat higher in dense PLK of A film, 1.45eV, may be because its composition is

not entirely identical, comparing with the others among the present three samples. In case of C film exposed to plasma, its degree of deformation is higher than that of B film at the identical porosity and composition. This result is attributable to the loss of methyl groups(-CH_3) caused by plasma processing, resulting in additional increase of Si-OH formation due to the reaction with water molecules and Si dangling bonds generated by the scission of methyl groups.

In the case of mechanical load effect, based on the chemical bonds change in the FT-IR spectra of the unindented and indented areas, the applied mechanical load scissions Si-CH_3, leading to the generation of Si dangling bond by the loss of methyl bond (-CH_3). The Si dangling bond causes absorption of water molecules to form Si-OH bonds. Also, further breakage of Si-O-Si bonds occurs by the mechanical load, corresponding to the decrease in FT-IR spectra for Si-O-Si bonds in the indented region shown in Figure 4.8 (b). The unsaturated Si-O bond reacts with H molecules in the broken CH_3, resulting in additional Si-OH formation. As a result, this indicates that the Si-OH bond can be produced by not only thermal load, but also mechanical load.

From the possible mechanism that we suggest, we believe that the viscoplasticity observed in our investigation is fundamentally driven by the viscous flow but chemical reaction can act as a catalyst for making the PLK films to be viscous. More specifically, the viscous flow of Newtonian solid (amorphous solid) occurs by body translation of entire solid under stress. In case of PLK films under test conditions used in our test, body translation may be difficult to achieve because silicate backbone provides a reasonable strong resistance against it. In order for the backbone molecule to

move, it requires momentary breakage of the bond and re-bond, which is known to require activation energy over 4eV. However, when there is a chain of weak links in the bond network, the resistance against body translation may be reduced because the colony that is encompassed by the weak link may act as one moving solid (like the grain boundary in crystalline solid). In this case, all the principle behaviors of viscoplastic deformation appear to follow the viscous flow yet activation energy can be significantly lower because colony motion does not require breakage of high energy bond. We believe that Si-OH (or Si-H) may serve as the defective bond and exist in PLK films due to 1) trapped defects during deposition, 2) damage to Si-O-CH_3 bond due to plasma damage, and 3) reaction with trapped moisture. This explains the low activation energy seen in all PLK films and also keen dependence of indentation kinetics on PLK film condition. The PLK films with plasma damage and moisture uptake would show faster deformation rate because the colony size is much smaller than the others. However, since the principle deformation mechanism is controlled by the colony motion itself, the activation energy would not be a keen function of the film condition. This mechanism, chemically assisted viscous flow, appears to explain all observations seen in our investigation.

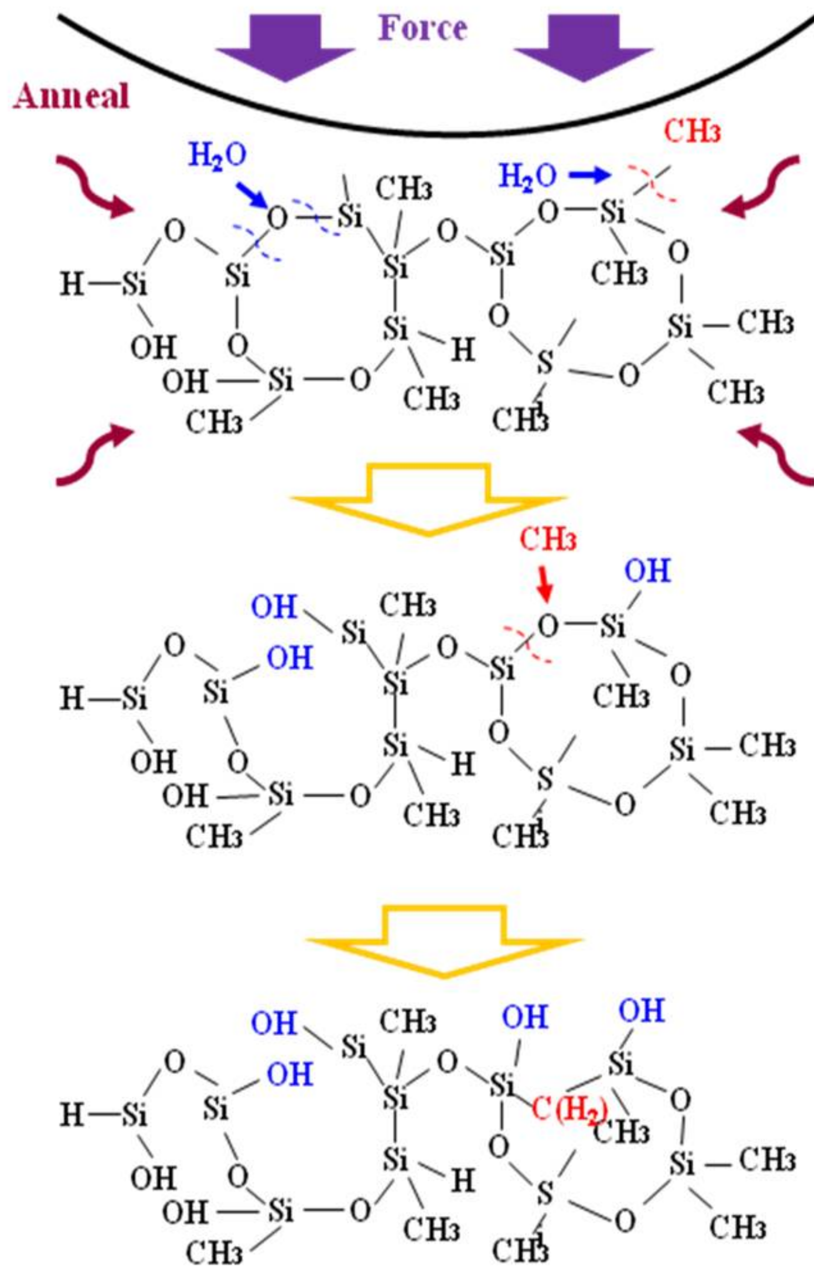

Figure 4.11 Schematic diagram showing the proposed mechanism leading to viscoplasticity of PLK film.

4.4 Summary

This investigation aims to identify the existence of the thermal and mechanical instabilities and understand the related mechanism in porous low-k dielectrics in Cu/porous low-k interconnects. For this reason, the ball indentation creep tests were conducted at various load and temperature conditions with variation in PLK conditions such as porosity and plasma-exposure. Essentially, this study leads us to four major findings. The first finding is that viscoplastic deformation does occur under a relevant load and temperature conditions of PLK processing, and second, it is also found that the viscoplastic deformation occurs by the mechanism of the viscous flow which is the well-known mechanism of glassy materials. This conclusion is obtained from the facts that the kinetics of the indentation creep match very well with the viscous flow model and the extracted stress exponent is close to unity, indicating that Newtonian viscous flow can be mechanism for viscoplastic deformation in the PLK film at given temperature and indentation load. In addition, this result is consistent with the fact that the mass build-up around the indented area occurs, meaning the sign of mass flow but fracture or a simple densification. Thirdly, our finding is that the deformation occurs with unexpectedly low activation energy (1.27eV to 1.45eV). This suggests that the viscous flow of PLK is controlled by chemical reaction happening in PLK matrix. Based on the FT-IR measurement for the examination of chemical bond reconfiguration, it is observed that the intensity of Si-OH bonds increases with the flow while that of Si-O-Si, -CH_3 and Si-CH_3 bonds decreases, indicating that chemical

reactions are involved in the deformation process. Last, the finding is that the degree of deformation is greatly influenced by PLK's intrinsic (porosity) and extrinsic (plasma damage) factors.

From these findings, it is concluded that the viscoplastic deformation in PLK films proceeds mainly by the viscous flow but is assisted by chemical reaction that reconfigure bonding configuration in the network (Si-OH or Si-H). This chemically assisted viscous flow mechanism may explain the low activation energy of viscoplastic deformation and an extreme dependence of the deformation kinetics on PLK conditions.

CHAPTER 5

EFFECT OF MOISTURE ABSORPTION AND INTEGRATION PROCESS STEPS ON THERMAL-MECHANICAL INSTABILITY OF POROUS LOW-K DIELECTRICS

5.1 Introduction

Successful implementation of porous low-k dielectrics (PLK) in Cu interconnect structures poses numerous challenges that appear in the integration of these materials into the semiconductor processes, including thermal and mechanical stability, as well as electrical and chemical characteristics. Although there are several low-k materials being used in integrated circuit fabrication, each of them has its own advantages and drawbacks, and none of them can completely replace the traditional silicon oxide [204]. Compared to their nonporous low-k materials and traditional SiO_2, porous dielectrics are expected to possess a much reduced mechanical strength and are more susceptible to the adsorption of reactive chemicals (moisture or organics), which not only occurs in the ambient environment of the cleaning room, but is also caused in patterning processes, wet and dry cleaning processes during device fabrication [205-209]. The adsorption of moisture in PLK is one of the most concerned subjects in microelectronic industry because the moisture adsorption negatively impacts both the electrical performance of the devices and their mechanical integrity, leading to the degradation of interconnect reliability [210,211]. In spite of considerable efforts, the mechanism of

moisture effect on thermal and mechanical instability of PLK in Cu interconnects has not been adequately studied and fully understood.

This chapter presents our attempts to investigate the impact of the moisture adsorption as an extrinsic factor on thermal and mechanical instability of PLK. Since it has been suggested in the last chapter that the principle of viscoplastic deformation mechanism is the viscous flow but chemical reaction related to the water (H_2O) molecules due to the presence/production of silanol bonds (Si-OH) in PLK films is involved in creating the viscous flow, an investigation into the effect of moisture adsorption is expected to allow us to prove our mechanism proposed in earlier chapter. The primary means of investigating the moisture effect on thermo-mechanical instability of PLK in this chapter is the measurement of indentation depth in variation of the presence/absence of moisture, time and temperatures by the ball indentation creep test technique with a proven track record in the previous chapter. In order to characterize the indentation depth and the indented surface morphology in post-test samples, the optical profilometer technique is also used.

In this study with this ball indentation creep test, we first characterize the effect of water exposure on plastic deformation behavior as a function of time in PLK films. Second, in order to reveal the mechanism behind plasticity of PLK exposed to moisture, we conduct indentation creep testing at various temperature conditions (300˚C~400˚C) of PLK processing. Interpreting the result from time-dependent plastic deformation and temperature dependence allows us to identify the associated mechanism of PLK in

ambient moisture. The implications of our study for the viscoplastic deformation of PLK dielectrics in the presence of water are discussed.

In this chapter, also, the influence of integration process steps on thermo-mechanical instability of PLK was investigated. While it is evident that lowering the density and mechanical strength by the introduction of porosity into the existing low-k film to generate further low-k films (or PLKs) make the PLK vulnerable to be damaged by integration processes such as plasma etch, ash, cure and chemical mechanical polishing, it is still unclear that how much integration damage is induced by each process steps and little is known if the integration damage is cumulative with individual process. Therefore, it is important examine the impact of each integration process steps to PLK stability so as to develop effective PLK process methods to minimize the damages in PLK resulting from integration processes and find a proper way to make PLK to be stable by restoring its original stability. Our previous studies find that viscoplastic deformation, measured by our ball indentation technique, correctly reflects the change in the chemical back-bone of PLK films and therefore can be used for tracking damage in PLK bond structure in variations with the integration process steps. This study will allow us to identify the integration damage in PLK with processing steps. This chapter will detail such findings by presenting experimental evidence.

5.2 Experimental

PLK films which are made using industry standard PECVD processes were prepared following the same procedure as described in the experimental section of Chapter 4. First, in order to study how the moisture affects the deformation behavior,

indentations were carried out using the test PLK films with variation in porosity (effective k~2.2), controlled plasma and moisture exposure. The ball indentation creep testing setup we developed is identical depicted in the Chapter 2. It relies on an application of a constant load on top of porous low-k film and measures the penetration depth (h) as a function of time (t). Indentation creep experiments were performed at different temperatures from 300 ˚C - 400 ˚C for the PLK films using a wide range of loading time from 1 to 8 hours in N_2 atmosphere. Note that all PLK films were evacuated and purged with N_2 alternately to remove water from the films at room temperature. Based on the preliminary test to determine minimum temperature for degassing process, summarized in Table 5.1, it was found that the indentation depth of PLK after prebaking at the temperature of 100°C was larger than that of PLK without prebaking, as shown in Figure 5.1, indicating that the PLK film should not be degassed at any elevated temperature due to the formation of silanol(Si-OH) or its pre-form even at the temperature of 100°C exposure. Accordingly, the (iv) procedure as standard degassing process in our study was carried for all PLK films before the indentation creep testing. Also, N_2 gas was kept flowing to protect the PLK film from water or possible defects. The load that we apply in this study was mostly 60gf, corresponding to 140MPa of maximum pressure stress developed at real process. The annealing temperatures are varied from 300 to 400 ^{o}C and the creep time is applied from 1 to 8 hours. For indentation in the environment of water, a water-filled small flask with 5.0 ml was simply placed near to the sample stage inside the chamber.

Table 5.1 Summary of the degree of deformation with different degassing procedures under 60gf at 300°C for 4 hours

Process / Sample	Evacuation	Baking Chamber (100°C-1hr)	N_2 flowing **(30 min)**	Prebaking w/N_2 flowing	Degree of Deformation	**Note**
(i)	**No**	**No**	**Yes**	**No**	**Middle**	**X**
(ii)	**No**	**Yes**	**Yes**	**No**	**Largest**	**X**
(iii)	**No**	**Yes**	**Yes**	**Yes**	**Same as (b)**	**X**
(iv)	**Yes (1hr-3times)**	**No**	**Yes (30min-3times)**	**No**	**smallest**	**standard test condition**

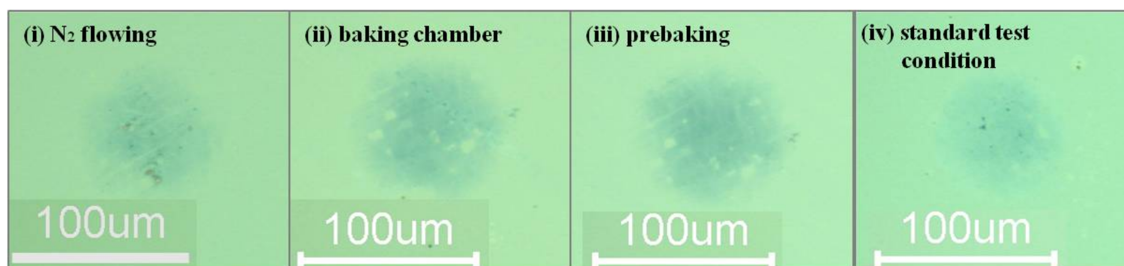

Figure 5.1 Optical microscope images showing the residual indentation regions in PLK films tested with different degassing processes under 60gf at 300°C for 4 hours.

Table 5.2 Experimental splits of integration process steps

Wafer Id(#)	Film Descriptoin	Plasma Etch	Wet Clean1	Ash	Wet Clean2	Wet Clean3	Polish	Cure	Post Thx (Ang)
14	PLK (k=2.3) + CAP (~10nm)	No	No	No	No	No	No	No	2512.91
16	PLK (k=2.3) + CAP (~10nm)	Yes	Yes	No	Yes	Yes	No	No	2164.08
17	PLK (k=2.3) + CAP (~10nm)	Yes	Yes	Yes	Yes	Yes	No	No	2079.23
18	PLK (k=2.3) + CAP (~10nm)	Yes	Yes	No	Yes	Yes	Yes	No	1891.27
19	PLK (k=2.3) + CAP (~10nm)	Yes	Yes	Yes	Yes	Yes	Yes	No	1981.97
20	PLK (k=2.3) + CAP (~10nm)	Yes	Yes	No	Yes	Yes	Yes	Yes	1846
34	PLK (k=2.3) + CAP (~10nm)	Yes	Yes	Yes	Yes	Yes	Yes	Yes	1914.52

Secondly, for the experiment with respect to the influence of process steps to PLK instability, The blanket PLK films were partially exposed to various combinations of PLK integration process steps, including plasma etching, ashing, CMP, and cure. The complete process splits for this study are shown in Table 5.2. Blank PLK films for the initiative test were processed by Intel Co. These PLK films had a dielectric constant of 2.3 and SiCN capping layer of 10 nm deposited. The ball indentation creep test was conducted for all PLK samples at 400 ^{o}C under 60gf for 4 hour.

The indentation surfaces were observed after each experiment using an optical microscope and then, the depth of indentation was measured by using a Wyko model NT9100 optical profilometer equipped with Vision software and averaged from five indentations.

5.3 Results and Discussions

5.3.1 Effect of moisture adsorption

To identify effectively how the moisture affect the thermal and mechanical instability of PLK films, a number of PLK films were exposed to moisture ambient during a ball indentation creep test. They were also subjected to a thermal and mechanical load conditions in N_2 environment at 300 ^{o}C under 60gf for 8 hours, and their surface morphology and indentation depth were examined subsequently. Figure 5.2 shows the optic and surface topography images for B film with a k value of 2.2 and C film exposed to plasma but same k value as B film with the absence/presence of moisture after the ball indentation creep test. The average residual indentation depth is

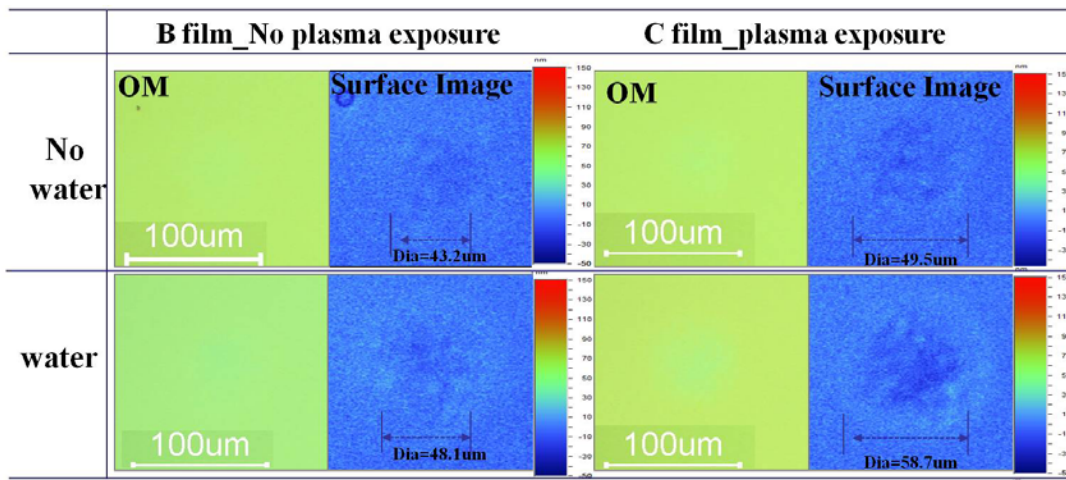

Figure 5.2 Optic and surface topography images presenting indentation regions with the absence/presence of moisture for B film and C film tested at 300°C with 60g loading for 8 hours, respectively.

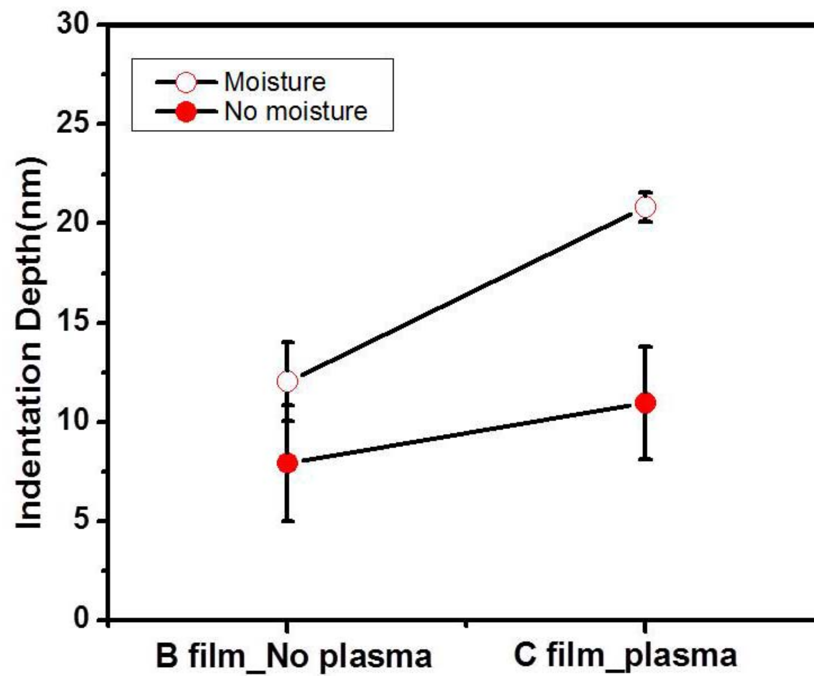

Figure 5.3 A plot showing indentation depth of B and C films with the absence/presence of moisture measured from the result of Figure 5.2.

subsequently plotted in Figure 5.3. It is clearly observed that the degree of deformation in both films is increased when the films are exposed to moisture. This indicates that the absorption of moisture has a significant negative influence on the stability of PLK film. Moreover, it can be seen that the change in the indentation depth for the C film exposed to plasma under water uptake is quite larger than for the B film without plasma exposure at the identical environment. This result is consistent with the first observations of a residual indentation depth noted in Chapter 4, implying the adverse effect of plasma-exposure on the thermal-mechanical stability of PLK films.

5.3.2 Observation of viscoplastic deformation of PLK in moisture ambient

As observed in Figure 5.2 and 5.3, it was found that the stability of PLK films was very prone to the existence of moisture, as well as the bond-damaged by plasma. Accordingly, the next step of the investigation is to examine the time effect on plastic deformation behavior of the PLK film under the moisture ambient. B film without moisture and D film with moisture were chosen for comparison. Fig. 5.4 shows the observations of the indented area using an optical surface profilometer in PLK films at the temperature of 400 ^{o}C under the constant mechanical load of 60gf in N_2 ambient. It is found that the depth of indentation representing the plastic deformation increases as a function of time in both PLK samples, while the increase is more pronounced in the D film with the absorption of moisture. Noticed is the fact that injection of moisture to PLK films significantly increases the indentation rate, indicating that moisture uptake to PLK results in acceleration of viscoplastic deformation. Subsequently, the indentation depth is measured to present true viscoplasticity of both PLK films.

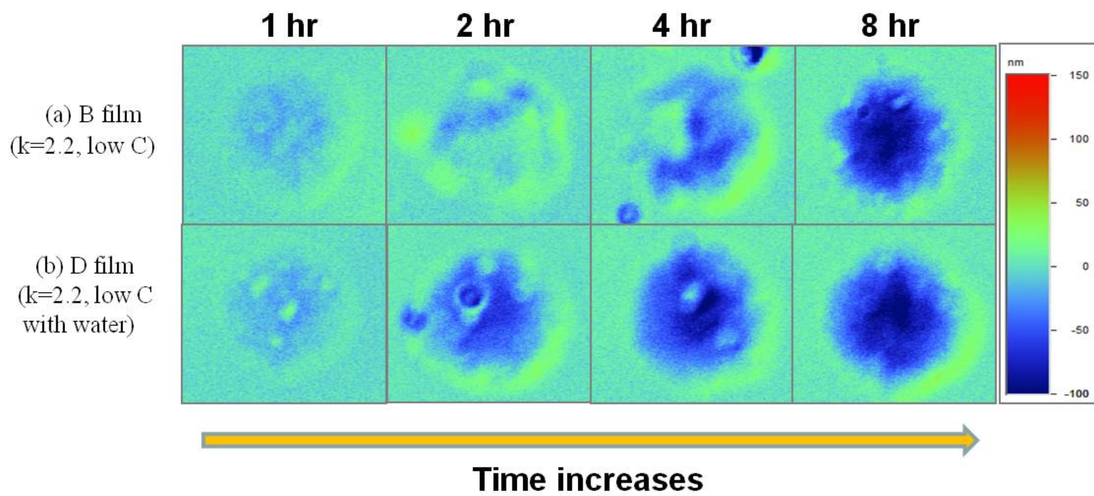

Figure 5.4 Surface topography images showing the residual indentation regions in (a) B film and (b) D film at 400°C under 60gf as a function of time.

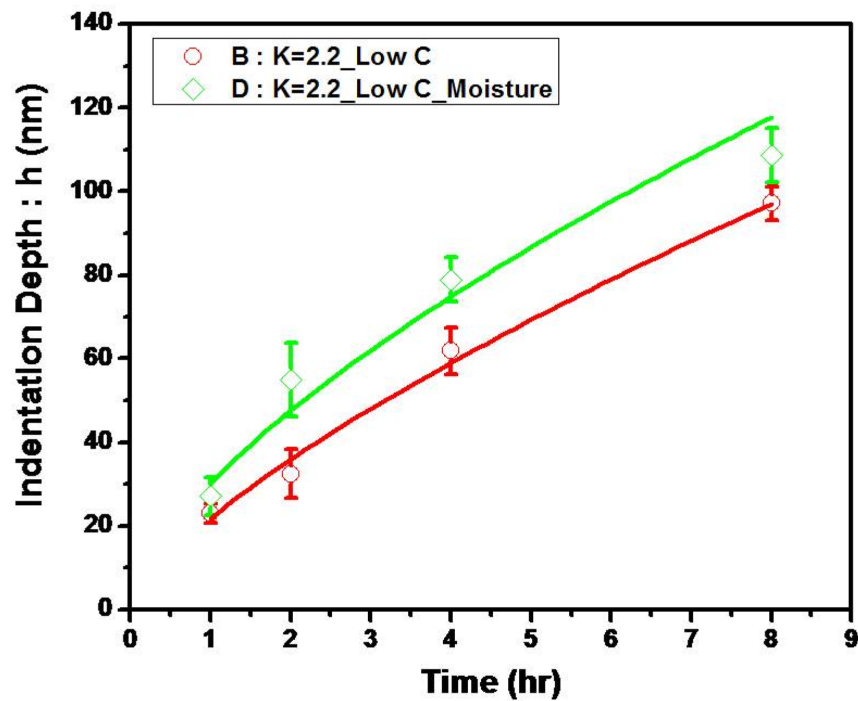

Figure 5.5 Plots showing the comparison of indentation depth as a function of time for B film without moisture and D film with moisture, respectively.

From the measurement of the residual indentation depths with an optical surface profilometer, the indentation depths of the PLK films as a function of creep time are plotted in Figure 5.5. It is confirmed that the stability of PLK film is strongly dependent on the moisture absorption as an extrinsic factor, indicating that the moisture uptake makes the PLK film to be more vulnerable to viscoplaticity. Similar results have been observed in other indentation testing conditions. Therefore, based on the results shown in Figure 5.4 and 5.5, we believe that the PLK instability is significantly affected by the existence of moisture as an extrinsic factor.

5.3.3 Kinetics of PLK exposed to moisture for the ball indentation creep test

Figure 5.6 shows that the indentation depth with a power of 3/2 varies linearly as a function of time by fitting curve of the indentation depth and creep time depicted in Figure 5.5. It is found that this result corresponds to the kinetic expression (see Equation (4.1) on Chapter 4) which was developed by Douglas *et al* [172], who suggested that the viscosity could be determined with the indentation rate of a ball indenter in Newtonian viscous material. As stated in Chapter 4, since the kinetic equation is applied for viscous flow materials in a ball indenter, this result observed in the presence of moisture thus confirms that the principle behavior of viscoplastic deformation seen in PLK films follows the viscous flow at the given temperature and load conditions. Furthermore, as shown in Figure 5.4, the piling-up effect of the PLK film exposed to moisture is clearly observed around the indentation, strongly suggesting the deformation mechanics of Newtonian fluid by viscous flow.

5.3.4 Temperature dependence

In Chapter 4, it has been proved that there is a significant dependence of PLK film instability on temperature. In the case of the PLK film exposed to moisture, similar

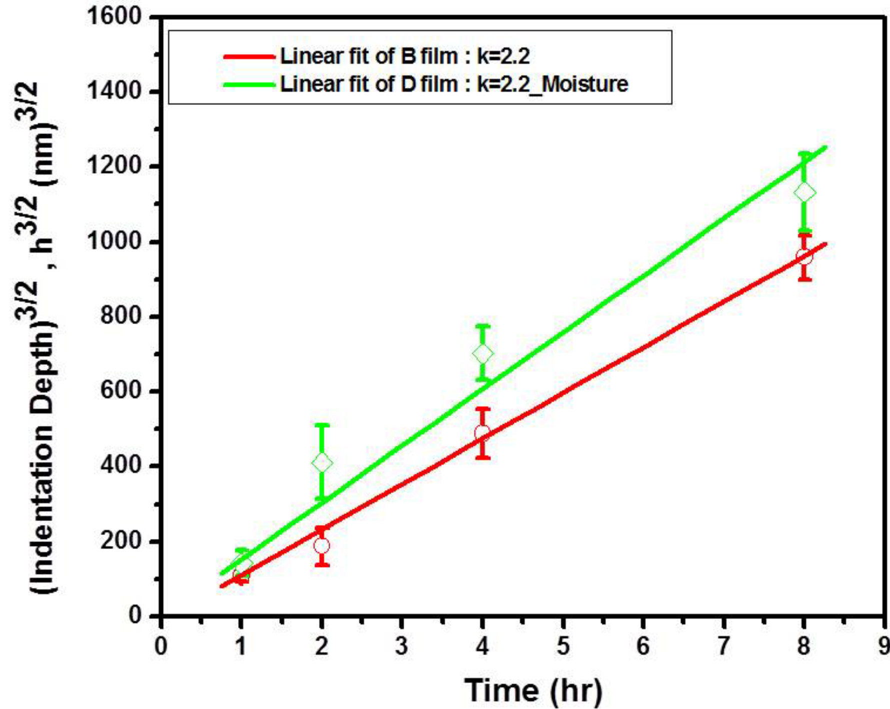

Figure 5.6 Plots showing the indentation depth with a power of 3/2 as a function of time for B film without moisture and D film with moisture, respectively.

behavior is observed in variation with temperatures as presented in Figure 5.7. Subsequently, the indentation creep test was performed at various temperatures (300°C ~400°C) under the constant load of 60gf so as to study the temperature dependence on the instability of the PLK film in ambient moistures, In the case when the permanent deformation arises from viscous flow, it is related to the viscosity (*η)* which is strongly dependent on the temperature. Based on the experimental data acquired through a ball

indentation test, as shown in Figure 5.5, the viscosity of the PLK film can be also easily determined by using the kinetic relation noted in previous chapter (see Equation (4.1) on Chapter 4). The activation energy of the viscous flow can be determined from the temperature dependence of the viscosity by using the Arrhenius relation as referred in previous chapter (see Equation (4.6) on Chapter 4). Figure 5.8 demonstrates the $\ln\eta$-1/T diagram for the moisture-absorbed PLK sample. It is found that the activation energy achieved for PLK film exposed to moisture exhibits 1.32eV in the temperature of 300 ^{o}C ~400°C. This value is relatively close to that obtained for other PLK films in Chapter 4. It should be thus note that the variation of activation energies obtained for all PLK films is not much wide, implying that the mechanism in viscoplastic deformation of porous low-k dielectrics is not different at given load and temperature conditions. This finding also supports the result that the viscous flow of PLK is controlled by chemical reaction consisting of reaction between water molecules and Si-O-Si bonds, and the generation of Si-OH bonds in PLK matrix.

Therefore, our findings in this chapter clearly evidence that when the PLK film is exposed to silanol bonds (Si-OH), the chemical reaction associated with water molecules results in the weakening of the local bond, leading to the viscous flow of the PLK film. The low activation energy of viscoplastic deformation and an extreme dependence of the deformation kinetics on PLK conditions may be due to the chemically-assisted viscous flow mechanism.

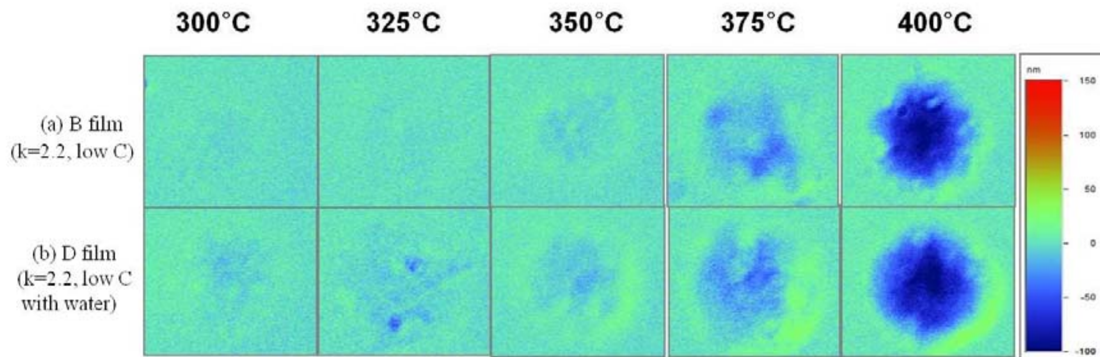

Figure 5.7 Surface topography images showing variations in the indentation depth as a function of temperature for (a)B and (b) D films. The indentation test is done at the constant load of 60g for 8 hours.

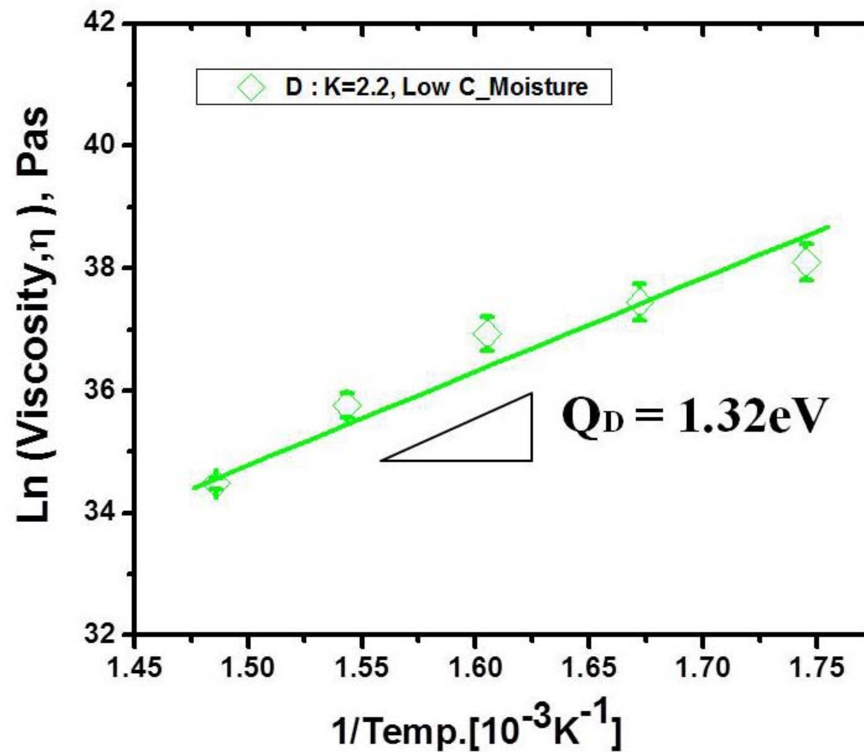

Figure 5.8 Viscosity in PLK film of D film exposed to moisture as a function of inverse temperature, showing Arrhenius-type behavior.

5.3.5 The influence of integration processes on the Thermo-Mechanical PLK stability

In order to investigate the influence of each process step used in Cu/PLK interconnect integration on PLK stability using the ball indentation creep testing, a variety of PLK films which were partially etched, ashed, chemical-mechanical polished (CMP) and cured by UV (Ultra Violet) were prepared. They were also subjected to a thermal and mechanical stress in N_2 environment at 400 ^{o}C under 60gf for 4 hours, and their indentation depths were subsequently examined by using a Wyko model NT9100 optical profilometer equipped with Vision software. Table 5.3 represents the change in mean indentation depth depending on the variations of process history. The mean indentation depth is subsequently plotted in Figure 5.9. It is clearly observed that the indentation depth representing integration damage increases with integration process steps. Noticed is the fact that the damage to PLK films by each integration process is cumulative, implying the adverse influence of integration processes on the PLK stability. Especially, the damage to PLK stability is the most pronounced in the PLK films exposed to plasma etching and ashing processes. This results are consistent with the fact that among various integration processes, plasma treatment such as etch/ash process has been generally known to generate most vexing damage to PLK through the bond-network reconfiguration such as the loss of Si-O-Si or Si-CH_3 and the formation of Si-OH or Si-H bonds, while it is widely used as one of critical integration processes in advanced Cu/PLK interconnects [212,213]. Judging from this point view, the results suggest that rigorous plasma process optimization such as modification of process and/or post-treatment of PLK films is required to successfully integrate these films.

Table 5.3 Mean indentation depth depending on the variations of process history

Wafer Id(#)	Film Descriptoin	Plasma Etch	Wet Clean1	Ash	Wet Clean2	Wet Clean3	Polish	Cure	Post Thx (Ang)	Mean Indentation depth (nm)
14	PLK (k=2.3) + CAP (~10nm)	No	No	No	No	No	No	No	2512.91	6.9
16	PLK (k=2.3) + CAP (~10nm)	Yes	Yes	No	Yes	Yes	No	No	2164.08	11.6
17	PLK (k=2.3) + CAP (~10nm)	Yes	Yes	Yes	Yes	Yes	No	No	2079.23	14.4
18	PLK (k=2.3) + CAP (~10nm)	Yes	Yes	No	Yes	Yes	Yes	No	1891.27	17.0
19	PLK (k=2.3) + CAP (~10nm)	Yes	Yes	Yes	Yes	Yes	Yes	No	1981.97	16.0
20	PLK (k=2.3) + CAP (~10nm)	Yes	Yes	No	Yes	Yes	Yes	Yes	1846	20.4
34	PLK (k=2.3) + CAP (~10nm)	Yes	Yes	Yes	Yes	Yes	Yes	Yes	1914.52	27.9

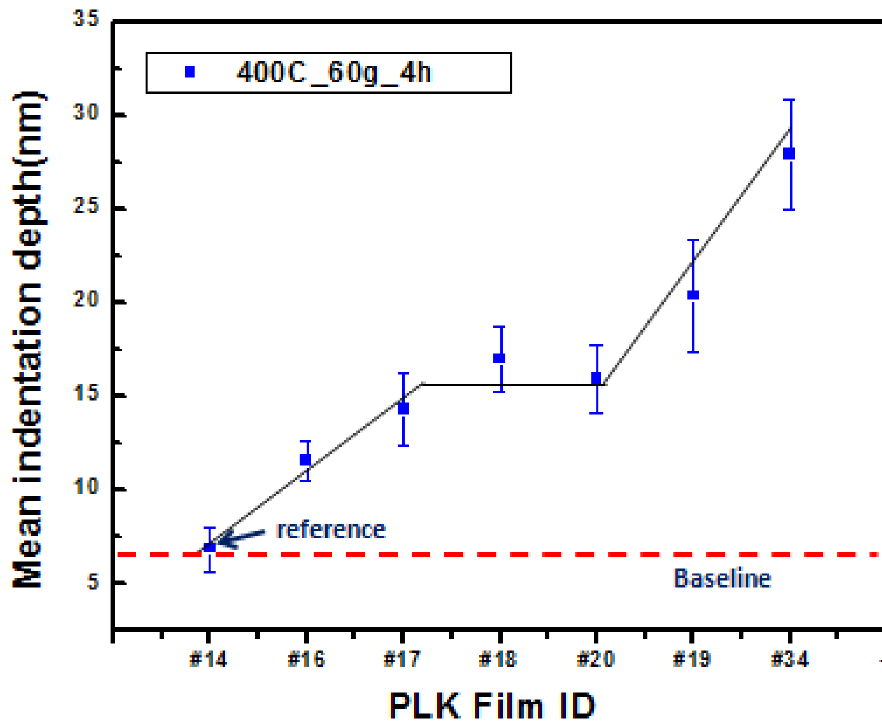

Figure 5.9 Mean indentation depth in PLK films exposed to various integration processes after indentation testing at 400°C under 60gf for 4 hours.

In the same manner, as depicted in Table 5.3 and Figure 5.9, the comparison of indentation depths of PLK films between #17 and #19 shows that the damage in the #19 PLK film exposed to additional CMP process is more marked, compared to that of #17 PLK film. It is indicated that PLK stability is greatly influenced by CMP process, leading to the damage into PLK films. This result may be due to the fact that CMP is basically a frictional process that generates a lot of heat, resulting in the decrease of film strength. Also, traces of slurry used in CMP and residue of the chemicals from the polished surface can be critical in reducing the mechanical strength of PLK films because they can diffuse into PLK film and create additional unsaturated and/or weak terminal bonds.

Ultra-violet (UV) irradiation curing has shown to be the most promising method in terms of increasing the mechanical strength of low-*k* materials by a pronounced rearrangement in the bonding structure of PLK films involving no significant compositional change or film densification. That is that UV radiation with cure breaks the relatively weak bonds like -OH and -H bonds and increases the degree of cross-linking of the PLK matrix, leading to the formation of more stable Si-O-Si bonds. However, in our study, it is found that UV irradiation with cure makes the PLK stability to be more deteriorated. This result may be related to the fact that the heat coming from UV radiation can make the properties of PLK worse if the formation of –OH from H_2O present in the film occurs during UV radiation with cure. Based on our results, it is thus reasonable to be assumed that UV is not effective for restoration. Ultimately, it is

necessary to find a practical method to make PLK stability to be enhanced by repairing the integration damage.

5.4 Summary

In this chapter, first, the effect of the moisture adsorption as an extrinsic factor on thermal and mechanical instability of PLK has been investigated. Using a ball indentation technique introduced in previous chapter, detailed characterization of PLK viscoplasticity with variation in moisture uptake has been carried out. This chapter describes the findings that PLK film exposed to moisture show significant viscoplastic deformation beyond any doubt and that PLK with moisture absorption makes the deformation to occur faster, indicating that PLK stability is greatly affected by moisture uptake. Besides, it is found that the deformation kinetics follows the mechanism of viscous flow of Newtonian solids. Based on the results of temperature dependence in PLK in moisture ambient, it is also found that the extracted activation energy for PLK with moisture uptake is 1.32eV, which is comparable to that obtained for other PLK films in previous chapter but far lower than the usual activation energy for glass viscosity. These findings from this chapter strongly support the mechanism proposed in Chapter 4 that the viscoplastic deformation proceeds mainly by the viscous flow but is assisted by chemical reaction that reconfigure bonding configuration in the network. Second, the effect of integration process steps to PLK stability has been studied by using the ball indentation creep testing. Our study reveals that current processes used for PLK integration generates cumulative damage to PLK stability, and also that plasma treatment such as etch and ash is the most barrier process induced damage to PLK film.

CHAPTER 6

CONCLUSIONS AND FUTURE WORK

6.1 Conclusions

The objectives of this dissertation were (1) to identify the mechanism leading to thermo-mechanical instability of PLK dielectrics observed in Cu/PLK interconnects; (2) to investigate the effect of porosity as an intrinsic and plasma damage and moisture absorption as extrinsic factors on thermal and mechanical instability of PLK and reveal the associated mechanism.

The occurrence of viscoplastic deformation leading to instability in PLK has been decisively evidenced by a ball indentation creep technique. In this study, the involved mechanism for viscoplastic deformation in PLK as well as the influence of the intrinsic/extrinsic factors on the viscoplasticity behavior of PLK has been investigated.

6.1.1 Detection of viscoplastic deformation in PLK

One of the key advances in microelectronics technology is the implementation of porous low-k dielectrics (PLK) in interconnect structures. The use of PLK is necessary to increase the device operation speed, yet its implementation has been seriously delayed due mainly to the reliability failure of interconnects integrated with PLK. While several reliability failure mechanisms instigated by PLK have been identified, the linkage between those mechanisms and properties of PLK itself has been elusive. To effectively identify the mechanism leading to PLK instability, a ball indentation creep

test technique has been introduced in our study. According to theoretical silicate structure properties, PLK should not show plasticity at interconnect processing temperatures due to the stability of cross-linked bonding networks. However, our experiment produces evidence showing the opposite. The ball indentation creep test demonstrated that the residual indentation depth increased with time. This result clearly evidences that PLK dielectrics shows significantly viscoplastic deformation (or time-dependent plastic deformation) under a relevant load and temperature conditions of PLK integration processing. Furthermore, the ball indentation creep test can be used as a simple yet effective method to reveal the thermo-mechanical instability of PLK in advanced Cu/PLK interconnects.

6.1.2 Study on viscoplasticity mechanism in PLK

The ultimate goal of this study is to identify the mechanism behind viscoplasticity of PLK. For this, the ball indentation creep tests were performed in variation with load and temperature conditions for PLK films. From the measurement of indentation depth with time for all PLK films, our finding is that the experimental creep curve are in very good agreement with the theoretical kinetic equation developed for viscous flow materials under the ball indentation. Based on the results of which the extracted stress exponent value is close to unity, it is confirmed that PLK films deform by Newtonian viscous flow at the given load and temperature conditions. Also consistent is the fact that the piling-up effect is obviously observed around the indented area, meaning the sign of mass flow. The ball indentation creep testing at various temperature (300˚C~400˚C) demonstrated that there is an extreme dependence of PLK

viscoplasticity kinetics on temperature. With the results of temperature dependence of PLK films, it is found that the deformation occurs with unexpectedly low activation energy (1.27eV to 1.45eV). This suggests that the viscous flow of PLK is controlled by chemical reaction happening in PLK matrix. From the FT-IR measurement for the examination of chemical bond reconfiguration, it is observed that the intensity of Si-OH bonds increases with the flow while that of Si-O-Si, $-CH_3$ and $Si-CH_3$ bonds decreases, indicating that chemical reactions are involved in the deformation process. This result means that the decomposition of $CH_x/Si-CH_3$ and Si-O-Si bonds can result in the generation of Si-OH bonds. Therefore, it is our conclusion that presence of Si-OH bond or production of by decomposition of $CH_x/Si-CH_3$ and Si-O-Si bonds or cross-links and their subsequent evolution to H_2O is responsible for the lowering of activation energy for viscous flow, leading to the occurrence of viscoplasticity observed in all PLK films.

6.1.3 Effect of contributing factors including porosity, plasma damage and moisture on thermo-mechanical instability of PLK

To investigate the impact of porosity, plasma exposure and moisture uptake on thermo-mechanical instability of PLK, the ball indentation creep tests were performed in variation with the PLK conditions under the constant load and temperature conditions. In this study, it is found that the indentation depth increases with time in all PLK films while the increase is more pronounced in films with higher porosity, plasma exposure, and moisture absorption in the PLK. It is thus believed that PLK viscoplasticity is significantly affected by porosity as an intrinsic factor and plasma damage, ambient moisture as extrinsic factors. On the basis of the finding that PLK viscoplasticity is

fundamentally driven by the viscous flow but assisted significantly by chemical reactions resulting in the formation of Si-OH bonds, the weak-link bonds such as -OH or dangling bonds can be increased by chemical reactions resulting from thermal and mechanical loads. Accordingly, it is possible that as the indentation creep test proceeds, the number of the colony with the weak-link bonds in the PLK matrix increases and its size becomes smaller, leading to the viscous flow yet lower activation energy due to the low energy to break the colony motion. This appears to explain the low activation energy seen in all PLK films and also strong dependence of indentation kinetics on PLK film condition. Therefore, the PLK films with plasma damage and moisture uptake would show faster deformation rate because the colony size is much smaller than the others.

For the present PLK films to be reliable as porous low-k materials in the advanced Cu/PLK interconnects, it is very important that viscoplasticity of PLK must be considered to avoid dimensional change when the Cu/PLK interconnect is designed.

6.2 Future Work

6.2.1 Influence of Process Conditions on the Thermo-Mechanical Stability of PLK

Enhancing mechanical and chemical stability of porous low-k (PLK) dielectrics is becoming of the critical technical challenge in PLK technology because it is determined to be the key to the successful integration of PLK into interconnect structure. Inherently inferior mechanical strength of PLK dielectrics combined with chemical reaction of PLK with process gases and liquid, possible due to their permeability through pore network, makes PLK films to be extremely prone to structural and/or functional failures during interconnect processing and in service. For this reason, there has been extensive number of studies conducted in recent years with a hope to find effective routes to enhance the PLK stability and thus resolve the reliability concern. However, the progress has been slow and hasn't yielded comprehensive identification of PLK failure condition as well as related mechanism. One of the leading sources of the slow progress is related to the fact that the mechanical failure is tightly linked with the chemical failure of PLK, that is that chemical reaction leads to mechanical instability of PLK. In order to properly investigate the failure possibility of PLK dielectrics, it is necessary to determine the degree of chemical reaction at each process steps and track the resulting change in the mechanical properties of PLK. Our previous studies find that viscoplastic deformation, measured by our ball indentation technique, correctly reflects the change in the chemical back-bone of PLK films and therefore can be used for tracking damage in PLK bond structure due to various process conditions. This study will allow us to identify the PLK instability with processing

conditions with an aim to demonstrate the close linkage between chemical and mechanical instability of PLK dielectrics.

6.2. Exploration of repair bond damage in PLK and strengthen resistance of PLK against viscoplasticity

The viscoplasticity of PLK discovered in our study indicates that it can be a serious source of integration and reliability problems. The troublesome feature of the viscoplasticity is the fact that it is slowly progressing that its occurrence becomes difficult to identify. Further, the failure in PLK/Cu integration due to the viscoplastic deformation in PLK layer appears much later stages of processing or in use condition. Of many contributing factors to PLK instability, it is found that extrinsic factors such as moisture uptake and plasma damage are the ones that are most influential to PLK viscoplasticity and such factors must be removed before PLK proceeds to next process. Based on the result that the viscoplasticity is due to combination of chemical reaction and the viscous flow, the resistance against viscoplasticity can be achieved by eliminating or reducing the Si-OH or Si-H bond. With reduction in Si-OH or Si-H bond, the colony size increases and so does the PLK's resistance against the viscous flow. There appears to be several routes to remove such factors. We are currently exploring a few methods of achieving such condition, including a use of low-energy radiation or thermo-chemical treatment with silylating agent to remove Si-OH or Si-H and restore Si-O-CH_3 bond. The current exploration will lead to a practical method to make PLK to be more stable by restoring bond completeness after damage and also to a supporting evidence for the chemically-assisted viscous flow mechanism we propose.

REFERENCES

[1]. S. P. Jeng, R. H. Havemann, and M. C. Chang, “Process integration and manufacturability issues for high performance multilevel interconnects”, *Mater.Res. Soc. Symp. Proc.* 337,25-31 (1994).

[2]. Shyam P. Murarka, and Steven W. Hymes, “Copper metallization for ULSI and beyond”,*Crit. Rev. Solid State Mater. Sci. 20, 87-124* (1995).

[3]. H.J.Frost and M. F. Ashby, *Deformation-Mechanism Maps* (Pergamon Press. Oxford, 1982) p.15.

[4]. D. Halliday and R. Resnick, *Fundamentals of Phys*. (1988) p. 453.

[5]. W. Koster and H. Franz, *Metall. Rev.* vol. 6 (1961).

[6]. Makarem A. Hussein, and Jun He, “Materials’ impact on interconnect process Technology and reliability”, IEEE Trans. Semiconductor. Manuf. 18, 69-85(2005).

[7]. R. Frankovic, and G.H. Bernstein, “Electromigration Drift and threshold in Cu Thin-Film Interconnects”, IEEE Transaction.

[8]. J. R. Lloyd, “Electromigration in integrated circuit conductors”, *J. Phys. D : Appl.Phys.* 32, R109-R118(1999).

[9]. Jens Lienig, “Interconnect and current density stress: an introduction to electromigration aware design”, *Proceeding of the 2006 International Symposium on Physical Design,* 39-46(2005).

[10]. C. K. Hu, and B. Luther, “Electromigration in two-level interconnects of Cu and Al alloys”, *Mater. Chem. Phys*. 41, 1-7 (1995).

[11]. Baozhen Li, Timothy D. Sullivan, Tom C. Lee, and Dinesh Badami, “Reliability challenges for copper interconnects”, *Microelectron Reliab* 44, 265-380 (2004).

[12]. J. Tao, N. W. Cheung, and C. Hu, “Electromigration characteristics of copper interconnects”, *IEEE Electron Dev. Lett.* 14, 249-252 (1993).

[13]. C. W. Park, and R. W. Vook, “Activation energy for electromigration in Cu

films", *Appl.Phys. Lett.* 59, 175-177 (1991).

[14]. C. K. Hu, B. Luther, F. B. Kaufman, J. Hummel, C. Uzoh, and D. J. Pearson, "Cu interconnection integration and reliability", *Thin Solid Films* 262, 84-92 (1995).

[15]. C. K. Hu, D. C. Edelstein, C. Uzoh, and T. Sullivan, "Comparison of electromigration in submicron Al(Cu) and Cu thin films lines", *Stress-induced Phenomena in Metallization* (1995) p. 152-168.

[16]. R. Rosenberg, D. C. Edelstein, C.–K. Hu, and K. P. Rodbell, "Cu Metallization for high performance silicon tech.", *Annu. Rev. Mater. Sci.* 30, 229-62 (2000).

[17]. D. Edelstein, J. Heidenreich, R. Goldblatt, W. Cote, C. Uzoh, N. Lustig, P. Roper, T. McDevitt, A. Stamper, W. Motsiff, A. Simon, J. Dukovic, R. Wachnik, P. McLaughlin, T. Katsetos, H. Rathore, R. Schulz, L. Su, S. Luce, N. Rohrer, and J. Slattery, *Tech. Dig. IEEE IEDM*, 376 (1997).

[18]. R. Rosenberg, D. C. Edelstein, C. –K. Hu, and K. P. Rodbell, "Copper metallization for high performance silicon technology", *Annu. Rev. Mater. Sci.* 30 229-62 (2000).

[19]. S. Venkatesan *et al. Tech. Dig. IEEE IEDM*, 769 (1997).

[20]. Davis, J.A., et al., *Interconnect limits on gigascale integration (GSI) in the 21st century.* Proceedings of the IEEE, 2001. 89(3): p. 305-324.

[21]. The International Technology Roadmap for Semiconductors, 2009. http://www.itrs.net/Links/2009ITRS/2009Chapters_2009Tables/2009_Interconnect.pdf

[22]. A.R.Blythe, *Electrical Properties of polymers*, Cambridge University Press 1979.

[23]. K. Maex, M. R. Baklanov, D. Shamiryan, F. Iacopi, S. H. Brongersma, and Z. S. Yanovitskaya, "Low dielectric constant materials for microelectronics", *J. Appl. Phys.* 93, 8793-8841 (2003).

[24]. M. Morgen, E. Todd Ryan, J.-H. Zhao, C. Hu, T. Cho, P.S. Ho. Low Dielectric Constant Materials for ULSI Interconnects. Annual Review of Materials Science. Vol. 30. No.1, 2000, p.645-p.683.

[25]. Kwak SI, Jeong KH, Rhee SW. 2004. Nanocomposite low-k SiCOH films by direct PECVD using vinyltrimethylsilane. *J. Electrochem. Soc.* 151:F11–16.

[26]. Tada M, Kawahara J, Hayashi Y. 2001. Characterization of plasma-polymerized divinylsiloxane benzocyclobutene (DVS-BCB) polymer film. *Mater. Res. Soc. Conf. Proc.* ULSI XVI:579–85.

[27]. Tada M, Yamamoto H, Ito F, Takeuchi T, Furutake N, Hayashi Y. 2007. Chemical structure effects of ring-type siloxane precursor on properties of plasma-polymerized porous SiCOH films. *J. Electrochem. Soc.* 154:D354–61.

[28]. Kawahara J, Kinimi N, Kinoshita K, Nakano A, Komatsu M, et al. 2007. An organic low-k film deposited by plasma-enhanced copoloymerization. *J. Electrochem. Soc.* 154:H147–52.

[29]. Wu Q, Gleason KK. 2003. Plasma-enhanced CVD of organosilicate glass (OSG) films deposited from octamethyltrisiloxane, bis(trimethylsiloxy)methylsilanes, and 1,1,3,3-tetramethyldisiloxane. *Plasmas Polym.* 8:31-41.

[30]. Grill, A. *Journal of Applied Physics.* 93, no. 3. 2003. pg. 1785.

[31]. R. M. A. Azzam, N. M. Bashara. Ellipsometry and Polarized Light. Elsevier, Amsterdam,1977.

[32]. C. Le Cornec, F. Ciaramella, V. Jousseaume, P. Leduc, A. Zenasni, and G.Passemard. K Value Improvement of ULK Dielectrics by Wet Activation. Microelectronic engineering, Vol.83, No.11-12, Nov.-Dec. 2006, p.2122 -p.2125.

[33]. Paul S Ho, *Material Issues And Impact on Reliability of Cu/Low-k interconnects*, APS March meeting, 2003.

[34]. J.G. Ryan, Copper and Low-k Dielectric Integration Challenges, SEMICON West 2000.

[35]. K. Carter, The road to Low Dielectric Constant Materials, Proceedings from the Ninth Meeting of the Symposium on Polymers for microelectronics, Wilmington DE 2000.

[36]. M. McCoy, *2000 C&EN*, 17, (2000).

[37]. L. Peters, *Semiconductor International*, 23(6), 108 (2000).

[38]. A. Grill, *Cold Plasma in Materials Fabrication: From Fundamentals to Applications,* Wiley-IEEE Press, Hoboken, NJ, 2001.

[39]. A. Grill, V. Patel, and C. Jahnes, *J. Electrochemical Soc*., 145, 1649 (1998).

[40]. B.D. Hatton, K. Landskron, W.J. Hunks, M.R. Bennett, D. Shukaris, D.D. Perovic, and G.A. Ozin. Materials Chemistry for Low-k Materials. Materials Today. Vol. 9, No. 3, March 2006, p.22 - p.25.

[41]. C. Case. Low-k Dielectrics: Was the Roadmap Wrong? Future Fab International, No.17, June 21, 2004.

[42]. A.T. Kohl, R. Mimna, R. Shick, L. Rhodes, Z. L. Wang, and P. A. Kohla. Low-k, Porous Methyl Silsesquioxane and Spin-On-Glass. Electrochemical and Solid-State Letters. Vol.2, No. 2, Feb. 1999, p.77 - p.79.

[43]. Hedrick, J. L., Miller, R. D., Hawker, C. J., Carter, K. R., Volksen, W., Yoon, D.Y., Trollsås, M. Adv. Mater. 10, 1049 (1998).

[44]. Hedrick, J. L., Carter, K. R., Labadie, J. W., Miller, R. D., Volksen, W.,Hawker, C. J., Yoon, D. Y., Russell, T. P., McGrath, J. E., Breiber, R. M. Adv. Polym. Sci., 141, 1 (1999).

[45]. Kim, S. M.; Yoon, D. Y.; Nguyen, C. V.; Han, J.; Jaffe, R. L. Mater. Res. Soc. Symp. Proc. 511, 39 (1998).

[46]. Cook, R. F.; Liniger, E. G.; Klaus, D. P.; Simonyi, E. E.; Cohen, S. A. Mater. Res. Soc. Symp. Proc., 511, 33 (1998).

[47]. Kim, S. M.; Yoon, D. Y.; Nguyen, C. V.; Han, J.; Jaffe, R. L. Mater. Res. Soc. Symp. Proc., 511, 39 (1998).

[48]. Cook, R. F.; Liniger, E. G.; Klaus, D. P.; Simonyi, E. E.; Cohen, S. A. Mater. Res. Soc. Symp. Proc., 511,33(1998).

[49]. C. Yang, W. Chen, L. Chen, and C. Wang. Characterization of Poly (silsesquioxane) by Thermal Curing. Proc. Natl. Sci. Counc. ROC (A), Vol.25, No.6, 2001, p.339 - p.343.

[50]. Ramkumar, K.; Saxena, A. N. *J. Electrochem. Soc.* 1992, *139*, 1437.

[51]. Ramkumar, K.; Ghosh, S. K.; Saxena, A. N. *J. Electrochem. Soc.*1993, *140*, 2669.

[52]. Stadtmueller, M. *J. Electrochem. Soc.* 1992, *139*, 3669.

[53]. G. Meggy, W.L. Peter, L. Xia, and E. Yieh. The Case for CVD Low-K Technology. Semiconductor Fabtech, 15th Edition, http://www.fabtech.org, 2005, p.179 - p.183.

[54]. N.P. Hacker, MRS Bulletin, pp.22-33(1997).

[55]. R.J. Gutmann, W.N. Gill, T.M. Lu, J.F. McDonald, S.P. Murarka, and E.J. Rymaszewski, Advanced Metallization Conference in 1996 (MRS, Pittsburgh, PA, 1997).

[56]. E.T. Ryan, A.J.McKerrow, J.Leu, and P.S. Ho, MRS Bulletin, 22, 49(1997).

[57]. M. Clarke, Introducing Low-k Dielectrics into Semiconductor Processing, Application notes, Mykrolis, http://mykrolis.com/

[58]. Grill A., Evolution of SiCOH dielectrics to ultralow-k and extreme low-k values. *Proc. VMIC, 23rd, Fremont, CA*, 23:165–72. Fermont, CA:VMIC(2006).

[59]. Ruessac V, Favennec L, Remiat B, Jousseaume V, Passemard G, Durand J., Precursor chemistry for U.K. CVD. *Microelectron. Eng.* 82:333–40 (2005).

[60]. Gates SM, Neumayer DAH, Sherwood MH, Grill A,Wang X, Sankarapandian M., Preparation and structure of porous dielectrics by plasma enhanced chemical vapor deposition. *J. Appl. Phys.* 101:094103 (2007).

[61]. Grill A, Neumayer DA., Structure of low dielectric constant to extreme low dielectric constant SiCOH films: Fourier transform infrared spectroscopy characterization. *J. Appl. Phys.* 94:6697–707(2003).

[62]. Vrtis R, O'Neill M,Vincent J, Lukas L, Peterson B, et al., Plasma enhanced chemical vapor deposition of porous organosilicate glass ILD films with k < 2.4. *Mater. Res. Soc. Symp. Proc.* 766:259–64(2003).

[63]. Yang J, Lee S, Park H, Jung D, Chae H., Characterization of low dielectric constant plasma polymer films deposited by plasma-enhanced chemical vapor deposition using decamethyl-cyclopentasiloxane and cyclohexane as precursors. *J. Vac. Sci. Technol.* A24:165–69(2006).

[64]. Favennec L, Jousseaume V, Gerbaud G, Zenasni A, Passemard G., Ultralow k using a plasma enhanced chemical vapor deposition porogen approach: matrix structure and porgenloading influences. *J. Appl. Phys.* 102:064107(2007).

[65]. Volksen, W., R.D. Miller, and G. Dubois, *Low dielectric constant materials.* Chemical Reviews, 110(1): p. 56-110(2010).

[66]. Grill, A., et al. *Optimization of SiCOH dielectrics for integration in a 90nm CMOS technology,* in *Interconnect Technology Conference.* (2004).

[67]. McGahay, V., et al. *65nm Cu integration and interconnect reliability in low stress k=2.75 SiCOH.* in *Interconnect Technology Conference, 2006 International* (2006).

[68]. M. J. Hampden-Smith, and T. T. Kodas, "Copper etching: new chemical approaches", *Mater. Res. Soc. Bull.* 18, 39 (1993).

[69]. Th. Kruck, and M. Schober, "Low-temperature dry etching of copper using a new chemical approach", *Microelectron. Eng*. 50, 417-423 (2000).

[70]. J. G. Ryan, J. E. Heidenreich, W. J. Cote, R. M. Geffken, and T. N. Theis, "Technology challenges for advanced interconnects", Advanced Metallization and Interconnect Systems for ULSI Applications 1997, p. 399-404.

[71]. C. W. Kaanta, S. G. Bombardier, W. J. Cote, W. R. Hill, G. Kerszykowski, H. S. Landies, D. J. Poindexter, C. W. Pollard, G. H. Ross, J. G. Ryan, S. Wolff, and J. E. Cronin, "Dual damascene: a ULSI wiring technology", *Proceedings of the VLSI Multilevel Interconnection Conference*, June 1991, p. 144-152.

[72]. J. Kriz, C. Angelkort, M. Szekalla, S. Huth, D. Meinhold, A. Pohl, S. Schulte, A. Thamm, and S. Wallace, "Overview of dual damascene integration schemes in Cu BEOL integration",*Microelectron. Eng*. 85, 2128-2132 (2008).

[73]. The International Technology Roadmap for Semiconductors, 2009. http://www.itrs.net/Links/2009ITRS/2009Chapters_2009Tables/2009_Interconnect.pdf

[74]. The International Technology Roadmap for Semiconductors, 2009 edition, interconnect, The Semiconductor Industry Association, http://public.itrs.net.

[75]. Eb Andideh, Evaluation and Evolution of Low-k Inter-Layer Dielectric(ILD) Material and Integration Schemes, 2003 MIT, http://www.erc.arizona.edu/seminar/protected/Current-2003/Eb-Andideh_MIT_1-9-03.pdf

[76]. A.K. Sikderl, P.Zantyel, S. Thagellal, Asho Kumar, B. Vinogradov and N. Gitis, Delamination studies in Cu-Ultra Low-k Stack, CMP-MIC Conference (2003).

[77]. C.L. Borst, D.G. Thakurta, W.N. Gill and R.J. Gutmann, J.Electron. Packaging 124, 362, (2002).

[78]. J-H Zhao, T. Ryan, P. Ho, A.J. McKerrow, and W-Y. Shih. Measurement of Elastic Modulus, Poisson Ratio, and Coefficient of Thermal Expansion of Onwafer Sub-micron Films. Journal of Applied Physics, Vol.85, No.9, 1999, p.6421-p. 6424.

[79]. D.R. Lide. Handbook of Chemistry and Physics. Boca Raton, FL: CRC, (1993).

[80]. S.Arkalgud, SEMATECH, TEL Seminar, (2005).

[81]. D. Shamiryan, T. Abell, F. Iacopi and K. Maex, "Low-k Dielectric Materials", Review Feature, Materials Today, January, (2004).

[82]. M. Morgen, E. Todd Ryan, J.-H. Zhao, C. Hu, T. Cho, P.S. Ho. Low Dielectric Constant Materials for ULSI Interconnects. Annual Review of Materials Science. Vol. 30. No.1, 2000, p.645-p.683.

[83]. H. Miyajima, R. Katsumata, Y. Nakasaki, Y. Nishiyama and N. Hayasaka. Water Absorption Properties of Fluorine-Doped SiO2 Films Using Plasma-Enhanced Chemical Vapor Deposition. Jpn. J. Appl. Phys, Vol.35, Part 1, No.12A., Dec. 1996, p.6217 - p.6225.

[84]. S. J. Martin, J. P. Godschalx, M. E. Mills, E. O. Shaffer II, P. H. Townsend. Development of a Low-Dielectric-Constant Polymer for the Fabrication of Integrated Circuit Interconnect, Adv. Mater. Vol.12, No.23, December, 2000, p.1769 - p.1778.

[85]. J. Yao, A. Iqbal, H. Juneja, and F. Shadman. Moisture Uptake and Outgassing in Patterned and Capped Porous Low-k Dielectric Films. Journal of The Electrochemical Society, Vol.154, No.10, 2007, p.G199 - p.G 206.

[86]. A. Iqbal, H. Juneja, J. Yao, and F. Shadman. Removal of Moisture Contamination from Porous Polymeric Low-k Dielectric Films. AICHE, Vol. 52, No.4, 2006, p.1586 - p.1593.

[87]. Shaw, T.M., et al. *Advanced Metallization Conference 2003 Proceeding (AMC2003)* 2003. Montreal, Quebec, Canada and Tokyo, Japan Materials Research Society, Warrendale, PA.

[88]. Guyer, E.P., J. Gantz, and R.H. Dauskardt, *Aqueous solution diffusion in hydrophobic nanoporous thin-film glasses.* Journal of Materials Research, 2007. 22(3): p. 710-718.

[89]. Tsui, T.Y., A.J. McKerrow, and J.J. Vlassak, *The effect of water diffusion on the adhesion of organosilicate glass film stacks.* Journal of the Mechanics and Physics of Solids, 2006. 54(5): p. 887-903.

[90]. Lin, Y.B., T.Y. Tsui, and J.J. Vlassak, *Water diffusion and fracture in organosilicate glass film stacks.* Acta Materialia, 2007. 55(7): p. 2455-2464.

[91]. H. Yanazawa, T. Fukuda, Y. Uchida, I. Katou. Water Sorbability of low-k Dielectrics Measured by Thermal Desorption Spectroscopy. Surface Science, Vol. 566–568, 2004, p.566 - p.570.

[92]. A.A. Kumbhar, S.K. Singh, and R.O. Dusane. Enhancement of Moisture Resistance of Spin-on Low-k HSQ Films by Hot Wire Generated Atomic Hydrogen Treatment. Thin Solid Films, 501 (May, 2006) 329 - 331.

[93]. Natarajan, S., et al., *A 32nm Logic Technology Featuring 2(nd)-Generation High k plus Metal-Gate Transistors, Enhanced Channel Strain and 0.171 mu m(2)SRAM Cell Size in a 291Mb Array.* Ieee International Electron Devices Meeting 2008, Technical Digest, 2008: p. 941-943.

[94]. P. T. Liu, T. C. Chang, S. M. Sze, F. M. Pan, Y. J. Mei, W. F. Wu, M. S. Tsai, B. T. Dai, C.Y. Chang, F. Y. Shih, and H. D. Huang, "The effects of plasma treatment for low dielectric constant hydrogen silsequioxane (HSQ) ", *Thin Solid Films* 332, 345-350 (1998).

[95]. Aurelie Humbert, Didem Ernur Badaroglu, and Romano J. O. M. Hoofman, "The effect of plasma damage on the material composition and electrical performance of different generations of SiCO(H) low-k films", *Mater. Res. Soc. Symp. Proc.* 914, 0914-F04-03,(2006).

[96]. Thomas Abell, Jeffrey Lee, and Mansour, Moinpour, "Challenges of ultra low-k dielectric measurement and plasma damage assessment", *Mater. Res. Soc. Symp. Proc*. 914,0914-F04-02 (2006).

[97]. Steven A. Vitale, and Herbert H. Sawin, "Etching of organosilicate glass low-k dielectric films in halogen plasmas", *J. Vac. Sci. Technol. A* 20, 651-660 (2001).

[98]. Hao Cui, Richard, J. Carter, Darren L. Moore, Hua-Gen Peng, David W. Gidley, and Peter A. Burke, “Impact of reductive N2/H2 plasma on porous low-dielectric constant SiCOH thin films”, *J. Appl. Phys*. 97, 113302 (2005).

[99]. S. Zimmermann, N. Ahner, F. Blaschta, M. Schaller, H. Rulke, S. E. Schulz, and T. Gessner, “Analysis of the impact of different additives during etch processes of dense and porous low-k with OES and QMS”, *Microelectron. Eng*. 87, 337-342 (2010).

[100]. Tsung-Kuei Kang, “Plasma cleaning technology in the dual damascene process”, *Microelectron. Eng*. 71, 21-27 (2004).

[101]. Chung-Hsien Chen and Fon-Shan Huang, “Surface modification of low dielectric constant material – methylsilsequioxiane”, Thin Solid Films 441, 248-254 (2003).

[102]. Darren Moore, Richard Carter, Hao Cui, Peter Burke, Peter McGrath, S. Q. Gu, David Gidley, and Huagen Peng, “Process integration compatibility of low-k and ultra-low-k dielectrics”, *J. Vac. Sci. Technol. B* 23, 332-335 (2005).

[103]. Yunlong Li, Zsolt Tokei, Joke Van Aelst, Laureen Carbonell, Mikhail R. Baklanov, Olivier Richard, Hugo Bender, Guido Groeseneken, and Karen Maex, “Plasma ash modulation of TDDB thermal activation energy in damascene SiOC:H”, *Semicond. Sci. Technol*. 22, 320-325 (2007).

[104]. D. Shamiryan, M. R. Baklanov, S. Vanhaelemeersch, and K. Maex, “Comparative study of SiCOH low-k films with varied porosity interacting with etching and cleaning plasma”, *J.Vac. Sci. Technol.* 20, 1923-1928 (2002).

[105]. S. Xu, C. Qin, L. Diao, D. Gilbert, L. Hou, A. Wiesnoski, E. Busch, R. McGowan, B.White, F. Weber, *J. Vac. Sci. Technol.* B 25 (1), 156 (2007).

[106]. J. Bao, H. Shi, J. Liu, H. Huang, P.S. Ho, M.D. Goodner, M. Moinpour, G.M. Kloster, *J. Vac. Sci. Technol.* B 26 (1), (2008).

[107]. K. N. Tu, “Recent advances on electromigration in vary-large-scale-integration of interconnects”, *J. Appl. Phys*. 94, 5451-5473 (2003).

[108]. K. Mosig, T. Jacobs, K. Brennan, M. Rasco, J. Wolf, and R. Augur, “Integration challenges of porous ultra low-k spin-on dielectrics”, *Microelectron. Eng*. 64, 11-24 (2002).

[109]. R. J. O. Hoofman, G. J. A. M. Verheijden, J. Michelon, F. Iacopi, Y. Travaly, M. R.Baklanov, Zs. Tokei, G. P. Beyer, “Challenges in the implementation of low-k dielectrics in the back-end of line”, *Microelectron. Eng*. 80, 337-344 (2005).

[110]. Richard A. Gottscho, K. Nojiri, J. LaCara, “Challenges in etch: what’s new?”, *Thin Solid Films* 516, 3493-3496 (2008).

[111]. M. Fayolle, G. Passemard, O. Louveau, F. Fusalba, and J. Cluzel, “Challenges of back end of the line for sub 65nm generation”, *Microelectron. Eng*. 70, 255-266 (2003).

[112]. F. Chen, O. Bravo, D. Harmon, M. Shinosky, and J. Aitken, “Cu/low-k dielectric TDDB reliability issues for advanced CMOS technology”, *Microelectron. Relib*. 48, 1375-1383 (2008).

[113]. K. Heo, S. -G. Park, J. Yoon, K. S. Jin, S. Jin, S. -W. Rhee and M. Ree, *J. Phys. Chem*. C, 111 (29), 10848 (2007).

[114]. D. M. Meng, N. L. Michael, Y. J. Park, and C. U. Kim, *Appl. Phys. Lett.* 88, 261911 (2006).

[115]. D. M. Meng, N. L. Michael, Y. J. Park, and C. U. Kim, *J. Electron. Mat.* 37, 429 (2008).

[116]. L. S. Chen, W. H. Bang, S. H. Kang, E. Zin, K.H. Oh, Y. J. Park, and C. U. Kim, “Study of thermo-mechanical instability of pores in porous low-k/Cu interconnects”, *TECHCON 2008*, Austin, TX (2008).

[117]. H. O‘Neill, *Hardness Measurements of Metals and Alloys*, (Chapman and Hall, London, 1967).

[118]. H. J. Frost and M. F. Ashby, *Deformation-Mechanism Maps, (The Plasticity and Creep of Metals and Ceramics*, Pergamon Press, (1982).

[119]. H. Rawson, Glass Sci. Tech., 3, *Properties and Application of Glass*, (1980).

[120]. J.S. Field and M.V. Swain, *J. Mater. Res*., Vol 8 (No.2), p 297-306, (1993).

[121]. O. D. Sherby, T. A. Trozera J. E. Dom, “Effects of creep stress history at high temperatures on the creep of aluminum alloys”, Proc. ASTM, vol. 56, p 789-804, (1956).

[122]. A. Dasgupta, J. M. Hu, “Failure mechanism models for plastic deformations”, *IEEE Trans. Reliability,* vol 41, 1992 Jun, pp 168-174.

[123]. G. E. Dieter, *Mechanical Metallurgy* (3rd edition), 1986, p 441; McGraw-Hill.

[124]. T. G. Langdon, Mat. Sci. Eng. A137 (1991) 1.

[125]. N. Q. Chinh, P. Tasnádi, A. Juhász, P. Szommer, E. Szép-Kiss, I. Kovács, Key Eng. Mat. 97/98, 159, (1994).

[126]. M. F. Ashby, A. M. Brown, proc. 2nd Risø Int. Symp. Metall. and Mat. Sci. (1981).

[127]. Spaepen F 1977 *Acta. Metall.* Vol. **25** 407.

[128]. Argon A S 1979 *Acta. Metall.* Vol. **27** 47.

[129]. Falk M L and Langer J S 1998 *Phys. Rev.* E Vol. **57** 7192.

[130]. Langer J S 2001 *Phys. Rev.* E Vol. **64** 011504.

[131]. Falk M L, Langer J S and Pechenik L 2004 *Phys. Rev.* E Vol 70 011507.

[132]. D. W. Hadley and I. M. Ward, Rep. Prog. Phys. 38,1143 (1975).

[133]. P.W. Bridgman, I. Simon, J. Appl. Phys. 24(1953) 405.

[134]. S. Yoshida, Jean-Christophe Sangleboeuf, Tanguy Rouxel, Int. J. Mat. Res. 98 (2007) 5.

[135]. W.C. Oliver, G.M. Pharr, J. Mater. Res. 19 (2004) 3.

[136]. S. L. Robinson, O. D. Sherby, “Activation energy for lattice self-diffusion in aluminum”, physica status solidi (a), vol. 1, Issue 3, p k119-k122, March (1970).

[137]. G. Cseh, N. Q. Chinh, P. Tasnádi, P. Szommer and A. Juhász, “Indentation test for the investigation of plasticity of glasses”, J. Mat. Sci., 32, 1733-1739(1997).

[138]. S.-P. Hannula, D. Stone, and C.-Y. Li. Determination of Time-Dependent Plastic Properties by Mentation Load Relaxation Techniques. In *Mater. Res. Soc. Symp. Proc. Vol. 40,* pages 217-224, Pittsburgh, PA, USA, 1985. Materials Research Society.

[139]. P. M. Sargent andM. F. Ashby. Indentation creep. *Mater. Sci. Technol. (UK),* 8:594-601, 1992.

[140]. W. B. Li and R. Warren. A Model for Nano-Indentation Creep. *Acta Metall. Mater.,* 10:3065-3069, 1993.

[141]. A. F. Bower, N. A. Fleck, A. Needleman, and N. Ogbonna. Indentation of a power law creeping solid.*Proc. Roy. Soc. Lond. A,* 441:97-124, 1993.

[142]. Nico M. Keulen. Indentation Creep of Hydrated Soda-Lime Silicate Glass Determined by Nanoindentation.*J. Am. Ceram. Soc,* 76:904-912, 1993.

[143]. D. S. Stone and K. B. Yoder. Division of the hardness of molybdenum into rate-dependent and rateindependent parts. *J. Mater. Res.,* 9:2524-2533, 1994.

[144]. W. H. Poisl, W. C. Oliver, and B. D. Fabes. The relationship between indentation and uniaxial creep in amorphous silicon. *J. Mater. Res.,* 10:2024-2032, 1995.

[145]. S. A. Syed Asif and J. B. Pethica. Nanoindentation creep of single-crystal tungsten and gallium arsenide. *Phil. Mag. A,* 76:1105-1118, 1997.

[146]. B. N. Lucas and W. C. Oliver. Indentation Power-Law Creep of High-Purity Indium. *Metall. Mater. Trans.,* 30A:601-610, 1999.

[147]. Yu. I. Golovin, Yu. L. Iunin, and A. I. Tyurin. Strain-Rate Sensitivity of the Hardness of Crystalline Materials under Dynamic Nanoindentation. *Doklady Academii Nauk,* 392:336-339, 2003. Appears in translation in *Doklady Physics,* 48:505-508, 2003.

[148]. Shuang Yang, Yong-Wei Zhang, and Kaiyang Zeng. Analysis of nanoindentation creep for polymeric materials. *J. Appl. Phys.,* 95:3655-3666, 2004.

[149]. A. C. Fischer-Cripps. A simple phenomenological approach to nanoindentation creep. *Mater. Sci. Eng. A,* 385:74-82, 2004.

[150]. David L. Goldsby, Andrei Rar, George M. Pharr, and Terry E. Tullis. Nanoindentation creep of quartz, with implications for rate- and state-variable friction laws relevant to earthquake mechanics. *J. Mater.Res.,* 19:357-365, 2004.

[151]. A. A. Elmustafa, S. Kose, and D. S. Stone. Strain rate sensitivity in nanoindentation creep of hard materials. *Mater. Res,* 22:926-936, 2007.

[152]. D. S. Stone and A. A. Elmustafa. Analysis of Indentation Creep. In *Mater. Res. Soc. Symp. Proc. Vol.1049,* pages 1049-AA10-02, Pittsburgh, PA, USA, 2008. Materials Research Society.

[153]. N.M. Keulen, J. Am. Ceram. Soc. 76 (4), 904, (1993).

[154]. W.T. Han and M. Tomozawa, J. Am. Ceram. Soc. 73,12 (1990) 3626.

[155]. O. Prakash and D.R.H. Jones, Acta. mater. 44, 3 (1996) 891.

[156]. Muktepavel and |I. Manika, J. Mat. Sci. letters 8 (1989) 4.

[157]. A.L. Yurkov, J. Mat. Sci. Letters, 12 (1993) 767.

[158]. A. Juhász, P. Tasnádi and I. Kovács, J. Mat. Sci. letters 5 (1986) 35.

[159]. W.B. Li, J.L. Henshall, R.M. Hooper and K.E. Easterling, Acta metall. mater. 39, 12, (1991) 3090.

[160]. A. Torre, P. Adeva, M. Aballe, J. Mat. Sci. 26 (1991) 4351.

[161]. P. Tasnádi, A. Juhász, N.Q. Chinh and I. Kovács, Key Eng. Mater. 97-98, (1994) 169.

[162]. Mayo MJ, Siegel RW, Narayansamy A, Nix WD. Mechanical properties of nanophase TiO2 as determined by nanoindentation. J Mater Res 1990;5:1073–81.

[163]. Raman V, Berriche R. “An investigation of the creep processes in tin and aluminium using a depth-sensing indentation technique”, J. Mater. Res 1992;7:627–38.

[164]. Asif SAS, Pethica JB. “Nano-scale indentation creep testing at non-ambient temperature”, J Adhesion 1998;67:153–65.

[165]. Jamari J, Schipper DJ. “Experimental investigation of fully plastic contact of a sphere against a hard flat. ASME J Tribol 2006 ; 128:230-5

[166]. T.O. Mulhearn and D. Tabor, J. Inst. Metals 89, 7 (1960).

[167]. F.M. Haggag, in: W.R. Corwin, F.M. Haggag, W.L. Server (Eds.), Small Specimen Test Technique Applied to Nuclear Reactor Vessel Thermal Annealing and Plant Life Extension, American Society for Testing and Materials, Philadelphia, 1993, p. 27 ASTM STP 1204.

[168]. R. Goodall, T.W. Clyne, Acta Materialia, 54(2006) 5489-5499.

[169]. M. Bletry, P. Guyot, Y. Brechet, J.J. Blandin, J.L. Soubeyroux, *Intermetallics*, 12 (2004) 1051.

[170]. E.C. Yu, J.C.M. Li, *Phil. Mag*. 36 (1977) 911.

[171]. D. F´atay, J. Gubicza, P. Szommer, J. Lendvai, M. Bl´etry, P. Guyot, *Mater. Sci. Eng*. A 387-389(2004), 1001.

[172]. R.W. Douglas, W.L. Armstrong, J.P. Edward and D. Hull, *Glass Technol*. 6 (1965) 52-55.

[173]. R.Morrel and K.H.G. Ashbee: J.Mater. Sci. 8, 1253, (1973).

[174]. T.Fett, K. Keller, M. Missbach, D. Munz and L. Pintschovius: *J. Am. Ceram. Soc*. 71, 1046, (1988).

[175]. H. Rawson, Glass Sci. Tech., 3, *Properties and Application of Glass*, (1980).

[176]. H. Scholze and N.J. Kreidl, "Technological Aspects of Viscosity", pp.233-274 in *Glass Science and Technology* Volume 3: Viscosity and Relaxation, Edited by D.R. Uhlmann and N.J. Kreidl. Academic Press, Orlando, (1986).

[177]. H.E. Hagy, "Experimental Evaluation of Beam-Bending Method of determining Glass Viscosiies in the range 10^8 to 10^{15} Poises, " *Journal of the American Ceramic Society*, 46 [2] (1963) 93-97.

[178]. A.V. Cardoso and A.B. Seddon, "Penetration Viscometry Using a Thermal Mechanical Analyzer", *Glass Technology*, 32 [5] (1991), 174-176.

[179]. F.T. Trouton: Proc. R. Soc. Lond. A 519, 426 (1906).

[180]. Timoshenko, S. and Goodier, J.N. (1951). *"Theory of Elasticity"*, p.372. McGraw-Hill, London.

[181]. S.M Cox, "A Method of Viscosity Measurement in the region 10^8 Poises", *Journal of Scientific Instruments*, 20 (1943), 113-114.

[182]. J.N. Goodier, "Slow Viscous flow and Elastic Deformation", *Philosophical magazine*, 22 (1936), 678-681.

[183]. A. Grill, DA. Neumayer, *J. Appl. Phys*., 94, 6697 (2003).

[184]. Alfred Grill, “Porous pSiCOH Ultralow-*k* Dielectrics for Chip Interconnects Prepared by PECVD”, Annual Rev. Mater. Res., 39:49–69, (2009).

[185]. G.B. Alers, D.Dornisch, J.Siri,K.Kattige,L.Tam, E. Broadbent and G.W.Ray, Proc.
39 th IEEE Int. Reliab. Phys. Symp.,(IEEE International, Orlando, FL,2001)
p.350.

[186]. K. H. Yang, K. Foster, J. Im, J. Waeterloos, E. Shaffer, D. Frye, M. Mills,and P. Townsend, American Society of Mechanical Engineers ASME meeting 2001, 9–12 September, Pittsburgh, PA; IMEC, unpublished results.

[187]. Veeco Metrology Group, *Wyko Surface Profilers - Technical Reference Manual*. 2008, Veeco Instruments, Inc: USA.

[188]. Smith, B.C. *Fundamentals of Fourier Transform Infrared Spectroscopy*, Boca Raton Florida, CRC Press LLC, 1996.

[189]. Gunzler, H. and Gremlich, H. IR Spectroscopy: An Introduction. Wiley-VCH., 2002.

[190]. Stuart, B., George, W.O., McIntyre P.S. *Modern Infrared Spectroscopy,* Edited by D.J. Ando, England, John Wiley & Sons Ltd, 1998.

[191]. Harrick, N.J., Beckmann, K.H. “Internal Reflection Spectroscopy” In *Characterization of Solid Surfaces*, edited by P.F. Kane, G.B. Larrabee, New York, Plenum Press, 1974.

[192]. D.D. Burkey, K.K. Gleason, *J. Appl. Phys*., Vol. 93, No. 9, 1 May (2003).

[193]. S.H. Rhee, M.D. Radwin, M.F. ng, J.I. Martin, and D. Erb, Appl. Phys. Lett. 83, 2644, (2003).

[194]. E. Kandoh, M. R. Baklanov, H. Bender, K. Max, Electro-Chem. Solid State Lett.1
224,(1998).

[195]. Storåkers B and Larsson P L, *J. Mech. Phys. Solids,* 42 307, (1994).

[196]. Hill R, *Proc. R. Soc. Lond.* A 436 617, (1992).

[197]. Tabor D, *The Hardness of Metals,* (1951) (Oxford: Clarendon).

[198]. I. Burn and J. P. Roberts, Phys. Chem. Glasses 11, 106 (1970).

[199]. T. Bakos, S. N. Rashkeev, and S. T. Pantelides, *Phys. Rev. B, vol. 69, Article* No.195206, (2004).

[200]. Chao Ye, Zhaoyuan Ning, Tingting Wang, Xiaozhu Yu, Yu Xin, Thin Solid Films 496, 221 – 226, (2006).

[201]. J. C. Mikkelsen, Appl. Phys. Lett. 39, 903 (1981).

[202]. D.L. Goldsby, DIFFUSION CREEP OF ICE: CONSTRAINTS FROM LABORATORY CREEP EXPERIMENTS, Lunar and Planetary Science XXXVIII (2007).

[203]. Y. Shioya, T. Ohdaira, R. Suzuki, Y. Seino, K. Omote, J. of Non-Crystalline Solids, 354, 2973-2982 (2008).

[204]. Edited by M. Baklanov, M. Green, and K. Maex. Dielectric Films for Advanced Microelectronics. Chapter 2: Geraud Dubois, Robert D. Miller, and Willi Volksen. Spin-on Dielectric Materials. John Wiley & Sons Ltd, UK, 2007.

[205]. D. Lu, R. Kumar, and C.-K. Chang, A.-Y. Du, T.K.S. Wong. Analysis of Surface Contamination on Organosilicate Low-*k* Dielectric Materials. Microelectronic Engineering, Vol.77, No.1, January 2005, p.63 - p.70.

[206]. Y. Furukawa, R. Wolters, H. Roosen, J.H.M. Snijders, R. Hoofman. Etch and Strip Induced Material Modification of Porous Low-*k* (k = 2.2) Dielectric. Microelectronic Engineering, Vol.76, No.1-4, October 2004, p.25 - p.31.

[207]. Y.S. Tan, S.Y.M. Chooi, C.-Y. Sin, P.-Y. Ee, M.P. Srinivasan, and S.O.Pehkonen. Characterization of Low-*k* Dielectric Trench Surface Cleaning after a Fluorocarbon Etch. Thin Solid Films, Vol.462-463, Sep. 2004, p.250 - p.256.

[208]. W. Puyrenier, V. Rouessac, L. Broussous, D. Rébiscoul, and A. Ayral. Effect of Plasma Treatments on a Porous Low-*k* Material - Study of Pore Sealing. Microporous and Mesoporous Materials, Vol.106, No.1-3, Nov. 2007, p.40 - p.48.

[209]. Y.L. Cheng, Y.L. Wang, J.K. Lan, G.J. Hwang, M.L. O'Neil, and C. F. Chen, Heat, Moisture and Chemical Resistance on Kow Dielectric Constant (low-*k*) Film Using Diethoxymethylsilane (DEMS) Prepared by Plasma Enhanced Chemical Vapor Deposition. Surface and Coatings Technology, Vol.200, No.10, Feb. 2006, p.3127 - p.3133.

[210]. R. J. O. Hoofman, G. J. A. M. Verheijden, J. Michelon, F. Iacopi, Y. Travaly, M.R. Baklanov, Zs. Tokei, G. P. Beyer, "Challenges in the implementation of low-k dielectrics in the back-end of line", *Microelectron. Eng*. 80, 337-344 (2005).

[211]. Thomas Abell, Jeffrey Lee, and Mansour, Moinpour, "Challenges of ultra low-k dielectric measurement and plasma damage assessment", *Mater. Res. Soc. Symp. Proc*. 914, 0914-F04-02 (2006).

[212]. D. Kim, Y. Lee, N. Park, Appl. Phys. Lett. 69 (1996) 2779.

[213]. S. Sugahara, K. Usami, M. Matsumura, Jpn. J. App. Phys. 38 (1999) 1428.

BIOGRAPHICAL INFORMATION

Emil Hyunbae Zin earned his B.S. in Metallurgical Engineering in 1999 in Pusan National University in Korea. After he finished his Master degree in Materials Science and Engineering in 2001 from Seoul National University, where he worked on studying analysis of duplex powder compaction process using finite element method, he was a packaging engineer in Samsung Electro-Mechanics Co. Ltd., Suwon, South Korea, where he worked on the development of advanced electronic packaging technologies including embedding passive devices into organic substrates for five and a half years. He has pursued a PhD. degree in Materials Science and Engineering Department at the University of Texas at Arlington since 2007 under the supervision of Dr. Choong-Un Kim. During his doctoral program in the University of Texas at Arlington, he was an intern in Texas Instruments Co. Ltd., where he worked on the development of characterization techniques for mechanical properties of materials. His research interests include time-dependent properties of various materials such as polymeric glasses (Porous Low-k dielectrics), metals and ceramics and reliability assessment in advanced Cu/PLK interconnects, as well as the development of next generation of electronic packaging.